Voltage-dependent and Synaptic Characteristics of Rostral Hypothalamic Kisspeptin Neurons and Their Role in the Neuroendocrine Control of Ovulation

by

Joseph Rudolph Starrett

A dissertation submitted in partial fulfillment
of the requirements for the degree of
Doctor of Philosophy
(Molecular and Integrative Physiology)
in the University of Michigan
2023

Doctoral Committee:

Professor Suzanne M. Moenter, Chair
Assistant Professor Bo Duan
Professor Carol F. Elias
Professor Michael A. Sutton

Joseph Rudolph Starrett

jstarret@umich.edu

ORCID iD: 0000-0002-0073-0252

Acknowledgements

I owe a great debt to many people for their help in completing this work.

The members of my thesis committee, Dr. Carol Elias, Dr. Michael Sutton, and Dr. Bo Duan all provided guidance. I received additional input and support from many MIP faculty, staff, and students at seminars and in conversation.

Dr. Laura Burger and Beth Wagenmaker spent many hours preparing solutions and managing a mouse colony. Jenn Jaime shared an electrophysiology rig with me and helped troubleshoot electrical noise issues. Amanda Gibson helped set up optogenetics equipment and also shared a rig. Chrystian Phillips taught me how to perform stereotaxic injections. Drs. Xi Chen, Luhong Wang, Caroline Adams, Tova Berg, Eden Dulka, Marina Silveira, Jeff Phumsatitpong, and Charlotte Vanacker were all excellent role models regarding their science, professionalism, and diligence. These people all provided valuable insight and were a pleasure to work with over the years.

Dr. Luke Remage-Healey ushered me into the world of scientific research with a great deal of patience and support. He fostered my interests in neuroendocrinology, steroid hormones, and electrophysiology which led me to this dissertation topic.

Dr. Tony Defazio was invaluable to many aspects of this work. I have enormous respect for his breadth of expertise, which he offered generously.

Ben Abdon, Kristy Weaver, Vi Tang, and Stefan Sweha discussed this work with me on many occasions over the years. They were with me in times of joy and distress, and I am very grateful for their continued friendship.

Julia Paulson was a pillar of emotional support during the closing months of this work.

I would not be poised to accomplish anything if not for the love, generosity, and stability provided by my parents, Annie and Dave Starrett, and the support of my siblings, Nikki and Doug. My nonna, Margaret, also cheered me on at every opportunity.

Finally, my utmost thanks and appreciation go to my advisor, Dr. Sue Moenter. She provided exceptional mentorship and support throughout, and I owe her an enormous debt for the role she has played in honing my scientific thoughts and writings. Her dedication to bolstering the development and success of everyone in her lab (and many outside it) is unmatched. I am incredibly fortunate to have been her student.

Table of Contents

List of Tables

List of Figures

Abstract

Anovulation is a common presentation of infertility, yet in many cases the root cause is unknown. This is, in part, due to an incomplete understanding of how ovarian estradiol normally acts in the brain to initiate the cascade of physiological events leading up to ovulation. In spontaneously-ovulating mammals, this cascade is known as estradiol positive feedback, and involves ovarian estradiol facilitating a surge of gonadotropin-releasing hormone (GnRH) release from the hypothalamus. The neurophysiological basis for GnRH surge generation is not well-defined. Initiation of the GnRH surge is thought to involve neurons in the rostral hypothalamus that express the neuropeptide kisspeptin, a strong activator of GnRH release. In mice, these estradiol-sensitive neurons are in the anteroventral-periventricular area (AVPV). This dissertation involved study of the intrinsic electrical properties of AVPV kisspeptin neurons and their neural circuit interactions with GnRH neurons. Voltage-gated potassium currents of AVPV kisspeptin neurons were biophysically characterized and found to have different amplitude and voltage sensitivity in neurons from diestrous vs proestrous mice. Simulations of spiking activity suggested concomitant increases in T-type calcium, persistent sodium, and hyperpolarization activated currents during proestrus promote burst-firing activity. This is likely to contribute to increased kisspeptin release by these cells during the GnRH surge.

Signaling between AVPV kisspeptin and GnRH neurons was studied in diestrous, proestrous, ovariectomized, and ovariectomized-estradiol-treated mice. It was found that GnRH neurons exhibit immediate and delayed increases in spike rate upon photoactivation of AVPV kisspeptin neurons. Immediate increases in spike rate were due to evoked monosynaptic excitatory GABAergic PSCs, and were absent in ovariectomized mice. Delayed increases in firing did not require a monosynaptic connection, suggesting peptidergic transmission can occur in absence of co-transmitted

activators of ionotropic receptors. The evoked increase in GnRH neuron firing rate was not different between diestrous and proestrous mice, suggesting increased activation of this circuit during positive feedback is not primarily driven by modulation of synaptic strength or an increase in the efficacy of metabotropic transmission. This places increased emphasis on AVPV kisspeptin neuron spiking activity as a primary determinant of GnRH surge initiation.

Chapter 1: Introduction

The hypothalamo-pituitary-gonadal axis

The hypothalamo-pituitary-gonadal (HPG) axis plays a central role in the regulation of reproduction in vertebrates. The hypothalamus, and in some species nearby areas of the forebrain, contains neurons that produce gonadotropin-releasing hormone (GnRH) and release it from nerve terminals near the primary pituitary portal capillaries at the median eminence (Pelletier et al., 1974; Bennett et al., 1975; Hoffman and Finch, 1986; Wray and Hoffman, 1986; Standish et al., 1987; Zoeller et al., 1988; Ronnekleiv et al., 1989; Silverman et al., 1994; Hoffman and Berghorn, 1997). GnRH released in this neuroendocrine fashion acts on gonadotropes in the anterior pituitary driving the synthesis and secretion of the gonadotropins luteinizing hormone (LH) and follicle-stimulating hormone (FSH) (Schally et al., 1971; Conn et al., 1987; Haisenleder et al., 1991). Gonadotropins then act on the gonads regulating gametogenesis and the synthesis of the sex steroids progesterone, testosterone, and estradiol (Hunzicker-Dunn and Mayo, 2006; Smith and Walker, 2014). Sex steroids have widespread effects on physiology. Within the HPG axis, they provide information to the brain and pituitary about the status of the gonads via feedback loops.

In a control system, a feedback loop is formed when an output of a system is fed into its input, creating a closed loop. Closed-loop feedback can take two forms: negative and positive. In negative feedback, the output has an inhibitory effect on the system. Negative feedback therefore promotes stability of the system around a steady-state and is common in physiology due to the need for stability of the organism's internal environment (i.e., homeostasis). In positive feedback, the output has a stimulatory effect on the system. Positive feedback leads to exponential increases in output, typically up to the limit of the system or until something disrupts the feedback loop. Positive feedback systems are relatively uncommon in physiology, likely due to their inherent instability. However, they are often found in contexts that demand deviation from a steady state.

The HPG axis is an interesting physiologic system because sex steroid feedback can take either the negative or positive form. Furthermore, the modes of GnRH and LH secretion differ between the two forms of feedback. In gonadectomized animals, which represent the "open-loop" feedback condition, GnRH is secreted in a pulsatile pattern required to maintain pituitary responsiveness to GnRH (Belchetz et al., 1978; Caraty et al., 1982; Clarke and Cummins, 1982; Moenter et al., 1992c). Pulses of GnRH evoke pulses of LH from the pituitary. When gonadectomized animals are treated with sex-steroids (closed-loop), negative feedback lowers the mean circulating concentration of LH compared to the open-loop condition. This is accomplished by reducing the

amplitude and frequency of GnRH and resulting LH pulses (Goodman and Karsch, 1980; Karsch et al., 1987a; Terasawa, 1994; Evans et al., 1995).The male HPG axis operates in a persistent negative feedback state, whereas females cycle between negative-feedback and positive-feedback states. Positive feedback is induced when high levels of estradiol produced by preovulatory ovarian follicles stimulate a change from pulsatile to continuous and markedly elevated GnRH release, an event called a surge (Sarkar et al., 1976a; Moenter et al., 1990, 1992a; Pau et al., 1993). GnRH surges can also be induced by administration of high physiologic doses of estradiol. The GnRH surge induces an LH surge, which acts at the ovarian follicle triggering ovulation.

Estradiol is thus particularly interesting for the regulation of the female HPG axis because it can act as both a negative-feedback carrier and a positive-feedback initiator. Both functions are critical for female fertility, one promoting growth of follicles in waves and the other initiating ovulation. Both also depend on the α form of the estradiol receptor (ERα), as evidenced by the finding that ERα knockout mice are hypogonadal and do not surge (Couse et al., 2003). Interestingly, despite its key role in the regulation of GnRH secretion, ERα is rarely detected in GnRH neurons (Hrabovszky et al., 2000). This apparent lack of ERα expression has motivated extensive investigations of estradiol-sensitive afferents of GnRH neurons and the mechanisms they utilize to relay feedback. Over the past two decades, research in this area has focused heavily on the neuropeptide kisspeptin, the hypothalamic neurons that produce it, and their

interactions with GnRH neurons via kisspeptin and other mediators. Kisspeptin-producing neurons in the anteroventral-periventricular area (AVPV) of the hypothalamus are theorized to mediate estradiol positive-feedback and to initiate the GnRH surge (Dungan et al., 2006). This dissertation examines the electrophysiological properties of these neurons and their interactions with GnRH neurons, including their regulation by estradiol feedback.

The neuroendocrine basis of estradiol negative and positive feedback

The dynamics of GnRH, gonadotropin, and steroid concentrations in blood began to be studied intensively when the development of the radioimmunoassay allowed researchers to quantify hormones beginning in the 1960s (Berson et al., 1956). This technological advancement led to discovery of the pulsatile (i.e., rhythmic peaks and nadirs) secretion pattern of LH measured in serial blood samples from ovariectomized rhesus monkeys (Dierschke et al., 1970). GnRH had not yet been isolated at this time, but the existence of a hypothalamic releasing factor that drives gonadotropin secretion was strongly suggested by the prior works of Harris, Everett, and Sawyer. Thus, from the discovery of LH pulses, it was inferred the hypothalamic releasing factor must be secreted in pulses that drive gonadotropin pulses from the pituitary. The existence of GnRH was confirmed when it was isolated by the labs of Roger Guillemin and Andrew Schally, who would later share the Nobel Prize in Physiology or Medicine with Rosalyn Yalow, who developed the radioimmunoassay (Schally et al., 1971; Burgus et al., 1972).

Even with modern technology (some 50 years later), it is not yet possible to measure GnRH in peripheral blood due to the minute amount of hormone secreted, its heavy dilution into the peripheral circulation, and its short half-life. Thus, it took another six years after the isolation of GnRH for researchers to develop surgical methods that allowed serial sampling of pituitary portal blood from which GnRH could be measured. Measurements from rhesus monkeys revealed GnRH was indeed secreted episodically, however, the relationship to gonadotropin secretion pattern could not be observed directly because the method used to collect portal blood (pituitary stalk resection) precluded simultaneous measurement of gonadotropins (Carmel et al., 1976). Nonetheless, the pulse pattern of GnRH secretion was established as a critical element of its function when it was discovered that pulsatile, but not continuous infusion of exogenous GnRH restored gonadotropin levels in ovariectomized rhesus monkeys with hypothalamic lesions (Belchetz et al., 1978). A few years after this finding, the right choice of animal model, sampling technique, and surgical expertise finally allowed GnRH and LH pulses to be measured simultaneously in portal capillaries and peripheral blood (respectively) in ewes (Caraty et al., 1982; Clarke and Cummins, 1982; Moenter and Evans, 2022). GnRH has now been measured in other species including monkeys, rats, horses and rabbits (Neill et al., 1977; Levine and Ramirez, 1982; Kaynard et al., 1990; Irvine and Alexander, 1994). This led to a rapid advancement in our knowledge of the endocrine control of reproduction including the feedback effects of gonadal steroids.

One longstanding question at the time concerned the seemingly biphasic nature of the gonadotropin response to estradiol in females. As early as 1940 it was understood that gonadal factors had a generally “depressing effect” on the release of gonad-stimulating factors from the pituitary (Moore and Price, 1932). However, it was also observed that single injections of high-dose estrogens could induce corpora lutea formation (a sign of ovulation) in immature rats, and that this effect was dependent on the pituitary (Hohlweg, 1934; Hohlweg & Chamorro, 1937). It was theorized “the pituitary maintains growth and development of the ovary continuously, with increased estrin[estrogens] acting as a stimulus to the pituitary whose increased output is demonstrated by the appearance of the gonadotropin peak" (D’Amour, 1940). However, the physiologic mechanisms that supported these dichotomous effects remained a mystery.

In the 1960s, “negative and positive feedback”, terms adopted from systems control theory, began to be used to describe the depressive and stimulatory effects of estradiol. Recognition that the hypothalamus exerts humoral control over the pituitary presented the question of where feedback is exerted. Work by Ernst Knobil’s lab suggested estradiol action at the pituitary is sufficient for positive-feedback induction of the LH surge in female monkeys and humans. Mainly, rhesus monkeys lacking endogenous GnRH secretion due to targeted lesions of the mediobasal hypothalamus (MBH) could still generate LH surges when administered GnRH at fixed intervals (Belchetz et al., 1978). Along a similar thread, GnRH-insufficient monkeys display menstrual cyclicity

and women can successfully conceive when given GnRH at regular intervals via infusion pump (Knobil et al., 1980; Martin et al., 1990). Simultaneous measurements of GnRH and LH in sheep, however, suggested gonadal steroid feedback effects on LH secretion to be controlled, at least partially, by modulation of the pattern of upstream GnRH pulses (Karsch et al., 1987a; Wu et al., 1987; Evans et al., 1994, 1995; Skinner et al., 1998). Modulation of frequency, primarily, was found to influence the mean concentration of LH and FSH in the blood and to drive preferential gonadotropin secretion i.e., high GnRH pulse frequency promoted LH synthesis and release whereas low frequency promoted FSH synthesis and release (Wildt et al., 1981; Dalkin et al., 1989). Furthermore, the LH surge in ewes was found to be induced by a GnRH surge that is itself induced by a follicular phase rise in estradiol (Caraty et al., 1989; Moenter et al., 1990, 1992b). Estradiol positive feedback-induced GnRH surges were also observed via direct measurement of GnRH in rats, mares, and monkeys (Sarkar et al., 1976a; Levine et al., 1985; Xia et al., 1992; Irvine and Alexander, 1994). These findings defined modulation of GnRH secretion as a key element of negative and positive-feedback effects of estradiol, and research into the neuroanatomy and physiology GnRH neurons soon intensified.

GnRH neurons: neuroanatomical distribution and innervation

When reliable antibodies became available to use for immunolabeling GnRH, researchers began to use light and electron microscopy to study the anatomical

distribution and morphology of GnRH neurons. It was soon discovered the number of GnRH neurons is relatively few. There are ~2500 GnRH neurons in humans and monkeys, and sheep, and ~800-1500 in rodents. In these species, GnRH neuron perikarya are scattered diffusely along the mid-ventral diencephalon, with some species variation in relative distribution. Displaying a typically bipolar morphology, most GnRH neurons direct a millimeters-long projection towards the median eminence where they release hormone in a neuroendocrine fashion. However, a minority of GnRH neurons do not seem to project to the median eminence and may therefore serve a neuromodulatory rather than neuroendocrine function. GnRH has been detected at synapses in the preoptic area, and GnRH modulates electrical activity in the preoptic area and elsewhere, making a neuromodulatory function likely, although it is not clear what role this function may play in physiology (Jennes et al., 1985; Silverman, 1984; Leranth et al., 1985b; Moss and Dudley, 1978; Dyer and Dyball, 1974). An interesting possibility is that GnRH may be involved in the coordination of GnRH neuron activity. This is suggested by multiple, but rare and seemingly species-dependent, findings of GnRH at synapses between GnRH neurons (Leranth et al., 1985b). Changes in local GnRH concentration at junctions between GnRH neurites has been detected electrochemically in mouse brain slices, indicating GnRH is released locally in the POA and in the vicinity of other GnRH neurons (Glanowska and Moenter, 2015). However, a role for autocrine and/or local circuit GnRH action in coordination of the GnRH neuron network has not been demonstrated conclusively.

GnRH neurons receive synaptic input at their somata and along their dendrites, as demonstrated by numerous electron microscopy studies (Hisano et al., 1981; Silverman, 1984; Leranth et al., 1985a, 1985b; Silverman and Witkin, 1985; Lehman et al., 1988; Lehman and Silverman, 1988). In most species studied, synaptic inputs are scarce both in absolute number and by comparison to surrounding non-GnRH neurons (Kozlowski et al., 1980; Witkin and Silverman, 1985; Witkin, 1987; Lehman and Silverman, 1988; Thind and Goldsmith, 1988; Witkin, 1989; Romero et al., 1994). Glia may play a contributing role here, as studies in monkeys, sheep, and rats have reported glial lamellae encasing portions of the GnRH neuron and/or nearby terminals, likely acting as physical barriers to transmission (Jennes et al., 1985; Lehman et al., 1988; Thind and Goldsmith, 1988; Witkin et al., 1991; Romero et al., 1994). Because the size of these lamellae is below the resolution of light microscopy, studies that use light-based techniques to draw conclusions about connectivity should be interpreted cautiously; a sequential confocal-electron microscopy approach examining GnRH neurons in sheep also reported numerous false-positives (Xiong et al., 1997). Electron microscopy therefore represents the most reliable, though laborious, method for anatomically mapping synaptic inputs to GnRH neurons. The technique has been used to show that GnRH neurons synapse with glutamate and GAD-positive terminals, as well as terminals containing neuropeptides and hormones (Leranth et al., 1985a; Thind and Goldsmith, 1988; Witkin, 1992a).

Synaptic contacts onto GnRH neurons are particularly interesting due to the potential for structural plasticity in relation to reproductive function and steroids. A classic example of reproduction-related, structural plasticity occurs in the brains of songbirds such as canaries. In these species, areas of the brain associated with song grow in volume at the start of the breeding season, when song is produced, and then regress when the breeding season ends (Nottebohm, 1981). This seminal discovery was made as researchers were publishing initial findings related to GnRH neuron ultrastructure in mammalian species, and may have motivated study of structural plasticity at the GnRH neuron across reproductive conditions. Seasonal and steroid-related plasticity was studied in sheep, and it was discovered that GnRH neurons in ewes received twice as much innervation during the breeding season compared to anestrous animals (Lehman et al., 1997; Xiong et al., 1997; Adams et al., 2006; Sergeeva and Jansen, 2009). However, this was not attributed to changes in gonadal steroids because a similar result was seen in intact vs. ovariectomized, estradiol-treated ewes. In rhesus monkeys, ovariectomy was found to decrease synaptic innervation of GnRH neurons while ovariectomy plus estradiol implantation did not induce a decrease, indicating steroids regulate structure of synaptic inputs in this species (Witkin et al., 1991). In monkeys ovariectomy caused an increase in glial ensheathment of GnRH neurons, which was similarly suggested in the study of ewes but not quantified, suggesting glia may take an active role in reshaping inputs to GnRH neurons in response to changes in the steroid

mileu (Witkin et al., 1991; Xiong et al., 1997). Reshaping of GnRH neuron glial ensheathment also appears to occur across development, since it is more extensive in pubertal monkeys and prepubertal rats, compared to adult conspecifics (Witkin and Romero, 1995; Witkin et al., 1995). Steroids may exert organizational effects, as suggested by a study in sheep which found GnRH neurons in female yearlings were more densely innervated than both males and females that were prenatally exposed to testosterone (Kim et al., 1999).

An intriguing possibility is that structural plasticity may play a role in the cyclic changes between negative/positive feedback in females. Evidence in support of this comes from studies of dendritic spines, membrane specializations that typically receive synaptic input. Although not a definitive indicator of a change in synaptic input (spines do not always coincide with functional transmission), a change in dendritic spine density is a sign of structural plasticity that can be detected with light microscopy. In a seminal study, this approach was used in the rat hippocampus and combined with electrophysiologic methods to show that estradiol induces structural and functional synaptic plasticity at CA1 pyramidal cells (Woolley et al., 1997). As mentioned, synaptic inputs to GnRH neurons have been reported as rare when examined at the ultrastructural level (Silverman et al., 1994). Confocal microscopy studies in mice, however, report abundant spines along the dendrites and somata of adult GnRH neurons (Campbell et al., 2009; Chan et al., 2011; Herde et al., 2013). This

disagreement may be attributable to the use of cell-filling techniques in the confocal microscopy studies that were not used in earlier electron microscopy studies; it is possible inputs onto spines were missed in ultrastructural studies because spines were not filled with immunolabeled GnRH, which does not distribute evenly throughout the cytoplasm, unlike biocytin dialysed with a patch pipette or transgenically-expressed GFP. Supporting this, examination of cell-filled neurons under the electron microscope identified inputs onto spines (Campbell et al., 2009), however, it is not clear if these are a common since their occurrence was not quantified. Furthermore, since there are no published ultrastructural studies of non-filled GnRH neurons in mice for comparison, it is not clear if these findings are species-dependent or attributable to technical differences. With these uncertainties in mind, spines appear to be plastic features of GnRH neurons that are shaped by gonadal steroid milieu, development, and estradiol feedback state in mice. Ovariectomy reduces spine density at GnRH somata, in comparison to diestrous mice, and adult GnRH neurons have greater spine density than GnRH neurons from immature mice (Chan et al., 2011; Campbell et al., 2022). A very intriguing finding in regard to estradiol feedback is that spine density increases during the GnRH/LH surge. Specifically, this finding is limited to GnRH neurons that are activated at the time of the surge, vs those that are not, as indicated by expression of the activity marker *Fos*. This creates the interesting possibility that structural plasticity of inputs to GnRH neurons occurs as a across feedback states and may include an activity-dependent component.

GnRH neurons: basic electrical properties

How do synaptic and other inputs functionally regulate GnRH neurons? This question, and many others related to the electrophysiology of these cells, remained difficult to address for decades. Major obstacles were the scattered distribution of GnRH neurons and their low number, which made it difficult to measure their activity using methods that indiscriminately measure population-activity (e.g., multiunit recordings). Moreover, the somatic morphologies of GnRH neurons are not distinctive, making it challenging to use morphology to guide single-cell recording techniques. Around the year 2000, researchers were able to overcome some of these obstacles by generating transgenic mice expressing green fluorescent protein (GFP) under the GnRH promoter, allowing GnRH neurons to be identified in acute brain slices (Spergel et al., 1999; Suter et al., 2000; Han et al., 2004). Since then, much information about GnRH neuron electrical properties in mice has been generated.

GnRH neurons are electrically excitable. They fire fast, robust action potentials with characteristically large afterhyperpolarizations (Constantin et al., 2022). These may be generated at the soma or in dendrites. The classification of a GnRH neurite as dendrite or axon is somewhat tenuous because projections to the median eminence in mice have been shown to have qualities of both axons and dendrites, in that they receive synaptic input and possess spines, but also initiate and propagate action potentials (Herde et al., 2013; Moore et al., 2018). Spontaneous firing patterns of individual

neurons show peaks in activity interspersed by periods of lower activity or quiescence (Nunemaker et al., 2003b). In the short term, transient increases in firing frequency are known as bursts (Chu et al., 2012). Bursts are associated with neuroendocrine secretion by magnocellular neurons, but it is not clear if the same is true for GnRH neurons (Dutton and Dyball, 1979a). Long-term oscillations in firing activity are also displayed, with a frequency reminiscent of peaks in multiunit activity recorded in the mediobasal hypothalamus of monkeys. Interestingly, some GnRH neurons in brain slices display rhythmic activity even when ionotropic GABA and glutamate receptors are blocked, suggesting these signaling systems may not be totally necessary for rhythmicity, at least that of individual neurons (Nunemaker et al., 2002). Studies in which activity of two GnRH neurons have been simultaneously measured are limited and have produced little evidence of coordination or even communication among neurons (Campbell et al., 2011; Chu et al., 2012). However, these studies were performed in brain slices in which much afferent and efferent projections are likely severed, making their interpretation of network effects (or lack thereof) limited. The challenge of targeting scattered neurons deep in the brain is still a major obstacle to performing *in vivo* monitoring of GnRH neuron activity. Recent advances in optical techniques for estimating activity in vivo hold some promise (Moore et al., 2022), but have been hindered by difficulty in getting the necessary components expressed in GnRH neurons (unpublished observations). These methods can survey only a limited

area, thus further advances in technology will be necessary to understand how, or if, GnRH neurons operate as a coordinated network.

Relationship between electrical activity and GnRH release

Neural and humoral factors likely modulate GnRH release via modulation of GnRH neuron activity. This hypothesis is rooted in the principle that action potential firing induces transmitter release by neurons. This principle holds for neurosecretory release by magnocellular neurons (Dutton and Dyball, 1979a; Bicknell et al., 1982), but whether or not it applies to GnRH release is not definitively demonstrated. The challenge here, again, has been the neuroanatomy of the GnRH system. As mentioned previously there are major obstacles to measuring GnRH neuron activity in vivo, and sampling GnRH in portal blood is technically challenging, thus there have been no studies that directly measured a correlation between activity and release. Rather than direct measurement, GnRH release is more typically estimated indirectly by measuring circulating LH with serial samples. This is not definitive because it introduces the variable of pituitary responsiveness to GnRH. With this in mind, serial LH measurements combined with multiunit recordings of the mediobasal hypothalamus or preoptic area of monkeys, rats, goats, and ewes found that peaks in activity coincided with LH pulses, suggesting coordinated firing correlates with GnRH release (Wilson et al., 1984). However, this recording method does not delineate GnRH neuron-specific activity. A cell-specific estimation of integrated neural activity can be provided by Fos/GnRH co-

immunolabeling, and in numerous species GnRH neurons express Fos during times when GnRH release is known to be high, such as during the GnRH surge (Wintermantel et al., 2006; Chan et al., 2011; Hoffman et al., 2011; Gusmao et al., 2022). In mice, cell-specific optogenetic activation of GnRH neurons generates increases in LH (Campos and Herbison, 2014), supporting a positive correlation between action potential firing and release.

Simultaneous measurement of spiking activity and neurosecretory GnRH release from a single neuron, if accomplished, would represent an elegant demonstration of firing-release relationship. However, the high density of GnRH terminals at the median eminence precludes measuring GnRH release from a single neuron. In the preoptic area, GnRH fibers are more dispersed and here local GnRH release has been recorded in real-time at fiber-fiber appositions using fast-scan cyclic voltammetry in mouse brain slices (Glanowska et al., 2012; Glanowska and Moenter, 2015). Recently, this was combined with electrical recordings of one or both apposing neurons (Chen and Moenter, 2021). The correlation between firing activity and GnRH release was positive. Interestingly, results further indicated changes in local GnRH concentration at these fiber-fiber appositions can occur independent of short-term changes in firing rate of either cell. This agrees with a previous study which found the activity blocker tetrodotoxin (TTX) did not block GnRH release in the preoptic area but did in the median eminence (Glanowska and Moenter, 2015). The firing-release relationship may

therefore be region-dependent. This may reflect different controlling mechanisms and physiological functions of locally-released, potentially neuromodulatory GnRH released in the preoptic area vs neurosecretory GnRH released at the median eminence.

Mouse models used to study estradiol feedback

Development of GnRH-GFP lines quickly made mice the animal-of-choice for studying the electrophysiology of GnRH neurons and their afferents. Mice are the most-used mammalian species for neurophysiology studies for a few reasons. Mice are amenable to transgenic techniques and many transgenic mouse lines are now available. These include lines that target expression of reporter genes or Cre-recombinase specifically to specific types of neurons, making neuroanatomical, electrophysiologic, and conditional gene knockout studies possible. Cell-specific Cre-recombinase expression also enables use of genetically-encoded molecular tools such as calcium-indicators (Lin and Schnitzer, 2016), channelrhodopsins (Deisseroth, 2015), chemogenetic receptors (Roth, 2016), and ribosomal tags. These tools are useful for studying the brain and will be described briefly in a later section.

As with all animal models, caution should be used in extrapolating findings in mice to other species due to differences in underlying physiology. Mice are useful for studying the physiology of reproduction because the sequence of hormonal events leading up to ovulation in mice is similar to humans and other spontaneously-ovulating mammals.

Specifically, it is preceded by a persistent rise in estradiol that causes a switch from estradiol negative to positive feedback during the afternoon of the proestrous phase of the estrous cycle. A similar rise in estradiol occurs during the early-mid follicular phase in humans, leading to a positive feedback induced LH surge in the late-follicular phase. In rodents, the LH surge is tightly diurnally regulated and occurs just before the start of the active (dark) period during proestrus. However, in higher primates such as humans the diurnal timing of the LH surge is not absolute, though diurnal influence may not be totally absent (Kerdelhué et al., 2002). This represents a clear species difference that must be considered, but also adds to the utility of mice as an experimental model. The relatively predictable timing of the surge in mice allows experimenters to perform measurements during times when estradiol negative or positive feedback are likely to be occurring.

Studies of estradiol negative and positive feedback in mice typically utilize two classes of approach. In the first class, parameters are examined on estrous cycle days and times characterized a form of feedback. To study negative feedback measurements are typically made on diestrus and/or the morning of proestrus, when LH is suppressed. To study positive feedback, measurements are made around the time of the LH surge on proestrus – typically within a few hours prior to lights off. Progression through the estrous cycle is monitored via vaginal lavage and cytology, making this approach relatively non-invasive. However, observations cannot be attributed solely to changes in

estradiol feedback because other ovarian hormones, including progesterone, concurrently change during the estrous cycle. A second class of approach attempts to address this caveat by performing ovariectomy (OVX) to remove gonadal steroid synthesis, followed by replacement with estradiol or derivatized estrogens, such as estradiol benzoate, to cause prolonged elevation of estradiol in the blood. Within this class, one model commonly used in rodents involves treating with a low dose of estrogen for several days to suppress LH (negative feedback). A bolus injection of estrogen is then given in the morning to simulate the proestrus rise in estradiol, causing an LH surge in the afternoon (positive feedback); this will be referred to as the E rise model below. Another model uses ovariectomy followed by a constant release implant to generate high physiologic levels of estradiol (OVX+E). These mice exhibit daily diurnal shifts between negative feedback in the morning and positive feedback in the afternoon; this will be referred to as the daily surge model. While these replacement models can isolate the effects of estrogens, it is important to point out that they may miss effects attributable to other ovarian factors which may be important for the function of the intact system. With this in mind, comparing observations among these systems can be informative, and studies often incorporate multiple estradiol feedback models.

Common techniques used to measure and manipulate neural activity

A variety of techniques have been employed to study neural activity in mouse models of estradiol feedback. For simplicity, common techniques and caveats are summarized

below. This section may serve as reference; studies that utilized these techniques are cited throughout the dissertation.

c-Fos is an immediate early gene product used as a surrogate marker of neuronal activity. c-Fos expression increases when neurons are activated, and the protein can be detected with immunostaining to estimate levels of neuronal activity at the time the animal was sacrificed (Herdegen and Leah, 1998). c-Fos provides only an approximation of firing activity because expression can be regulated by activity-independent pathways (Kovács, 2008), and temporal resolution is poor because protein expression integrates activity over an many minutes or hours. Furthermore, c-Fos immunostaining can provide only a single snapshot of estimated activity since experiments are necessarily terminal.

Targeted extracellular recordings of fluorescently-identified cells in brain slices are used to measure action potential firing activity (Roberts and Almers, 1992; Nunemaker et al., 2003a). Slices are acutely prepared from mice that express a fluorophore in a cell-type of interest, and fluorescent microscopy is used to guide placement of a patch-clamp electrode near the cell membrane of a fluorescent neuron. A correctly placed electrode can detect action currents, which flow when a neuron fires action potentials, without perturbing the cytosol. This type of recording is particularly useful for stable, long-term (15 min+) measurements of action potential frequency.

Whole-cell recordings of fluorophore-identified cells in brain slices can measure ionotropic synaptic inputs, action-potential firing, voltage-gated currents, and intrinsic membrane properties (Sakmann and Neher, 1995). Unlike the extracellular technique, the whole-cell technique allows the experimenter to manipulate the membrane voltage or pass current into (stimulate) the neuron with the same electrode used to record activity. The perturbation of the cytosol required for this approach may modify spontaneous firing activity of the neuron or diminish the response to signals requiring cytosolic factors that are sensitive to intracellular dialysis.

Optogenetics and chemogenetics are methods for manipulating neuronal activity in brain slices or *in-vivo*. Cell-specific expression of light-activated channels (optogenetics) or designer receptors exclusively activated by designer drugs (chemo-genetics) allow experimenters to activate or inhibit firing of specific neuronal populations with pulses of light or with synthetic ligands such as clozapine n-oxide (Deisseroth, 2015; Roth, 2016). These techniques are useful for studying synaptic or circuit physiology (typically in slices) and for drawing associations between activation of specific neuronal populations and a downstream effect, such as a change in hormone concentration *(in vivo*). However, data should be interpreted cautiously as it is unlikely these tools generate activity that exactly phenocopies the underlying physiology.

Calcium-imaging is an optical method used to estimate neuronal activity indirectly by estimating changes in intracellular calcium levels. Genetically-encoded fluorescent calcium indicators, such as GCaMP (Lin and Schnitzer, 2016), are used to monitor calcium events in many neurons simultaneously at either the population (bulk) or single-cell resolution. This can be done in brain slices or *in-vivo* when combined with fiber photometry (bulk) or 2-photon microscopy for single-cell resolution. Although it is tempting to equate calcium events to action potential firing, this is not always the case as spikes can occur in the absence of a detected fluorescent signal, and calcium events can occur in the absence of spiking (Sanz et al., 2009; Huang et al., 2021). Ideally, the relationship between spiking and calcium events should be determined via control experiments involving simultaneous imaging and direct electrical measurements of spiking in the cell type of interest.

Synaptic input to GnRH neurons: functional measures and regulation by estradiol feedback

Perhaps the most conspicuous feature of GnRH neurons discovered over the past 30 years is their apparent lack of estrogen receptor alpha (ERα) – a receptor necessary for estradiol feedback effects but not detectable in GnRH neurons (Hrabovszky et al., 2000; Couse et al., 2003). This places particular emphasis on the afferent network, i.e., the system of ERα-positive cells that relays feedback to GnRH neurons via neurotransmitters, neuromodulators, gliotransmitters, etc. Synaptic transmission

represents a likely avenue for conveying feedback. Numerous studies have demonstrated effects of GABA and glutamate on the secretion of LH (Adler and Crowley, 1986; Urbanski and Ojeda, 1987; Jarry et al., 1991; Kimura and Jinnai, 1994; Ping et al., 1997). However, it is difficult to determine which, if any, effects are direct at GnRH neurons because many hypothalamic neurons are sensitive to glutamate/GABA and the methods utilized did not target GnRH neurons specifically. This section focuses on GnRH neuron-specific glutamate and GABA transmission.

GnRH neurons express receptors for GABA and glutamate and axon terminals containing markers of these transmitters form synapses with GnRH neurons (Leranth et al., 1985a; Witkin, 1992b; Goldsmith et al., 1994). In congruence with this anatomy, GnRH neurons display electrical signatures of glutamate- and GABA-mediated synaptic transmission. Post-synaptic currents (PSCs) flow when neurotransmitter binds to ionotropic receptors on the neuronal membrane, and in GnRH neurons GABAergic and glutamatergic PSCs are detected via whole-cell patch-clamp recordings made from the soma. Although PSCs can be mediated by classes of cholinergic, glycinergic, and serotonergic receptors, PSCs of these classes are not detected at GnRH neurons recorded in mouse brain slices (Constantin et al., 2022). It remains possible these systems operate in the intact animal, and/or in other species, however.

Glutamatergic transmission

Spines, putative sites of glutamatergic input, are present on GnRH neurons in mice (Campbell et al., 2005, 2009; Chan et al., 2011; Herde et al., 2013). Ultrastructural studies suggest glutamatergic inputs constitute a majority of synaptic inputs onto GnRH neurons (Goldsmith et al., 1994). In mice, estradiol feedback modulates spine density, which increases during positive feedback and decreases as a result of ovariectomy (Chan et al., 2011). These findings would seem to suggest glutamatergic transmission is a major regulator of GnRH neuron electrical activity, yet measures of PSCs in brain slices tell a different story in that glutamatergic PSCs are infrequent (Constantin et al., 2022). This curious disagreement between anatomy and function is hard to reconcile. One potential explanation is the experimental preparation may preclude observation of glutamatergic inputs. If glutamatergic input occurs predominantly along the distal dendrites, this input would be lost in brain slices. Glutamatergic inputs could alternatively be present but simply not spontaneously active in the slice or of low release-probability. There is evidence that glutamate PSC frequency decreases during estradiol negative feedback (Christian et al., 2009), but this is of questionable biological relevance due to their baseline infrequency.

GABAergic transmission

GnRH neurons are depolarized by GABA because they accumulate higher-than-typical levels of intracellular chloride, creating a chloride gradient that favors chloride efflux and membrane depolarization from the typical baseline membrane potential of -60 to -70 mV (DeFazio et al., 2002a). GABA-mediated depolarization can induce action potential firing. GABA therefore acts at GnRH neurons in a manner that is opposite to its more typical inhibitory role(Herbison and Moenter, 2011; Watanabe et al., 2014a).

GABAergic input to GnRH neurons is regulated by estradiol feedback in the daily surge model and in naturally cycling mice. In the daily surge model, GnRH neurons in slices from OVX+E mice have higher GABA PSC frequency and amplitude during the afternoon (positive feedback) compared to the morning and to OVX mice during either time of day (Christian and Moenter, 2007). In naturally cycling mice, PSC frequency is higher during afternoon of proestrus (positive feedback) compared to the morning of proestrus (negative feedback) (Adams et al., 2018a). GABA transmission to GnRH neurons did not show regulation by estradiol feedback in the estradiol rise model (Liu et al., 2017). This likely reflects underlying neurobiological differences between feedback models, time of day of the recordings that have been made and the manner in which they induce GnRH/surges.

GABA input to GnRH neurons may not be strictly necessary for GnRH surge generation. As stated, ERα is required for estradiol feedback including the positive-

feedback induced surge (Couse et al., 2003). Disruption of ERα in GABAergic neurons in mice disrupts the LH surge but this may be due to the fact that GABA is co-expressed in many hypothalamic neurons including those that express neuropeptides essential for reproduction (Cheong et al., 2015). Accordingly, GnRH neuron-specific knockdown of $GABA_A$ receptor does not impact surge generation despite a 70% reduction in GABA PSC frequency and amplitude (Lee et al., 2010). However, it is possible only a portion of GABA signaling is necessary to maintain surge capability.

The hypothalamic kisspeptin system

In 2003, patient-based research led to the discovery that inactivating mutations in the "orphan" G-protein coupled receptor gene *GPR54* could cause hypogonadotropic hypogonadism (de Roux et al., 2003; Seminara et al., 2003). This kicked off extensive research into the receptor, now referred to as KISS1R, its neuropeptide ligand kisspeptin, and the neurons involved in the kisspeptin signaling system (Gottsch et al., 2009). We now know that central kisspeptin signaling is an essential component of reproduction in mammalian and non-avian vertebrates. In this reproductive context, a critical site of kisspeptin action is at KISS1R expressed by GnRH neurons. This is supported by mouse models in which Kiss1R signaling is disrupted specifically at GnRH neurons, which display a hypogonadotropic phenotype similar to phenotypes of inactivating *KISS1R* mutations in humans (Novaira et al., 2014). At GnRH neurons, Kiss1R activation initiates a $G\alpha_{q/11}$- coupled mechanism that inhibits A-type and inward-

rectifying potassium currents and activates transient receptor potential type C (TRPC) currents, producing a minutes-long depolarization and increased action potential firing frequency (Rønnekleiv and Kelly, 2013). Kisspeptin delivered intravenously or via intracerebroventricular injection induces a robust increase in serum LH within 30 minutes of treatment (Gottsch et al., 2004; Tovar et al., 2006; Dhillo et al., 2007; Narayanaswamy et al., 2016). This effect is blocked by pre-treatment with GnRH receptor antagonists demonstrating the potent effect of kisspeptin on LH depends on GnRH action (Gottsch et al., 2004).

Neurons that synthesize kisspeptin are found throughout the brain including the hypothalamus, amygdala, lateral septum and bed nucleus of the stria terminalis (Oakley et al., 2009a). Of primary interest for the neuroendocrine control of reproduction are two populations in the hypothalamus: a caudal population in the arcuate nucleus, and a rostral population that displays species-dependent localization. A majority of research on the kisspeptin system has been performed in rodents, and in both mice and rats the rostral population is located in the anteroventral periventricular (AVPV) area and extends caudally into the periventricular nucleus. For simplicity, AVPV shall refer to the entire rostral population. Identification of kisspeptin expression in the arcuate and AVPV sparked great interest because it was known from prior studies that lesions of these areas affect reproductive outcomes and the release of LH (Plant et al., 1978; Soper and Weick, 1980). A majority of kisspeptin neurons in both regions were found to express

Erα revealing the intriguing possibility the hypothalamic kisspeptin neurons act as conduits for estradiol feedback and its regulation of GnRH and LH release (Smith et al., 2005a, 2006; Cravo et al., 2011). In line with this, knockout of ERα in kisspeptin- or calmodulin-kinase II-expressing neurons causes infertility and dysregulated LH (Mayer et al., 2010; Cheong et al., 2014).

In a seminal study, Robert Steiner's group discovered that estradiol differentially regulates kisspeptin expression in the arcuate and AVPV (Smith et al., 2005a). Compared to intact mice, ovariectomized mice display increased kisspeptin expression in the arcuate and decreased kisspeptin expression in the AVPV. Ovariectomized mice treated with a physiologic dose of estradiol display reduced expression in the arcuate but increased expression in the AVPV. From this, it was hypothesized the arcuate kisspeptin neurons relay estradiol negative feedback to GnRH neurons while the AVPV kisspeptin neurons relay estradiol positive feedback (Dungan et al., 2006; Oakley et al., 2009a). Relaying likely occurs via peptidergic and non-peptidergic neurotransmission via direct neuroanatomical projections from each population. Studies in rodents indicate the two hypothalamic kisspeptin populations project mostly to different subcellular locations of the GnRH neuron: the AVPV kisspeptin neurons project to both the somatic and terminal region of GnRH neurons, whereas the arcuate kisspeptin neurons project primarily to the terminal regions of GnRH neurons in the median eminence (Yip et al., 2015, 2021). There may be species differences in this trend (Lehman et al., 2013). In

mice, despite the relative abundance of kisspeptin-positive fibers apposing GnRH neurons at their somata in the POA and their distal projections in the arcuate/median eminence, a study that used viral transsynaptic tracing found only a small percentage of these fibers make direct synaptic contact with GnRH neurons (Kumar et al., 2015). This suggests an interesting possibility of non-synaptic mechanisms playing a role in transmission between these cell types, however, more work is needed to determine if this observation varies among species.

Arcuate kisspeptin neurons: evidence for their role in estradiol negative feedback

Estradiol negative feedback reduces overall GnRH and LH output primarily by reducing pulse amplitude (Evans et al., 1995). Negative feedback can also regulate pulse frequency, although effects on frequency seem to depend on factors such as concentration, dosing regimen and physiologic context(Goodman and Karsch, 1980; Evans et al., 1994). Low concentrations of estrogens reduce pulse frequency, compared to ovariectomized animals, whereas high concentrations first reduce frequency, then increase it leading up to an LH surge. These findings suggest negative feedback modulates the activity of a neural pulse-generating system. As previously discussed, pulsatile secretion is necessary for maintenance of pituitary sensitivity to GnRH (Belchetz et al., 1978). The neural basis of GnRH pulse generation has thus been a central focus of HPG axis research.

The arcuate nucleus was first hypothesized as a locus of pulse generation when it was found that lesions of the area abolish LH pulses in numerous species, and multiunit electrical recordings of the arcuate showed peaks in activity that correlated with LH pulses (Plant et al., 1978; Soper and Weick, 1980; Kawakami et al., 1982; Wilson et al., 1984; Martin and Thiéry, 1987; Mori et al., 1991). Discovery of kisspeptin neurons in the arcuate and their sensitivity to estradiol then pointed towards a specific cell type by which negative feedback may influence pulse generation. There is now accumulating evidence for a role of arcuate kisspeptin neurons in this process. When arcuate kisspeptin neurons are conditionally ablated (>97% reduction in cell number) and when transmitter release by these cells is blocked via conditional expression of tetanus toxin light chain, LH pulses become irregular and estrous cyclicity is abolished, marked by persistent diestrus (Mayer and Boehm, 2011; Padilla et al., 2019). Consistent with a role in pulse generation, arcuate kisspeptin neurons display rhythmic electrical activity when monitored in brain slices and, more recently, *in vivo*. These findings extend prior multiunit activity studies by attributing rhythmicity of the arcuate to an identified cell type.

Kisspeptin neurons in the arcuate co-express neurokinin B (NKB) and dynorphin, which are implicated in pulse generation and not found in other kisspeptin neuron populations. This molecular phenotype causes them to sometimes be referred to as KNDy neurons for the three neuropeptides they express: kisspeptin, neurokinin B and dynorphin. NKB has a stimulatory and dynorphin an inhibitory effect on LH pulse frequency

(Wakabayashi et al., 2010; Goodman et al., 2013). Local release of these signals in the arcuate, where they directly stimulate (NKB) or inhibit (dynorphin) firing activity, is thought to be the basis of pulse generation. However, the mechanisms that generate pulse activity are still being delineated.

To target specifically kisspeptin neurons in the arcuate region, a common approach involves stereotaxic injection of Cre-specific adeno-associated viral (AAV) vectors into the arcuate off Kiss1-Cre mice. Recombination in this case should only occur in Cre-expressing kisspeptin neurons, and the arcuate is targeted in exclusion of other kisspeptin cell populations due to limited diffusion of the virus. An alternative approach takes advantage of co-expression of neurokinin-B (tachykinin 2). Mice that express Cre under control of the tachykinin 2 promoter (Tac2-Cre) are crossed with mice carrying a transgene flanked by loxp sites to produce offspring that express the transgene specifically in tachykinin-producing cells. It should be noted that NKB is expressed in other non-kisspeptin-expressing cells, making this approach non-specific. Furthermore, the transgene is expressed persistently from the onset of Cre-expression, which may produce developmental effects.

Neurokinin B and dynorphin are not just avenues that allow genetic manipulation of arcuate kisspeptin neurons regulate LH pulses and may be critical to pulse generation (Wakabayashi et al., 2010; Goodman et al., 2013). With regard to estradiol feedback

effects, in addition to down-regulating kisspeptin mRNA expression, estradiol inhibits expression of neurokinin B mRNA and that of its receptor, NK3R, in arcuate kisspeptin neurons (Smith et al., 2005a, 2005b; Navarro et al., 2009). It also dampens the firing response of arcuate neurons to neurokinin B, and increases the inhibitory effect of dynorphin on firing in males (Ruka et al., 2013, 2013). Thus, estradiol modulates expression of the three namesake peptides of KNDy neurons in ways that are consistent with its homeostatic suppression of LH pulses. Whether or not homeostatic effects of estradiol are directly at kisspeptin cells was tested using KERKO (kisspeptin estrogen receptor knockout) mice, in which ERα is deleted from in kisspeptin cells from the onset of kisspeptin expression in that cell type (Mayer et al., 2010). KERKO mice exhibit advanced vaginal opening and constant estrus in adulthood, indicating direct effects of estradiol in kisspeptin-expressing cells somewhere in the body are critical for typical reproductive function. LH pulses in adult KERKO mice are irregular and more frequent than in controls suggesting a failure of estradiol negative feedback to regulate pulse generation (Wang et al., 2018).

Notably, the KERKO approach does not distinguish between arcuate, AVPV, or extra-hypothalamic kisspeptin-expressing cells and thus cannot delineate which populations contribute to the phenotypes observed. TERKO mice, which lack ERα in tachykinin2 (neurokinin B) cells, exhibit a similar phenotype to KERKO mice suggesting estradiol sensitivity in the arcuate population is critical for normal cyclicity (Greenwald-Yarnell et

al., 2016). However, since sensitivity is lost in all tachykinin cells, a role for non-KNDy neurons cannot be ruled out. Furthermore, both KERKO and TERKO are constitutive knockouts, with gene deletion initiated as soon as the respective promoters become active, making it difficult to determine if their phenotypes are due to absence of the receptor in their respective cell types influencing the development of the central reproductive network and/or due to loss of estradiol feedback post-puberty. To circumvent this, a recent study used an AAV-mediated CRISPR-Cas9-based approach to target guide RNAs to deplete ERα in arcuate kisspeptin neurons of adult female mice (Wang et al., 2019a). Importantly, and as with all AAV-based techniques, only a subset (~35%) of cells under-went recombination, resulting in knockdown rather than knockout. Nevertheless, knockdown mice exhibited disrupted cyclicity similar to KERKO and TERKO mice, suggesting neuroendocrine disruption. Notably, LH pulse frequency was not different from controls, which was speculated to be due to stress induced by single-housing of animals, and could also be related to the incomplete ablation of ERα or underpowering of the study. In line with estrogen sensitivity in only a fraction of KNDy neurons being necessary for pulse generation in rats. Specifically, pulsatile LH secretion was restored in global kisspeptin knockout rats by reintroducing kisspeptin expression into a subpopulation of arcuate Tac3 neurons of adults via AAV (Nagae et al., 2021).

The biophysical properties of arcuate kisspeptin neurons have also been studied in mouse brain slices. Because estradiol negative feedback and LH pulsatility are common

to both sexes, both males and females have been studied (Jamieson and Piet, 2022). Notably, comparison of results across studies is a complicated endeavor because of the diversity of animal models, sex, experimental timing and estradiol replacement approaches. Further, few studies utilized the same recording methodology. Despite this, some common trends emerge. For example, the spontaneous firing rates of arcuate kisspeptin neurons in slices from both KERKO and ERα knockdown (arcuate-targeted) female mice are higher than their respective controls, and firing rates of these cells in OVX+E and OVX KERKO mice are similarly elevated (Wang et al., 2018, 2019a). This suggests loss of estradiol sensitivity in arcuate neurons, or other kisspeptin-expressing cells, lifts homeostatic suppression of firing rate. Some of this suppression may be attributable to effects on synaptic transmission. Both GABA- and glutamate-driven fast transmission to arcuate kisspeptin neurons are modulated by estradiol feedback. Specifically, GABA PSC frequency to arcuate kisspeptin neurons is elevated in OVX+E mice compared to OVX, and glutamate transmission to arcuate neurons in KERKO mice is elevated relative to controls (DeFazio et al., 2014a; Wang et al., 2018). The effects on glutamate transmission could be indirect from non-kisspeptin cells and/or direct via connections between KNDy neurons, as KNDy neurons are predominantly glutamatergic and form local circuits (Cravo et al., 2011; Qiu et al., 2016).

Given findings in KERKO and knockdown mice, in mice with typical ERα expression, one may predict firing rates to be elevated in OVX mice compared to OVX+E due to

loss of peripheral estradiol. Data here, however, are less consistent, with some studies finding higher rates in OVX and others reporting no effect of gonadectomy or cycle stage (de Croft et al., 2012a; Wang et al., 2018; Phumsatitpong et al., 2020; Jamieson and Piet, 2022). Examination of methodologies suggests this could be attributed to numerous factors. Beyond evident differences in mouse line, time-of-day of experiments and estradiol dose, one less appreciated aspect may be the duration over which activity was sampled. Evidence from long-term (1–3.5 h) recordings of arcuate neurons in males indicates these cells exhibit peaks and nadirs in activity that may be truncated or absent in 5–15 min recordings that were typically used in prior studies (Vanacker et al., 2017). Indeed, many studies with shorter recordings report high percentages of quiescent cells that may have been transiently quiescent between active periods (de Croft et al., 2012a; Cholanian et al., 2014). In longer-term recordings, castration, which removes negative feedback from both testosterone and its metabolite estradiol, was found to reduce the duration of nadirs, consistent with an increase in LH pulse frequency and suggesting cyclically active cells are steroid sensitive (Vanacker et al., 2017). Interestingly, *in vivo* calcium-imaging of arcuate kisspeptin neurons in castrate males found population-level events occur every 2–58 min in a study that used bulk fiber photometry, and synchronized events among individual cells occurred every ~4 min in a study that used gradient-index (GRIN) lens, indicating loss of network interactions in slices may cause deviation from the endogenous rhythm of activity (Han et al., 2019; Moore et al., 2022). In the former study, intact males exhibited longer

intervals between bulk calcium signals (43–347 min) compared to castrates, consistent with the effect of gonadectomy on firing rates in slices and further indicating steroid feedback suppresses arcuate neuron activity and changes activity pattern.

In the daily surge model, GnRH neuron firing rates measured in the AM are elevated in OVX compared to OVX+E animals (Christian et al., 2005a), but the degree to which arcuate kisspeptin neurons contribute to this is unclear since the arcuate is excluded from the coronal slices that are predominantly used for recordings of GnRH neurons. Simultaneous monitoring of action potential firing by both cell types has not been performed to determine if they are correlated, and if any correlation is modulated by estradiol feedback. Optogenetic stimulation combined with serial LH measurements has provided the closest approximations of this relationship in intact male and female mice, but these measure response rather than spontaneous interactions. Photoactivation of arcuate kisspeptin neurons at 10 Hz for 1 min induced pulse-like secretion of LH (Han et al., 2015). The duration of this stimulus seems to be consistent with the endogenous duration of synchronized calcium events measured *in vivo* (Moore et al., 2022), but firing rates ≥ 10 Hz maintained for ≥ 1 min are rarely observed in recordings of these cells in brain slices. Caveats of both approaches need to be considered; LH release is only an approximation of GnRH release and likely even less accurate for estimating GnRH neuron firing (Moenter, 2015). The firing/neurosecretory release relationship in GnRH neurons is not yet well-defined. Optogenetic stimulations are also not conducive

to estimating firing-release relationships, since they induce a near-perfectly synchronous activation of the population, which does not appear to phenocopy what is observed endogenously in-vivo (Moore et al., 2022).

AVPV kisspeptin neurons: evidence for their role in estradiol positive feedback

Like the arcuate, the earliest studies indicating a role of the AVPV in regulating LH secretion involved lesion experiments. Rostral hypothalamic lesions that included the AVPV blocked the LH surge but did not block pulses (Wiegand et al., 1978, 1980; Wiegand and Terasawa, 1982), indicating mechanisms controlling surge and pulse functions may be spatially distinct in the brain despite both involving GnRH release. The AVPV was later found to be larger in females vs males in numerous species, to contain ERα-expressing neurons, and to send neuronal projections to GnRH neurons, all consistent with a role in estradiol feedback (Simerly, 1998a). The discovery of kisspeptin focused research on surge mechanisms to a specific cell type within the AVPV, and substantial evidence now suggests these cells are involved in positive feedback surge induction. As stated, estradiol stimulates kisspeptin expression in the AVPV (Smith et al., 2005a); this may function to prime the ability of AVPV neurons to activate GnRH neurons through increased neuropeptide availability. Retrograde tracing from GnRH neurons indicates AVPV kisspeptin neurons synapse with GnRH neurons (Kumar et al., 2015), and optogenetic activation of the AVPV population in brain slices confirmed firing of AVPV neurons excites GnRH neurons via kisspeptin- and GABA-

mediated mechanisms (Piet et al., 2018). The latter is consistent with most AVPV kisspeptin neurons expressing GAD67, the enzyme for GABA synthesis (Cravo et al., 2011). However, evoked PSCs in GnRH neurons have not been reported; therefore, monosynaptic input from the AVPV to GnRH neurons has not yet been firmly established. Notably, it is also unknown if estradiol modulates communication between AVPV kisspeptin and GnRH neurons because experiments have not been performed in full daily surge/E-rise models, at different cycle stages or even to compare gonadectomized to intact mice. Both of these are topics that will be investigated in this dissertation.

Optogenetic activation of AVPV kisspeptin neurons induces GnRH neuron firing and LH release (Piet et al., 2018), but it is not known if such activation occurs endogenously *in vivo*. Calcium imaging of these cells has not yet been reported, thus the best estimates are from the surrogate activity marker cFos. Both the endogenous proestrous and estradiol-induced LH surge coincide with increased expression of cFos in AVPV neurons of mice and rats (Clarkson and Herbison, 2006; Smith et al., 2006; As et al., 2007; Clarkson et al., 2008; Robertson et al., 2009) and preoptic kisspeptin neurons in monkeys and ewes (Smith et al., 2009; Merkley et al., 2012; Watanabe et al., 2014b). Interestingly, unlike in rodents, in monkeys and in goats estradiol can induce LH surges and cFos expression in the POA of both male and female castrates but it is unclear why surge mechanisms are conserved in males of these species and not others (Watanabe

et al., 2014b; Matsuda et al., 2015). Estradiol upregulation of kisspeptin expression and a concomitant increase in electrical activity of AVPV neurons are thus correlated with surges across species and, in some cases, sexes.

Electrical activity and biophysical properties of AVPV kisspeptin neurons and regulation by estradiol feedback

Spontaneous activity and biophysical properties of AVPV kisspeptin neurons have been studied in brain slices (Jamieson and Piet, 2022). Consistent with cFos findings, action potential firing rates of AVPV neurons in brain slices are higher during the afternoon of the LH surge on proestrus compared to the same time of day on diestrus. A similar finding comparing OVX+E during positive feedback vs OVX mice in the daily surge model suggests that estradiol at least in part drives the increased firing observed on proestrus (Wang et al., 2016a). These results and others suggest an activating effect of estradiol on firing activity as well as gene expression (Frazão et al., 2013; Zhang et al., 2015; Wang et al., 2016a, 2019a). Diurnal regulation of the firing rate of AVPV kisspeptin neurons has been comparatively less studied. One study of slices from intact female mice reported firing rate decreased after the time the surge is expected to begin (de Croft et al., 2012a), which may indicate the AVPV becomes less active once the surge is initiated, compared to earlier times during proestrus. This warrants further study, as most work has focused on surge induction rather than termination. Notably, this study remains the only examination of time-of-day effects on spontaneous firing

rates of AVPV kisspeptin neurons, which is surprising given the tight diurnal regulation of the GnRH/LH surge in rodents. It also indicates the necessity of precise timing of measurements of the properties of these cells. Seemingly small differences (1–3 h) in the Zeitgeber time brain slices are made and recordings performed may affect results, possibly explaining variation across studies.

The firing activity of AVPV kisspeptin neurons has been analyzed to extract patterns that may inform function. “Bursts”, clustering of action potentials into periods of rapid firing, are a pattern of particular interest because they are associated with neuropeptide or neuroendocrine release by various types of neurons. Several reports indicate AVPV neurons in brain slices exhibit burst firing (de Croft et al., 2012b; Piet et al., 2013a; Zhang et al., 2013; Wang et al., 2016a). Estradiol increased burst frequency in the afternoon of the daily surge model and addition of a progesterone injection the morning before afternoon recording (OVX+E+P) had no additional effect compared to estradiol alone. This suggests estradiol positive feedback promotes burst firing, which might be a mechanism increasing kisspeptin release during the surge. In gonadally-intact mice, the prevalence of bursts was higher in cells studied on proestrus versus diestrus in one study (Wang et al. 2016) but not affected by cycle stage in another (DeCroft et al., 2012). It is worth noting the definition of a “burst” varies across studies and few quantified burst properties, making comparison across studies complicated.

To determine the mechanisms that may drive increased AVPV kisspeptin neuron firing activity during estradiol positive feedback, researchers have studied the membrane properties of these cells, including voltage-gated currents. Notably, only a fraction of the suite of currents that may be expressed by these neurons have been measured. However, a shared finding across studies is that depolarizing currents that can be activated in the subthreshold membrane potential range increase in amplitude during positive feedback. Specifically, the amplitudes of persistent sodium current, transient low-voltage activated calcium current, and hyperpolarization-activated current increase at the time of the surge, likely promoting increased firing activity (Zhang et al., 2015; Wang et al., 2016a; Piet et al., 2013a; Zhang et al., 2013). These observations are strikingly consistent across different estradiol-induced surge models and during the natural surge. Measurements of passive membrane properties (capacitance, input capacitance) have produced less consistent observations. These measurements may have been impacted by methodological differences such as differences in membrane potential at which measurements were made, as well as differences in pharmacological ion-channel blockers present in the recording solution, however.

Since the amplitude of depolarizing currents increase during positive feedback, when AVPV kisspeptin neurons also fire more bursts, it seems plausible the shifts in voltage-gated currents promote increased burst firing. The validity of this hypothesis was difficult to discern because there was scarce information about other types of voltage-gated

currents expressed by these cells. For example, voltage-gated potassium currents are major regulators of neuronal excitability and firing behavior, yet were not examined. This fact, combined with observations that potassium currents are modulated by estradiol in other cell types, was the motivation for Chapter 2 of this dissertation.

AVPV kisspeptin neurons: necessity for the GnRH LH surge

While there is much evidence support the role of AVPV kisspeptin neurons in positive feedback, there have been no conclusive demonstrations of necessity. KERKO mice are infertile, which demonstrates the necessity of ERα in kisspeptin cells, without indicating which populations are required (Mayer et al., 2010). Wang et al., tested the necessity of ERα in AVPV kisspeptin neurons for surge generation by using an AAV-based, combined CRISPR/Cas9/Cre approach to knock down ERα in AVPV kisspeptin neurons of adult female mice (Wang et al., 2019a). Knockdown mice had normal cyclicity but severely blunted LH surges and reduced number of corpora lutea, consistent with AVPV kisspeptin neuron involvement in positive, but not negative feedback. Another study non-specifically knocked down ERα in the AVPV and saw similarly blunted LH surges but also disrupted cyclicity, which may indicate ERα in non-kisspeptin cells of the AVPV plays a role in cycles (Porteous and Herbison, 2019). In either case, blunted, rather than fully abolished, surges may have been due to the incomplete nature of the knockdowns; ERα expression in a minimal percentage of these cells may be required. Since neither complete knockout of ERα in AVPV kisspeptin

neurons nor specific ablation or silencing of these cells has been performed, their ultimate necessity for positive feedback and surge generation has yet to be determined. There is evidence that the AVPV cannot generate surges on its own, but rather requires input from other brain areas. For example, ablation of the suprachiasmatic nucleus (SCN) blocks LH surges likely due to loss of diurnal input to neurons, possibly including AVPV kisspeptin neurons. These receive vasopressin and GABA input from the SCN (Vida et al., 2010; Piet et al., 2013a). A recent study found AVPV kisspeptin neuron firing rate increases in response to photoactivation of SCN vasopressin neurons in brain slices (Jamieson et al., 2021). Interestingly, increases in firing were greater on proestrus than either diestrus or estrus. This effect was not attributed to changes in sensitivity to vasopressin since exogenous vasopressin evoked similar changes in AVPV neuron activity across all three cycle stages. Changes in SCN output during the cycle may thus play a role in positive feedback, and may itself be estradiol-dependent since SCN neurons express estrogen receptors at a low to moderate level (~5% ERα, ~25% ERβ) in the shell region, which contains vasopressin neurons (Vida et al., 2008).

Interactions between kisspeptin neurons and nitric-oxide (NO) producing neurons may play a role in estradiol feedback and ovulation. In the preoptic region, triple-label immunodetection revealed kisspeptin-positive fibers appose neurons that express both NO synthase (NOs) and kisspeptin receptor (Hanchate et al., 2012). During the afternoon of proestrus and in response to estradiol (E rise model), the proportion of

activated (phosphorylated) vs non-activated NOs in the median preoptic nucleus and organum vasculosum of the lamina terminalis increases suggesting a role of NO in surge generation (Hanchate et al., 2012). The effects of estradiol on preoptic NOs may be downstream of estradiol's effects on kisspeptin, since kisspeptin promotes phosphorylation of NOs but neither estradiol nor kisspeptin increase NOs phosphorylation in kisspeptin receptor-null mice. NOs-null mice are infertile and exhibit both abnormal ovarian cyclicity and few/no corpora lutea (Gyurko et al., 2002; Hanchate et al., 2012), suggesting NO may be important both for positive feedback/ovulation and negative feedback/cyclicity. Reproductive deficits in adult NOs-null mice may be due to altered development in the absence of NOs. This is suggested by a recent study demonstrating NO signaling during a critical period ranging from P10 to P21 is necessary for normal pubertal development and reproductive function in adulthood (Chachlaki et al., 2022).

Dissertation Preview

The main goal of this dissertation was to better understand how the neurophysiology of AVPV kisspeptin neurons changes during the estrous cycle, and how this may relate to the process of initiating the GnRH surge. The prevailing hypothesis of the field at the onset of the work was that during the afternoon proestrus, the time of the GnRH surge, AVPV kisspeptin neurons are electrically activated by estradiol positive feedback, and that this stimulates co-transmission of amino-acid derived and peptidergic transmitters

onto GnRH neurons. Chapter 1 relates to the first element of this hypothesis. A major class of voltage-gated ion currents, previously unexamined in these cells, was characterized during diestrus and proestrus. Empirical observations were contextualized with previous studies of voltage-gated currents by using biophysical computational modeling to perform *in silico* simulations. Chapter 2 relates to the second element of the hypothesis. Neurotransmission between AVPV kisspeptin neurons and GnRH neurons was measured during diestrus, proestrus, and in OVX mice. Together, these studies provide insight into how estradiol positive feedback is detected and processed by neurons, and how this is communicated to GnRH neurons.

Chapter 2: Reciprocal Changes in Voltage-gated Potassium Currents and Subthreshold Inward Currents Help Maintain Firing Dynamics of AVPV Kisspeptin Neurons During the Estrous Cycle

J. Rudolph Starrett, R. Anthony Defazio, Suzanne M. Moenter

This work was originally published in 2021 in the journal eNeuro. 2 Sep 2021

DOI: 10.1523/eneuro.0324-21.2021

Abstract

Kisspeptin-expressing neurons in the anteroventral-periventricular nucleus (AVPV) are part of a neural circuit generating the gonadotropin-releasing hormone (GnRH) surge. This process is estradiol-dependent and occurs on the afternoon of proestrus in female mice. On proestrus, AVPV kisspeptin neurons express more kisspeptin and exhibit higher frequency action potentials and burst firing compared to diestrus, which is characterized by a pulsatile rather than a prolonged surge of GnRH secretion. We hypothesized changes in voltage-gated potassium conductances shape activity profiles of these cells in a cycle-dependent manner. Whole-cell voltage-clamp recordings of GFP-identified AVPV kisspeptin neurons in brain slices from diestrous and proestrous mice revealed three subcomponents of the voltage-sensitive K^+ current: fast-inactivating, slow-inactivating, and residual. During proestrus, the V50 of inactivation of the fast-inactivating current was depolarized and the amplitude of the slow-inactivating component was reduced compared to diestrus; the residual component was consistent across both stages. Computational models were fit to experimental data, including

published estrous-cycle effects on other voltage-gated currents. Computer simulations suggest proestrus-typical K^+ currents are suppressive compared to diestrus. Interestingly, larger T-type, persistent-sodium, and hyperpolarization-activated currents during proestrus compensate for this suppressive effect while also enabling post-inhibitory rebound bursting. These findings suggest modulation of voltage-gated K^+ and multiple subthreshold depolarizing currents across the negative to positive feedback transition maintain AVPV kisspeptin neuron excitability in response to depolarizing stimuli. These changes also enable firing in response to hyperpolarization, providing a net increase in neuronal excitability, which may contribute to activation of this population leading up to the preovulatory GnRH surge.

Significance statement

GnRH neurons provide the central signal to initiate ovulation by releasing a surge of hormone. GnRH neurons are regulated by other cells including those expressing kisspeptin, a potent stimulator of GnRH secretion. Kisspeptin neurons in the anteroventral-periventricular nucleus (AVPV) express more kisspeptin and become more active during the afternoon of proestrus, the phase of the rodent estrous (reproductive) cycle when the GnRH surge occurs. We found voltage-dependent potassium currents in AVPV kisspeptin neurons change with phase of the estrous cycle. Firing simulations indicated these changes are suppressive if occurring in isolation. But proestrous-typical increases in subthreshold depolarizing currents overcome this suppression and promote greater excitability by increasing rebound firing, possibly contributing to the preovulatory activation of this system.

Introduction

The anteroventral-periventricular (AVPV) nucleus is a critical site involved in the regulation of female fertility, specifically the control of the estradiol-dependent process of ovulation (Kalra and McCann, 1975; Goodman, 1978; Wiegand and Terasawa, 1982;

Petersen and Barraclough, 1989; Petersen et al., 1989). The AVPV contains neurons that express both estrogen receptor a (ERa) and kisspeptin (Simerly, 1998b; Smith et al., 2005a), a neuropeptide that acts at gonadotropin-releasing hormone (GnRH) neurons to potently induce GnRH neuron activity and hormone secretion (Han et al., 2005; Messager et al., 2005; Pielecka-Fortuna et al., 2008; Zhang et al., 2008; Caraty et al., 2013). Ovulation is initiated by positive feedback actions of estradiol at the central and pituitary levels (Döcke and Dörner, 1965; Sarkar et al., 1976b; Moenter et al., 1991). In a prevailing theory, sustained elevation of circulating estradiol during the late follicular phase (the cycle day of proestrus in rodents) exerts positive feedback effects via ERa that drive increased kisspeptin expression in AVPV neurons (Smith et al., 2005a; Gottsch et al., 2006; Oakley et al., 2009b). Action potential firing by AVPV kisspeptin neurons is also increased on proestrus vs diestrus (a time of homeostatic negative feedback) (Wang et al., 2016b). Combined, these effects are thought to increase kisspeptin secretion onto the GnRH neuron, as increases in firing frequency are typically associated with increased neuropeptide release (Dutton and Dyball, 1979b; Cropper et al., 2018). Estradiol positive feedback is likely conveyed to GnRH neurons by increased kisspeptin signaling, causing a surge of GnRH release which stimulates a luteinizing hormone (LH) surge from the pituitary. The LH surge stimulates ovulation (Greep et al., 1942).

If the above theory is correct, the firing activity of AVPV kisspeptin neurons is a critical piece of this surge induction process, serving as a gating mechanism controlling kisspeptin release and thus the physiologic cascade culminating in ovulation. Several studies have focused upon the electrical properties of these cells and how they change across the reproductive cycle, measured via recordings performed in acutely prepared mouse brain slices during periods of estradiol negative (typically diestrus) vs. positive (proestrus) feedback. AVPV kisspeptin neurons recorded on proestrus maintain higher firing rates than on diestrus even when fast synaptic transmission was blocked,

suggesting a shift in intrinsic properties across the diestrus-proestrus transition enables increased firing during proestrus (Wang et al., 2016b). Voltage-gated conductances may provide a basis for these shifts in activity since they help control membrane potential and shape firing dynamics in electrically-excitable cells. T-type calcium, persistent sodium, and hyperpolarization-activated currents were all found to be larger in AVPV kisspeptin neurons during proestrus (Piet et al., 2013b; Zhang et al., 2015; Wang et al., 2016b). Increases in these depolarizing currents, which can be active at subthreshold membrane potentials, could promote greater firing activity. Potassium currents, which strongly influence firing onset of many neurons and are vital for proper repolarization of the membrane (Hille, 2001), remained uncharacterized in AVPV kisspeptin neurons. K^+ currents change across the estrous cycle and in response to estradiol in GnRH neurons and kisspeptin neurons in the arcuate nucleus (DeFazio et al., 2002b, 2019; Pielecka-Fortuna et al., 2011).

We hypothesized voltage-gated potassium currents in AVPV kisspeptin neurons are regulated by estrous cycle stage. Classic voltage-clamp approaches revealed three conductances contribute to the total voltage-gated potassium current in these cells, and each component was characterized during the afternoon of diestrus (negative feedback) and proestrus (positive feedback). It can be difficult to predict how multiple voltage-gated conductances interact to control the membrane voltage. Computational modeling studies were thus conducted to better understand how estrous cycle modulation of these and other currents influence action potential firing output.

Materials and Methods

Animals

The University of Michigan Institutional Animal Care and Use Committee approved all procedures. Adult female Kiss1-hrGFP mice (Cravo et al., 2011) which express humanized *Renilla* GFP under control of the kisspeptin promoter, were used for these

studies. Mice were provided with Harlan 2916 chow and water *ad libitum* and were held on a 14L:10D light cycle with lights on at 3:00 AM Eastern Standard Time. Estrous cycle stage was monitored by vaginal cytology for at least one week before experiments. Uterine mass was measured after brain slice preparation to confirm cycle stage. Uterine mass >100mg indicated *in vivo* exposure to a high concentration of estradiol, typical of proestrus, whereas mass <60mg indicated exposure to low estradiol, typical of diestrus (Shim et al., 2000a).

Experimental Design

Brain slices were prepared from cycling adult female mice (age 55-154 days) during cycle stages corresponding to estradiol negative feedback (afternoon of diestrus) or positive feedback (afternoon of proestrus). Whole-cell voltage-clamp recordings of hrGFP-identified AVPV kisspeptin neurons were used to characterize macroscopic voltage-gated potassium currents; three currents (fast transient, slow transient, residual) were identified and separated using pharmacological and/or voltage-based subtraction methods for characterization. Current-clamp recordings were used to monitor action potential firing. Computational modeling was used to predict how each type of potassium current regulates AVPV neuron excitability, and how changes in multiple voltage-gated currents across the estrous cycle may impact excitability.

Brain slice preparation

Chemicals were purchased from Sigma-Aldrich unless noted. All solutions were bubbled with 95% O2/5% CO2 for at least 15 minutes before exposure to tissue. All mice were euthanized at 3:00 to 4:00 PM Eastern Standard Time, and the brain was rapidly removed and placed in ice-cold sucrose saline solution containing the following (in mM): 250 sucrose, 3.5 KCl, 25 $NaHCO_3$, 10 D-glucose, 1.25 Na_2HPO_4, 1.2 $MgSO_4$, and 3.8 $MgCl_2$, at pH 7.6 and 345 mOsm. Coronal (300 μm) slices were cut with a VT1200S Microtome (Leica Biosystems). Slices were incubated in a 1:1 mixture of sucrose saline

and artificial cerebrospinal fluid (ACSF) containing (in mM) 135 NaCl, 3.5 KCl, 26 $NaHCO_3$, 10 D-glucose, 1.25 Na_2HPO_4, 1.2 $MgSO_4$, and 2.5 $CaCl_2$ at pH 7.4 and 305 mOsm for 30 min at room temperature (~21 to 23 °C) and then were transferred to 100% ACSF for an additional 30-180 min at room temperature before recording. For recording, slices were placed into a chamber and perfused (3 ml/min) with carboxygenated ACSF kept at 31°C with an inline heating unit (Warner Instruments). GFP-positive AVPV kisspeptin neurons were identified by brief illumination at 488 nm on an Olympus BX51WI microscope. Recordings were performed 1-4 h after brain slice preparation. No more than four cells were recorded per mouse; data values from cells from the same animal were not clustered in a manner that would typically contribute to reduced variability.

Voltage-clamp recordings

Recording micropipettes were pulled from borosilicate capillary glass using a Flaming/Brown P-97 puller (Sutter Instruments) to obtain pipettes with a resistance of 1.5-3.5 MΩ when filled with pipette solution, which consisted of (in mM) 135 K-gluconate, 10 KCl, 10 HEPES, 5 EGTA, 0.1 $CaCl_2$, 4 MgATP, and 0.4 NaGTP, 305 mOsm and pH 7.2 with NaOH. Pipettes were wrapped in Parafilm to reduce capacitive transients. All potentials reported were corrected on-line for a liquid junction potential of -15.7 mV(Barry, 1994). Recordings were performed with one channel of an EPC-10 dual patch-clamp amplifier and PatchMaster software (HEKA Elektronik). After achieving the on-cell configuration with seal resistance >2.0 GΩ, fast capacitive transients were minimized and the whole-cell configuration was achieved by rupturing the cell membrane with brief suction. The membrane potential was held at -70 mV between voltage-clamp protocols. Passive membrane properties and voltage-clamp quality were calculated from the averaged current response (after on-cell capacitive current subtraction) to sixteen -5 mV, 20 ms test pulses from a holding potential of -70

mV performed immediately before and after each protocol. To ensure adequate recording quality, the following criteria were required for inclusion for analysis: uncompensated series resistance (Rs) <20 MΩ, input resistance (Rinput) >500 MΩ, capacitance (Cm) between 8 pF and 30 pF, holding current (Ihold) between -60 and 10 pA. Rs was compensated 50-85% for all protocols and recordings were excluded from analysis if >20% change in Rs occurred during the experiment.

To isolate voltage-gated potassium currents, TTX (2.5 μM, Tocris Bioscience), $CdCl_2$ (100 μM), and $NiCl_2$ (300 μM) were included in the ACSF to block Na^+ and Ca^{2+} currents. Picrotoxin (100 μM) was used to block $GABA_A$-receptor-mediated currents and D-2-amino-5-phosphonovalerate (APV; 20 μMm, Tocris Bioscience), and 6-cyano-7-nitroquinoxaline-2,3-dione (CNQX; 10 μM) were used to block ionotropic glutamate receptor-mediated currents.

Total K^+ current

In initial recordings of the total voltage-gated potassium current, two temporally-distinct peaks were visible in voltage steps from -100 to -10 or 0 mV. Further, a persistent negative slope in the outward current suggested a component with slow inactivation was present at potentials depolarized to -10 mV. Lengthening the voltage-clamp protocols allowed for more complete removal or induction of inactivation before the test pulse. To measure the voltage dependence of activation of the total voltage-gated K^+ current, the membrane potential was held at -100 mV for 5 s to remove inactivation then stepped to test pulses of -70 to +40 mV (10 mV increments) for 1 s. To measure the voltage-dependence of inactivation, the membrane was held at potentials ranging from -100 to -10 mV (10mV increments) for 10s and then stepped to a test pulse of 0 mV for 1 s. The long duration of these protocols makes P/N subtraction (Armstrong and Bezanilla, 1977) unfeasible. Instead, slow capacitance and leak current subtraction were performed offline by subtracting the appropriately scaled average current

response to one hundred -5 mV test pulses with capacitance and series resistance compensation activated (Kimm et al., 2015). Averages were scaled for each voltage step used in the protocol.

Slow-transient K^+ current

To characterize the slow transient K^+ current, the same activation/inactivation protocols as above were repeated with 5 mM 4-aminopyridine (4-AP) included in the ACSF to reduce primarily the fast-transient current. To measure the time course of inactivation of the slow-transient K^+ current, the membrane was held at -100 mV for 5 s to remove inactivation, then at -10 mV for durations varying from 0-8 s, followed by a test pulse at 0 mV for 1 s. To measure the time-dependence of recovery from inactivation, the membrane was held at -10 mV for 10s to inactivate the current, then at -100 mV for durations varying from 0-8 s, followed by a test pulse at 0 mV for 1 s. Offline leak subtraction was used as for recordings of the total K^+ current (Kimm et al., 2015).

Fast-transient K^+ current

The fast-transient K^+ current was isolated and quantified using a voltage-based subtraction method after reducing primarily the slow-inactivating and residual components with ACSF in which 20 mM tetraethylammonium chloride (TEA) replaced 20 mM NaCl. To measure the voltage-dependence of activation, two protocols (A and B) were run in series. For protocol A, the membrane potential was held at -100 mV for 200 ms, then current was measured during 150 ms test pulses from -70 to +40 mV (10 mV increments). Protocol B was identical to protocol A, except that the membrane potential was held at -30 mV rather than -100 mV during the first 200 ms of the protocol. This fully inactivates the fast-transient current, isolating any remaining residual component during the test pulse. The current response during the test pulse of protocol B was subtracted from that of protocol A to yield the fast-transient current. To measure the voltage-dependence of inactivation, the membrane was held at -100 to -20 mV (10

mV increments) for 200 ms, before stepping to a test pulse at -10 mV (150 ms). Current occurring after a step from -30 mV holding potential was defined as residual current and was subtracted from earlier sweeps to yield isolated fast transient current. To measure the rate of inactivation of the fast-transient K^+ current, inactivation was fully removed by holding the membrane at -100 mV for 300 ms. The membrane was then stepped to -30 mV for 0-250 ms followed by a test pulse of 0 mV for 100 ms. The component of the current that did not inactivate (residual current) was subtracted from the prior series to isolate the fast-transient current. To measure the rate of the recovery from inactivation, the fast-transient current was fully inactivated by holding the membrane at 0 mV for 300 ms, then recovery prepulses at -100 mV were applied for 0-250 ms before measuring current at 0 mV (100 ms). The current after the 0 ms recovery prepulse was subtracted from each test pulse to isolate the fast-transient K^+ current. Slow capacitance and leak currents were corrected using P/-5 online leak subtraction with Vhold = -70 mV (Armstrong and Bezanilla, 1977).

It was not possible to quantify all parameters from every cell because not all cells remained within our quality control standards long enough for inclusion in the analysis of the time dependence of activation and inactivation. The number of cells and animals per measurement are shown in Tables 1-2 and 1-3

Total, fast-transient, slow-transient and residual K^+ current densities were calculated by dividing by capacitance. Peak values were divided by the driving force according to the Goldman-Hodgkin-Katz (GHK) current equation using the calculated reversal potential (-94 mV) (Clay, 2000, 2009). Conductance values were then normalized to the maximum conductance (g_{max}) to generate steady state activation/inactivation curves, which were fit with a Boltzmann function to calculate voltage of half (V50) activation or inactivation, and steepness (k). Inactivation and recovery from inactivation curves were fit to single exponentials to measure time constants *(τ).*

Current-clamp recordings

Depolarizing (2 to 28 pA, 2 pA increments) and hyperpolarizing (-25 to -5 pA, 5 pA increments) current pulses (500 ms) were applied in whole-cell configuration. The maximum amplitude of hyperpolarizing stimuli was limited to avoid hyperpolarizing the membrane beyond -100 mV, as further hyperpolarization was detrimental to recording stability. The targeted initial membrane potential was within 2 mV of -70 mV, which is close to the baseline membrane potential of these cells (DeFazio et al., 2014b). Spikes were counted as action potentials only if their peak value was depolarized relative to -10 mV; spike number was plotted as a function of current injection.

Modeling - Physiological data utilized

Mean ± SEM normalized activation, inactivation, recovery, and rate of inactivation curves were calculated for the total, fast-transient (fast), slow-transient (slow) and residual (resid) K^+ current densities in each group. Leak-subtracted current traces from activation protocols were averaged for each current at each voltage step to obtain mean ± SEM current traces used for fitting. T-type calcium and persistent sodium conductance data were collected from published measurements, which indicated larger amplitudes during proestrus (Zhang et al., 2015; Wang et al., 2016b). The hyperpolarization-activated conductance was estimated based on the amplitude and time course of the sag potential, which has larger amplitude during proestrus (Piet et al., 2013b; Wang et al., 2016b). Neurons were modeled as a single compartment with whole-cell capacitance of 17.62 pF based on the mean of experimentally-observed values (Table 2--1).

Modeling - Equations

Na^+, $Ca^{2+,}$ and hyperpolarization-activated currents were modeled based on Ohmic driving forces (Eq 1-2). K^+ currents were modeled based on nonlinear driving forces

described by the Goldman-Hodgkin-Katz (GHK) current equation (Clay, 2000, 2009) (Eq 3).

(1) $I = C_m \frac{dV}{dt} + I_{NaT} + I_{NaP} + I_{CaT} + I_h + I_{resid} + I_{fast} + I_{slow} + I_{Leak}$

(2) $I_a = \bar{g}_a m^r h(V - E_a)$, $a = Na_p, Ca_T, h, Leak$

(3) $I_b = \bar{g}_b mh \frac{qV}{kT} \frac{e^{\frac{q(V-E_b)}{kT}} - 1}{e^{\frac{qV}{kT}} - 1}$, $b = resid, fast, slow$

I is current (nA) across the neuronal membrane, C_m is the cell capacitance (pF), V_m is the membrane potential (mV), *t* is time (ms), $\bar{g}_a$ is the specific conductance (nS), E_a is the reversal potential (mV) of a given ion, *q* is the elementary charge, *k* is the Boltzmann constant, *T* is the absolute temperature, and *m* and *h* represent activation and inactivation variables, respectively. Exponents *r* represents the number of activation particles. These variables are governed by the following differential equations (Eq 4,5)

(4) $\frac{dm}{dt} = \frac{m_\infty(V) - m}{\tau_m(V)}$

(5) $\frac{dh}{dt} = \frac{h_\infty(V) - h}{\tau_h(V)}$

where $m_\infty(V)$ and $h_\infty(V)$ are the steady-state activation/inactivation functions for each variable and τ_m and τ_h are functions determining the voltage-dependent time constants (in ms) of activation/deactivation and inactivation/recovery, respectively. These functions take the form (Eq 6-9). *A*-*G* are free parameters adjusted during fitting.

(6) m_∞ , $h_\infty = \frac{1}{1 + e^{\frac{(V50_{m,h} - V)}{K_{m,h}}}}$

(7) $\tau_{m_a}, \tau_{h_a} = A + \frac{B}{1+e^{\left(\frac{V-C}{D}\right)}} * \frac{E}{1+e^{\left(\frac{V-F}{G}\right)}}$, $a = slow, resid$

(8) $\tau_{m_a}, \tau_{h_a} = A + \frac{B}{1+e^{\left(\frac{V-C}{D}\right)}}$, $a = fast, H, CaT$

(9) $\tau_{NaP} = \frac{E}{e^{\frac{A+V}{B}} + e^{\frac{C+V}{D}}} + F$

The transient sodium current (Na_T) was modeled used a Markov chain with three states, open (*O*), closed (*C*), or inactivated (*I*). Transitions between states were either voltage sensitive or constants. The model used was modified from Adams et al., 2018. (Eq. 10-14).

(10) $I_{NaT} = \bar{g}_{NaT} O^3 (V - E_{Na})$

(11) $\alpha(V), \beta(V), r_1(V), r_3(V) = \frac{r}{1 + e^{\frac{(V+s)}{k}}}$

(12) $\frac{dC}{dt} = \beta(\mathrm{V})\mathrm{O} + r_3(V)I - \alpha(\mathrm{V})\mathrm{C}$

(13) $\frac{dO}{dt} = \alpha(\mathrm{V})\mathrm{C} - (\beta(\mathrm{V}) + r_1(V))O$

(14) $I = 1 - C - O$

Modeling - Parameter optimization

Simulated voltage-clamp experiments were performed using Xolotl (Gorur-Shandilya et al., 2018). Voltage-step protocols matched those used experimentally for each conductance. Current traces generated by models were analyzed in the same manner as the slice recording data. For each voltage step, peak currents were converted to conductance and normalized to generate activation/inactivation curves. For K^+ models, permeability as calculated by the GHK current equation was used (Clay, 2000, 2009). m_∞ and h_∞ function parameters were adjusted manually until the normalized

activation/inactivation curves were well fit to the experimental data. τ_m, τ_h, and $\bar{g}$ parameters were also adjusted so that the rise and decay (where applicable) phases of the current trace and peak amplitudes were well fit to the data. This process was iterative and was greatly facilitated by xolotl's "puppeteer" function, which allowed for rapid-recalculation and visualization of simulation results following parameter adjustment. Separate models were generated for each experimental group to reproduce estrous cycle effects on each of the voltage-gated currents.

The total K^+ current was fit by simulating voltage-clamp of a cell containing the three K^+ conductance subcomponents (fast, slow, resid) as they were fit to their respective drug-separated recordings. To better fit the total K^+ recording, $\bar{g}$ parameters were optimized using particle swarm optimization (Global Optimization Toolbox, Mathworks), which sought to minimize the sum of squares error between the current trace generated by the model and the mean data for the respective conductance.

Modeling - Simulation of excitability

To study action potential firing, diestrous and proestrous neuron models were built with an identical sodium channel model. This model was made the same between groups because although there are no experimental data characterizing this conductance in AVPV kisspeptin neurons, action potential threshold (defined as when rate of rise exceeds 2V/s) and amplitude were the same between cycle stages (Wang et al., 2016b), and these characteristics are highly influenced by transient sodium current properties (Kress et al., 2010).

To examine how conductances alter firing, a suite of conductance models corresponding to the respective experimental group were added to single-compartment neuron models, and the voltage of the model was allowed to vary, i.e., "current clamp". Using the same protocols from *in vitro* recordings, firing was stimulated by applying increasing current steps (-30 to 0 pA at 10 pA intervals, 2-28 pA at 2 pA intervals) to the

model cell at a baseline membrane potential of -70 mV. The number of spikes fired during the stimulation is plotted against the stimulation amplitude to generate a firing-current (F-I) curve. To achieve this baseline potential, holding current and leak conductance were adjusted so that the membrane potential prior to the start of the current pulse was within 50 μV of -70 mV and input resistance was 1 GΩ (passive properties in Table 2--1). For diestrous and proestrous models, the simulated rheobase action potential waveform was compared to the peak-aligned mean rheobase action potential of the corresponding experimental group. This fit was improved by manually adjusting sodium conductance model parameters; adjustments were kept the same for the diestrous and proestrous models. To test predictions regarding estrous cycle effects or the role and/or interaction of various conductances, individual or multiple conductances fit to diestrous data were substituted into the proestrous model (and *vice versa*) for a particular simulation.

Statistics

Data were analyzed using Prism 9 (GraphPad). Shapiro-Wilk was used to test distribution of data. Parameters (mean ± SEM) were compared between cycle stages with unpaired statistical tests appropriate for experimental design and data distribution as indicated in the results section. The number of cells per group is indicated by n. For two-way ANOVAs and Mann-Whitney, difference of the means (Diff) was defined for cycle stage (diestrus–proestrus). For Kruskal-Wallis tests (Table 2--1), mean rank differences are reported as (total – slow), (total- fast), (slow – fast). Significance was set at $p < 0.05$.

Results

Passive properties

Series resistance, input resistance, capacitance, and holding current measurements were made before and after each protocol and values were averaged for each cell.

There were no statistical differences between cells recorded during diestrus vs proestrus for any of the measured properties (Table 2--1). Comparing across drug treatments that are discussed below, input resistance was higher during 4-AP or TEA treatment (Table 2--1). Dunn's multiple comparisons *post hoc* tests of input resistance revealed increases consistent with antagonism of channels active at baseline membrane potentials by the respective drugs (Dunn's, control vs 4-AP $p = 0.002$, control vs. TEA $p = 0.001$, 4-AP vs TEA $p > 0.99$).

Total voltage-dependent K^+ current in AVPV kisspeptin neurons has multiple components

In nocturnal rodents, positive feedback needed to generate the LH surge occurs during the afternoon of proestrus (Brown-Grant et al., 1970; Sarkar et al., 1976b). During this time, both overall firing rate and burst firing of AVPV kisspeptin neurons increase relative to diestrus (Wang et al., 2016b). Given the importance of K^+ currents in determining the excitability and firing patterns of neurons (Coetzee et al., 1999; Hille, 2001), we hypothesized voltage-gated potassium currents are targets of estradiol feedback in AVPV kisspeptin neurons; we tested this using whole-cell voltage-clamp. Figure 2-1A shows a representative recording of total voltage-dependent K^+ current activation. Examining this family of traces from the most hyperpolarized to the most depolarized command potentials revealed induction of one component with faster inactivation at more hyperpolarized potentials that merged with a component that activated at more depolarized potentials and only slowly inactivated. The slow kinetics of the macroscopic current resembled a K+ current previously observed in dorsal root ganglion neurons (Gold et al., 1996), and led us to extend the duration of the prepulses beyond what is used in a typical inactivation protocol to 10 s (Figure 2-1B). As described above, a fast component can be seen to activate and inactivate within ~50 ms at more hyperpolarized potentials during the prepulse (expanded in Figure 2-1C, left); this component is prominent as a spike during the test pulse following hyperpolarized

prepulses (expanded in Figure 2-1C, right). A second component required greater depolarization to begin activating and inactivated slowly only at more depolarized potentials. The peak total current density (derived from the voltage-clamp protocol in Figure 2-1A) was not different between diestrus and proestrus at any of the potentials tested (Figure 2-1D, two-way repeated-measures ANOVA for effect of cycle stage; Table 2--2). These observations, however, do not preclude latent changes attributable to individual components being differentially regulated.

Pharmacological treatments to isolate current components

To attempt to isolate the components of the total potassium current, recordings were made before and during application of the potassium channel blockers TEA (20 mM) or 4-AP (5 mM). TEA reduced the amplitude of both the fast and slow components, but the reduction in the slow component was proportionally greater, making the fast peak appear more prominent (Figure 2-2A). Lower concentrations of TEA (500 μM to 10 mM) did not block most of the slow peak amplitude and were thus less effective in revealing the fast component. The fast-transient component was markedly reduced by 5 mM 4-AP (Figure 2-2B, note right-shift of peak in red trace). Lower concentrations of 4-AP (100 μM to 1 mM) did not block the fast initial peak at -10 mV. These changes were attributable to drug action rather than rundown as the current remained stable in the absence of treatments over the ten minutes required for these recordings (Figure 2-2C).

Individual components of the total current may have distinct roles in determining firing output and may also be independently regulated by cycle stage. The differential effects of TEA and 4-AP were utilized to perform more detailed characterization of the sub-components of the total potassium current in AVPV neurons in slices from diestrous and proestrous mice. To increase recording yield, we switched from a within-cell design to a population (i.e., among-cell) design, with drug present from the time the slice was placed in the recording chamber. In these population studies, the longer exposure to

TEA caused a larger reduction in peak current density. Specifically, the peak current density at +40 mV during TEA treatment was 76.6 ± 5.1% of pretreatment values in within-cell experiments, but only 53.0 ± 3.7% of untreated cells in population studies. This greater reduction was not observed with 4-AP (the peak current density during 4-AP treatment was 76.6 ± 4.9% of the control period for within-cell studies (n=3), and 76.1% of untreated controls in population studies (n=4)).

The slow transient component is increased on diestrus

The extended duration voltage-clamp protocols were used to characterize the slow-transient potassium current in the presence of 4-AP; representative traces are shown in Figure 2-3. Peak current density was greater in cells from diestrous (n=12) than proestrous (n=13) mice at more depolarized potentials (Figure 2-3C, two-way repeated-measures ANOVA for effect of cycle stage; Table 2--2). The slow current was activated at command voltages at and depolarized relative to -20 mV. Normalized activation and inactivation curves were not different between groups (Figure 2-3D, two-tailed Student's *t*-test with Welch's correction for V50 activation, inactivation; Table 2--3). Timecourse of inactivation was not different between diestrus and proestrus (Figure 2-3F, two-way repeated-measures ANOVA for effect of cycle stage; Table 2--2). In contrast, recovery from inactivation was more rapid during proestrus (Figures 1-3G, H, two-way repeated-measures ANOVA for effect of cycle stage; Table 2--2). In recovery from inactivation experiments, the recovery of two currents was evident. The fast transient was visible when the hyperpolarizing recovery prepulse was shorter than 200 ms (Figure 2-3G, arrow). This may be attributable to the voltage-dependence of 4-AP action, in which the channel becomes unblocked during depolarization (Choquet and Korn, 1992; Kehl, 2017). The slow current was visible 70-150 ms into the test pulse. To avoid contamination with the fast current, for this protocol only the peak of the slow transient current was taken as the maximum current 70-150 ms after the start of the test pulse.

The inactivation curve of the fast-transient component is depolarized during proestrus

Bath-applied 20 mM TEA preferentially reduced the amplitude of the slow-transient current, allowing better characterization of the fast-transient current. Because this fast-transient component activated and inactivated quickly, voltage-clamp protocols with more traditional durations were utilized (Figure 2-4A). Under these recording conditions, a fast-transient current began to activate between -50 mV and -40 mV (Figure 2-4C); current reached a non-zero steady state by the end of the test pulse, suggesting a contribution by non- or slowly-inactivating channels. To isolate the fast-transient current from this non-inactivating residual component, a voltage-based subtraction method was used. Subtraction of the residual current following a depolarizing prepulse (Figure 2-4A, middle) yielded a transient current that was almost fully inactivated by the end of the test-pulse (Figure 2-4A, right). The V50 activation of the residual current was more depolarized than that of the fast-transient current at both cycle stages (Figure 2-4B-D diestrus n=11, proestrus n=13, one-way ANOVA $F(3,44) = 10.8$, $p<0.001$; Tukey residual vs fast $p=0.001$ for proestrus, residual vs fast $p=0.002$ for diestrus). There was no effect of cycle stage on the peak current density of either the fast-transient or residual component (Figure 2-4B, two-way repeated-measures ANOVA for effect of cycle stage; Table 2--2). In contrast, cycle stage affected voltage dependence of the fast-transient component. Specifically, inactivation of the fast transient occurred at more depolarized potentials on proestrus than diestrus (Figure 2-4C,E, two-way repeated-measures ANOVA for effect of cycle stage on inactivation; Table 2--2; unpaired two-tailed Student's *t*-test with Welch's correction of V50 inactivation; Table 2--3), Cycle stage did not, however, affect the voltage-dependence of activation (Figure 2-4C, two-way repeated-measures ANOVA for effect of cycle stage on activation curve; Table 2--2) or V50 activation (Figure 2-4D, unpaired two-tailed Student's *t*-test; Table 2--3). Full inactivation and full recovery of the fast transient occurred in less than 100 ms (Figure

2-4F, G). There was no group difference in either of these properties (two-way repeated-measures ANOVAs for effect of cycle stage; Table 2--2).

Modeling conductances

Computational modeling was used to better understand the role of estrous cycle modulation of multiple conductance types in the control of AVPV kisspeptin neuron firing. Specifically, we examined if estrous cycle-related shifts in K^+ current components and/or subthreshold depolarizing currents alter the firing dynamics of these cells. To model subcomponents *in silico*, Hodgkin-Huxley conductance models were fit to mean ± SEM recordings of drug- and voltage-separated subcomponents of the K^+ current: slow, fast and residual. This involved adding individual subcomponents to single-compartment neuron models and running such models through the same voltage-clamp protocols used experimentally, generating membrane current over time plots. Model output was compared to experimental data (Figure 2-5), and $m_\infty(V)$, $h_\infty(V)$, $\tau_m(V)$, and $\tau_h(V)$ function parameters were changed iteratively to improve the quality of fit. Steady-state activation and inactivation curves and I(density)-V plots were calculated from the model output and compared to experimental data for K^+ currents (Figure 2-6A, B, D) and for CaT (Figure 2-6C, F) and NaP (Figure 2-6E) currents reported (Zhang et al., 2015; Wang et al., 2016b).

To reconstruct the total K^+ current from the sum of the subcomponents, the set of I_{slow}, I_{fast}, and I_{resid} currents for each group were included in single neuron models, and the models were run through the same voltage-clamp protocol used for recordings in Figure 2-1A. Initial simulations indicated the sum of fast, slow, and residual currents as fit to their isolated recordings was not enough to account for the full amplitude of the total K^+ current, suggesting subcomponents were blocked to some degree by the drug used to isolate them (i.e., 4-AP blocked a portion of the slow current, TEA blocked some of the fast and residual currents). To overcome this problem, particle-swarm optimization was

used to minimize the error between the model-generated current trace and the mean ± SEM trace by optimizing $\bar{g}$ parameters of each subcomponent, with equal weighting across the trace. This preserved the voltage-sensitivity and kinetics of the subcomponents as fit in the drug- and voltage-separated recordings (Figure 2-5) while providing a better fit to the experimental data. Parameter values are shown in Tables 1-4-5. This approach provided a good fit to peak current density (Figure 2-7A) and the first ~250 ms of the total K^+ current (Figure 2-7B). The error between the model and data increased as the simulation progressed, however. This error could be reduced by decreasing the inactivation rate of I_{slow}, but this modification had no effect on firing behavior as measured in response to 500 ms current pulses, suggesting this shift in kinetics does not substantially influence firing output at these timescales (not shown).

Simulations of firing

K^+ conductance models from fits to the total K^+ current, CaT, NaP, and HCN conductances for the diestrous and proestrous groups were combined into single-compartment neuron models, thus creating neuron models with seven voltage-gated conductances and one leak conductance each. A transient sodium (NaT) conductance is needed to enable action-potential firing and was thus added to the models at this stage (Table 2--6). Transient sodium currents of AVPV kisspeptin neurons have not been measured. We thus estimated NaT parameters using action potential properties such as threshold and peak amplitude. NaT was kept identical between diestrus and proestrus as these action potential properties did not change with cycle stage previously (Wang et al., 2016b) or this study (threshold: diestrus -51.8 ± 1.0 mV, n = 12 cells from 5 animals, proestrus -51.6 ± 0.6 mV, n = 17 cells from 6 animals, two-tailed, unpaired Student's *t*-test, p = 0.85, t=0.1906, df=27, amplitude diestrus 82.1 ± 1.9 mV, n = 12, proestrus 80.5 ± 1.1 mV, n = 17, two-tailed unpaired Student's *t*-test, p = 0.4501, t=0.72, df=22) suggesting estrous cycle modulation of this conductance is minimal. Using the same NaT conductance in the diestrous and proestrous models generated action

potential shapes similar to experimental action potentials (Figure 2-8C). The diestrous and proestrous models were tested with the same current injection protocols used in recordings and demonstrated F-I curves similar to the mean ± SEM data, indicating that the models could reproduce the firing behavior of AVPV kisspeptin neurons recorded in brain slices (Figure 2-8D).

These models also faithfully reproduced cycle-dependent differences in post-hyperpolarization rebound firing behavior observed (Wang et al., 2016b). Specifically, cessation of hyperpolarization initiated rebound spikes in the proestrous but not the diestrous model (Figure 2-8B). To determine the basis for this difference as well as to further understand how each conductance influences firing behavior, we performed a series of simulations involving swapping individual or multiple conductances from one model into the other. In the diestrous model, replacing all K^+ conductances with their proestrus counterparts had a suppressive effect, depolarizing the rheobase and reducing the number of spikes fired in response to all depolarizing stimuli (Figure 2-8E). Of the three potassium current subcomponents, proestrous I_{slow} was the most suppressive when individually substituted into the diestrous model (Figure 2-8E). The diestrous model with only I_{fast} substituted for the proestrous counterpart had a depolarized rheobase but the F-I curve (Figure 2-8E) had a similar slope. Changing from diestrous to proestrus $I_{residual}$ did not change firing behavior (Figure 2-8E), consistent with this current being similar between groups (Figure 2-4). Of the subthreshold depolarizing conductances, proestrous CaT caused the greatest increase in excitability when substituted into the diestrous model, generating more spikes at every depolarizing stimulus after rheobase was achieved, but not changing rheobase itself (Figure 2-8F). Rebound firing only occurred in the diestrous model when all three subthreshold depolarizing currents were replaced with their proestrous counterparts (Figure 2-8F, G). This model, which had diestrous K^+ conductances and proestrus CaT,

NaP, and h-current, had the greatest excitability of any model tested. It is important to point out that changes in excitability were not attributable to differences in either baseline membrane potential or input resistance as these were the same among models. Comparing this hybrid model to the proestrus-only model thus further indicates the suppressive effect of proestrous K^+ currents.

Discussion

AVPV kisspeptin-expressing neurons are key mediators of estradiol positive feedback–a process critical for ovulation. We studied intrinsic properties of these neurons to determine how they become more active during proestrus, the phase of the rodent estrous cycle when positive feedback culminates in the ovulation-inducing GnRH/LH surge. AVPV kisspeptin neurons exhibit three types of voltage-gated potassium currents; two were modulated in an estrous-cycle dependent manner. Unexpectedly, effects of the proestrous K^+ currents were suppressive but countered by cycle-dependent shifts in inward currents active in the subthreshold range. The proestrous shift in K^+ currents did not, however, block increased rebound firing enabled by the proestrous shift in inward currents.

This finding that the K^+ currents on proestrus were suppressive was initially surprising given substantial evidence indicating AVPV kisspeptin neurons are activated during estradiol positive feedback (Zhang et al., 2015; Wang et al., 2016b, 2019b). Much of this evidence was gathered using experimental models of estradiol feedback involving ovariectomy plus estradiol replacement (OVX+E) as a constant-release implant producing daily surges (Christian et al., 2005b), or an implant followed several days later by an estradiol benzoate injection that triggers an LH surge the next day (Bronson and Vom Saal, 1979). These models allow study of estradiol feedback in isolation of other ovarian factors. In both models, AVPV kisspeptin neurons have increased c-fos expression during the LH surge (Adachi et al., 2007; Porteous and Herbison, 2019).

Increases in spontaneous firing rate during positive feedback in the daily surge model are similar to those observed in naturally cycling animals on proestrus (Wang et al., 2016b, 2019b). Interestingly, given the changes in spontaneous firing, no studies have reported that feedback or estrous cycle stage affect the F-I curve of AVPV kisspeptin neurons. Our data and simulations suggest this lack of effect on the F-I curve is attributable to more suppressive K^+ currents during proestrus counteracting larger inward currents during depolarization, without inhibiting rebound burst firing.

Estradiol feedback also affects voltage-gated K^+ currents in other central neurons controlling reproduction. In GnRH neurons, inactivation of the transient K^+ current is depolarized by positive feedback in the daily surge model to a similar degree observed in the present study (DeFazio et al., 2002b). In contrast to AVPV neurons, however, peak K^+ current densities in GnRH neurons are reduced during positive feedback, and excitability is increased (Adams et al., 2018b). Interestingly, positive feedback effects in GnRH neurons may be at least in part attributable to increased kisspeptin receptor activation, as kisspeptin treatment has similar effects on transient K^+ currents in these cells (Pielecka-Fortuna et al., 2011). In arcuate kisspeptin neurons, K^+ currents were compared between open-loop (OVX) and estradiol negative feedback (DeFazio et al., 2019), with negative feedback reducing peak transient and sustained K^+ currents compared to open-loop but not affecting voltage sensitivity of activation/inactivation. Together these observations suggest the effects of estradiol and cycle stage on voltage-gated K^+ currents in the reproductive neuroendocrine circuitry depend on both cell type and type of feedback involved.

The subcellular mechanisms linking estradiol feedback to these effects have not been extensively studied but may include changes in channel subunit expression/composition, subcellular location of channels, binding by partner proteins, and/or subunit phosphorylation state (Coetzee et al., 1999; Levitan, 2006). In GnRH neurons, estradiol or cycle stage regulates expression of Ca^{2+}, HCN, and SK channel

genes (Zhang et al., 2009; Bosch et al., 2013; Rønnekleiv et al., 2015; Vastagh et al., 2019). K^+ channel genes are also estradiol-sensitive in the paraventricular and arcuate nuclei (Qiu et al., 2006; Roepke et al., 2007; Lee et al., 2013; Yang et al., 2016). Estradiol affects transcription of ion channels outside the central nervous system in neural (Du et al., 2014) and non-neural tissue (Marni et al., 2009; Banciu et al., 2018). In addition to transcription, estradiol action through membrane-associated signaling pathways can rapidly modulate L- and R-type Ca^{2+} and K-ATP currents (Sun et al., 2010; Zhang et al., 2010). Estradiol positive feedback effects on K^+ currents in GnRH neurons are attenuated by a broad-spectrum kinase inhibitor, suggesting a role of phosphorylation (DeFazio and Moenter, 2002). Estradiol may also interact directly with channels, as with voltage-gated BK channels in vascular smooth muscle (Granados et al., 2019). Effects of estradiol on CaT currents in AVPV kisspeptin neurons, however, are dependent on actions via ERα as cre-lox or CRISPR mediated ERα knockdown in these cells eliminates estradiol effects (Wang et al., 2019b).

The present results add important information to a growing list of voltage-gated conductances in AVPV kisspeptin neurons that are modified by the estrous cycle (Piet et al., 2013b; Zhang et al., 2015; Wang et al., 2016b). We used *in silico* approaches to amalgamate multiple experimental findings into a more comprehensive understanding of how hormonal manipulations/estrous cycle shape the membrane response of these cells as in other reproductive neuroendocrine neurons (Moran et al., 2016; Adams et al., 2018b; Mendonça et al., 2018; DeFazio et al., 2019). Simulation results suggest modulation of K^+ currents across the negative to positive feedback transition do not increase AVPV neuron excitability or enable rebound burst firing, as had been suggested by blocking the fast-transient current with 4AP in current-clamp studies (Wang et al., 2016b). Rather, proestrous shifts in subthreshold inward currents CaT, NaP, and HCN counteract suppressive K^+ currents during proestrus and enable rebound firing. Involvement of the former currents in rebound firing is consistent with

their role in shaping firing behavior (Lüthi and McCormick, 1998; Bevan and Wilson, 1999; Hille, 2001; Perez-Reyes, 2003).

The finding that cycle-dependent changes in intrinsic properties lead to no net change in excitability begs the question of how increased firing rates during proestrus are maintained when receptors for fast glutamate and GABA transmission are blocked (Wang et al., 2016b). First, neuromodulation via metabotropic receptors could occur, and may alter non-voltage-sensitive mechanisms, such as GIRK channels (Kelly and Qiu, 2010). Second, proestrous increases in spontaneous firing rate may be due to the emergence of rebound bursting (Wang et al., 2016b). The suppressive K^+ current changes observed on proestrus did not inhibit this process and may bestow properties to the cell that are otherwise beneficial. For example, these more suppressive K^+ currents may serve a protective/ homeostatic function by limiting the increase in excitability enabled by increases in depolarizing currents. An optogenetic study examining the relationship between AVPV neuron stimulation and GnRH neuron firing found delayed activation of GnRH neurons characteristic of kisspeptin receptor activation plateaus at 10 Hz (Piet et al., 2018), suggesting firing frequencies above this are unnecessary. Third, excitation-release coupling in AVPV neurons may be regulated by the estrous cycle. Small increases in release probability or the readily releasable pool of kisspeptin could have substantial downstream effects on GnRH neuron activation with only modest differences in AVPV neuron firing frequency. Of note, kisspeptin expression by these cells is increased during positive feedback (Smith et al., 2005; Gottsch et al., 2006). An important consideration for brain slice preparations is the disruption of neuronal projections that likely play a role in cycle-dependent changes. In rodents, input from the circadian clock is critical for surge induction (van der Beek, 1996); these and other afferents may be regulators of AVPV neuron activity *in vivo* and would not be present in the slices used (Watson et al., 1995).

In silico approaches provide the advantage of being able to test multiple hypotheses quickly but also have several caveats. First, while we sought to make the models reasonably comprehensive by including characterizations of currents reported in the literature, there are likely uncharacterized currents expressed in AVPV neurons that may change with cycle stage and/or influence firing behavior that were not included. Second, and related to the first point, no studies have characterized the transient sodium current in AVPV neurons. We adapted a Markov model of NaT used in a GnRH neuron model to enable firing in these models (Adams et al., 2018b). Estimating this current was guided by fitting the rising phase of the action potential to experimental data, the phase of the action potential most highly influenced by sodium channel properties (Kress et al., 2010). Third, no computational model is ever a perfect representation, and it is possible that other combinations of properties for the components of this model could produce similar results in firing output. Despite these limitations, our voltage-clamp models are well fit, and the firing simulations reasonably approximated the firing behavior of these cells.

Together these results point to changes in multiple voltage-dependent currents in these cells through the reproductive cycle. Our data and firing simulations suggest estrous cycle effects on these currents are unlikely to explain the increase in AVPV kisspeptin neuron spontaneous activity during the afternoon of proestrus, as changes in typically hyperpolarizing and depolarizing currents exert reciprocal effects on excitability, though the latter contribute to the emergence of post-inhibitory rebound burst firing. These findings motivate further study of the inputs controlling firing behavior of these cells as well as the mechanisms regulating their neurochemical and peptidergic output to GnRH neurons, and how these contribute to GnRH/LH surge generation.

Figures and Legends

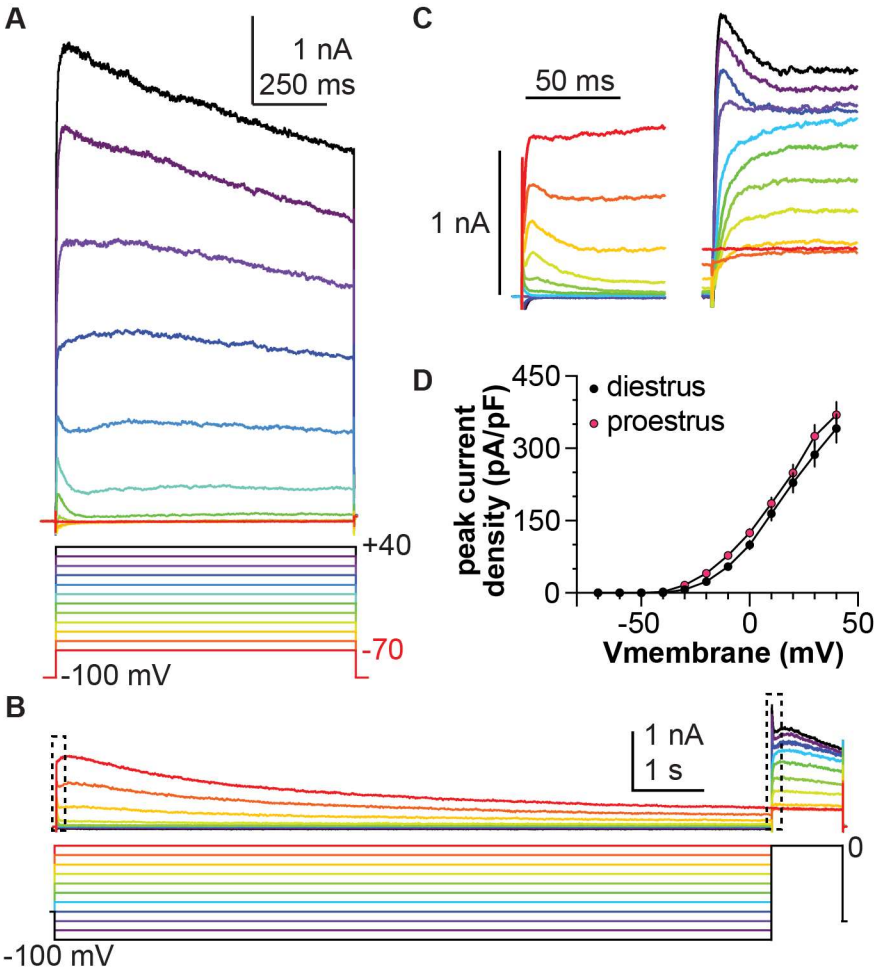

Figure 2-1 Total voltage-dependent K^+ current in AVPV kisspeptin neurons has three distinct components. **A.** Representative total K^+ current in response to the voltage-clamp protocol shown. **B.** Representative recording of total K^+ current from a different cell in response to the voltage protocol shown; both a slowly-inactivating and residual (sustained) component are evident during the extended prepulse. **C.** Expansions of the areas within the dashed boxes in B, showing the change in inactivation rates as more depolarizing prepulses are applied (left), and how this affects both activation and inactivation during the test pulse (right). **D.** Mean±SEM peak current density in cells from mice in diestrus (black symbols) and proestrus (magenta symbols). Error bars are smaller than symbols for some values.

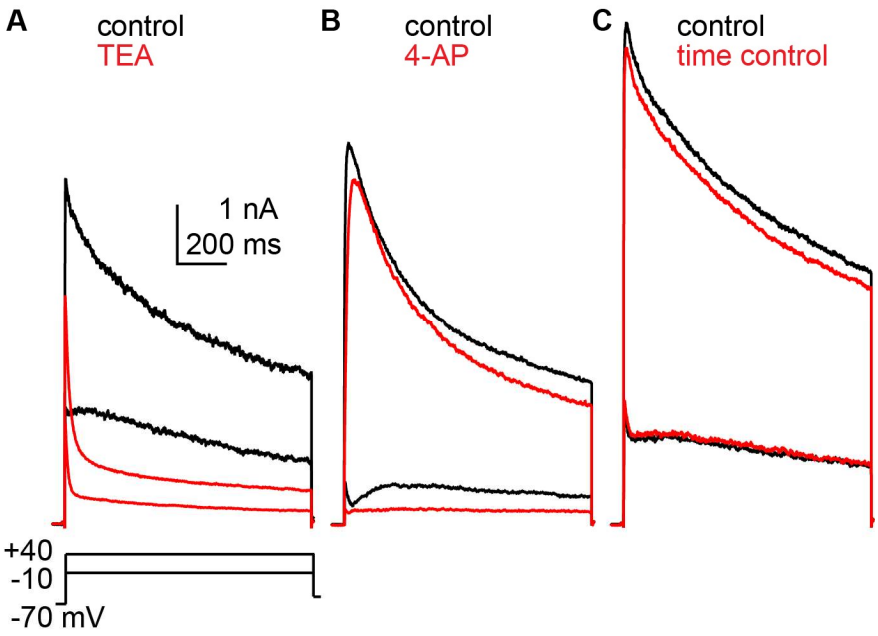

Figure 2-2 Potassium current recorded from three different cells before and during application of potassium channel blockers. **A.** 20 mM TEA. B. 5 mM 4-AP. **C.** time control.

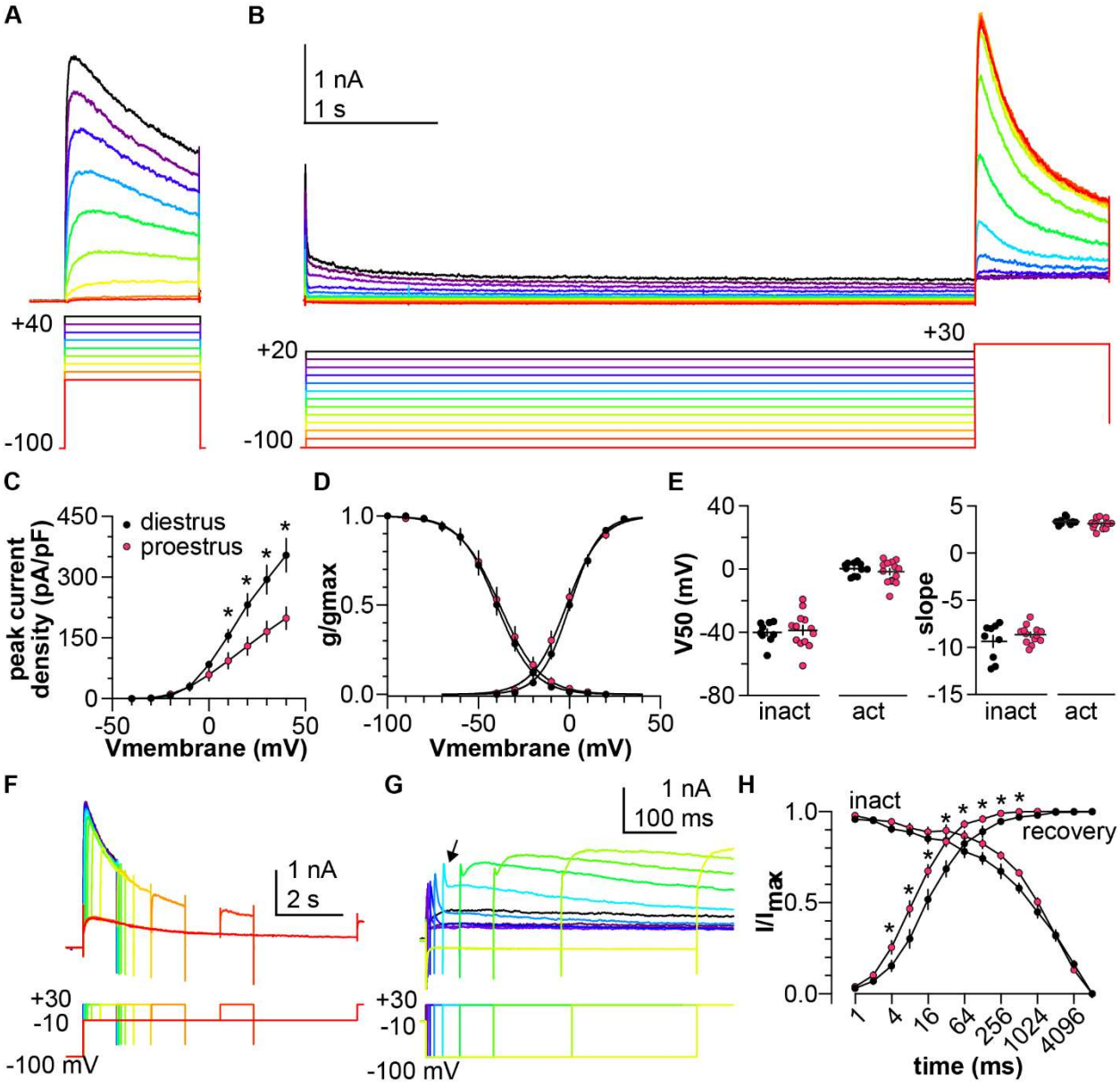

Figure 2-3 4-AP-resistant slow-transient voltage-dependent K^+ current is larger on diestrus. **A.** Representative traces (top) in response to the activation voltage-clamp protocol (bottom) in the presence of 5 mM 4-AP. **B.** Representative traces (top) in response to the inactivation voltage-clamp protocol (bottom). Offline leak subtraction was applied to test pulses only, hence the capacitance transient is visible at the start of the recording. **C.** Mean ± SEM peak current density from cells in mice in diestrus (black symbols) and proestrus (magenta symbols). **D.** Mean ± SEM normalized conductance. Solid lines are Boltzmann fits to the mean data. **E.**

Individual values and mean ± SEM parameters obtained from Boltzmann fits to normalized conductance curves for each cell. **F, G.** Representative traces (top) in response to the voltage-clamp protocol (bottom) used to measure the time-dependence of inactivation (F) and recovery (G). Arrow denotes peak of fast transient current. **H.** Mean ± SEM normalized peak current vs. prepulse duration for time-dependence of inactivation (inact) and recovery from inactivation. Error bars are smaller than symbols for some values. * p<0.05

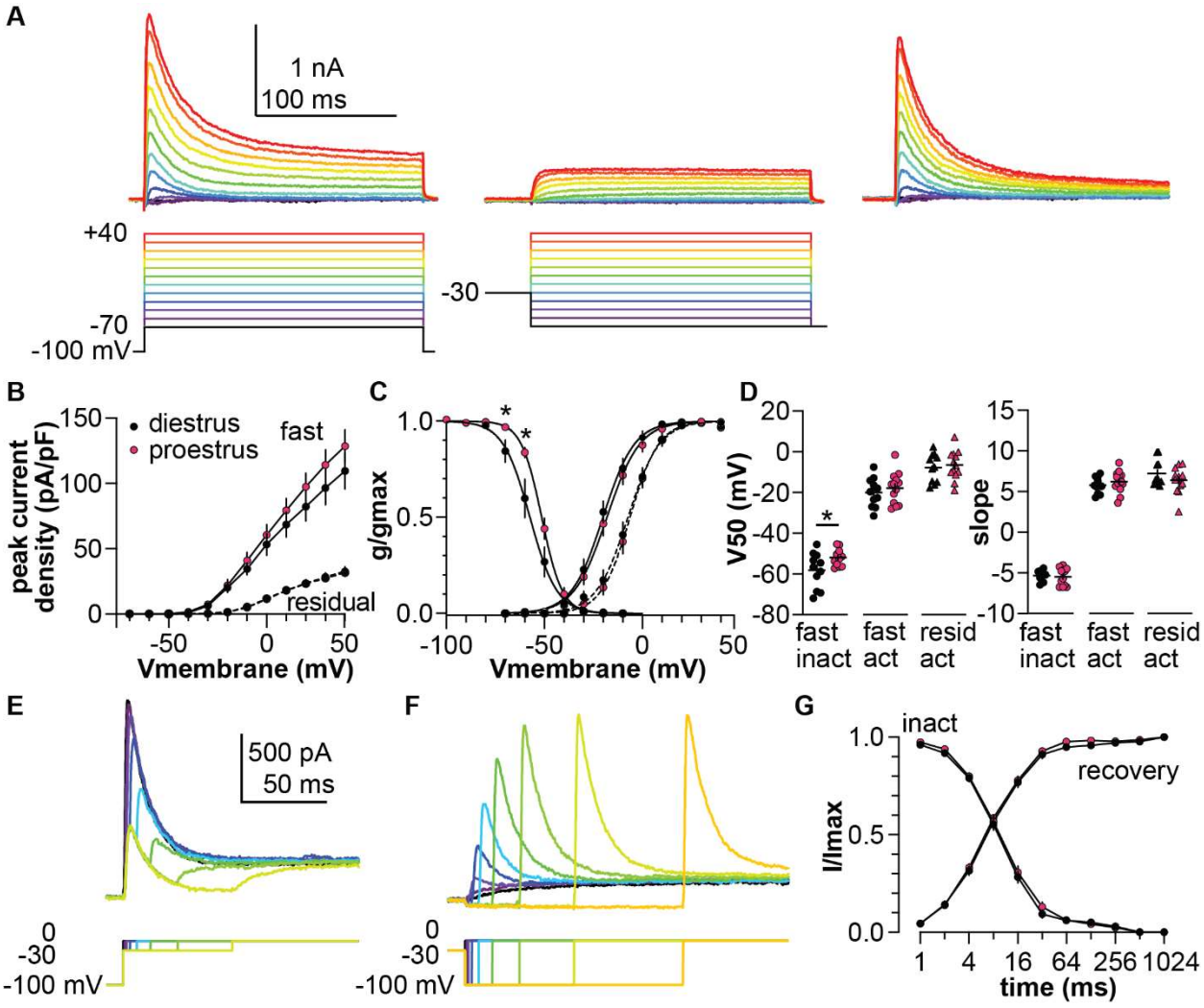

Figure 2-4 TEA-resistant fast-transient voltage-dependent K^+ current has a depolarized inactivation curve during proestrus**. A.** Left: Representative unsubtracted K^+ current (top) in response to the voltage-clamp protocol (bottom) in presence of 20 mM TEA. Middle: Residual current in the same cell with a -30 mV prepulse. Right: Fast transient current yielded by subtracting residual current from raw current. **B.** Mean ± SEM peak current density in cells from

mice in diestrus (black symbols) and proestrus (magenta symbols). **C.** Mean ± SEM normalized conductance. Solid lines represent Boltzmann sigmoidal fits to the mean data for the fast transient, dash lines the fits for the residual current. **D.** Individual values and mean ± SEM parameters obtained from Boltzmann fits to normalized conductance curves for each cell. **E,F.** Representative traces (top) in response to the voltage-clamp protocol (bottom) used to measure the time-dependence of inactivation (E) and recovery (F). **G.** Mean ± SEM normalized peak current vs. prepulse duration for time-dependence of inactivation (inact) and recovery from inactivation. Error bars are smaller than symbols for some values. * $p<0.05$

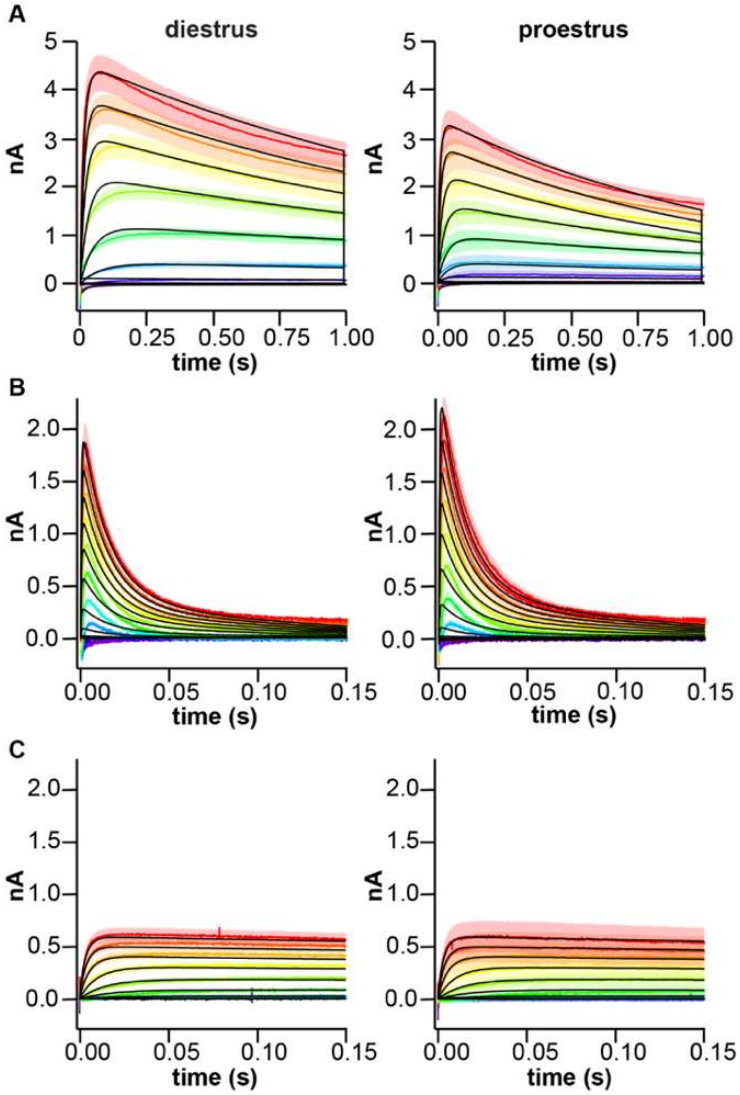

Figure 2-5 Potassium conductance model output vs experimental data for voltage steps. Rainbow colors indicate mean ± SEM current traces recorded at different test potentials; black lines show model simulations. In each panel, diestrus is on the left and proestrus on the right. **A.** Slow (voltage protocol as in Figure 2-3A). **B.** Fast (voltage protocol as in Figure 2-4A). **C.** Residual (voltage protocol as in Figure 2-4A).

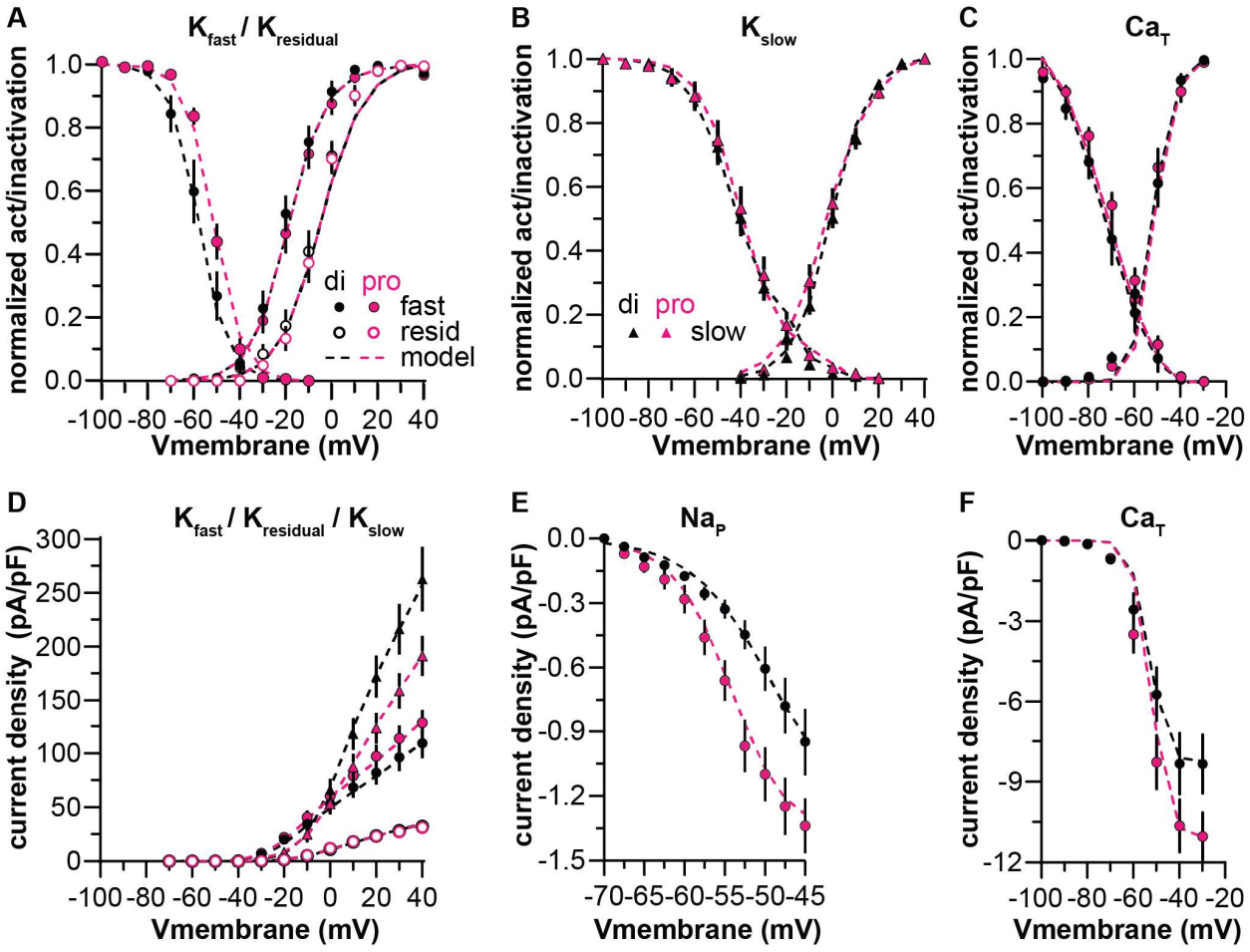

Figure 2-6 Conductance models vs data for steady state activation/inactivation and current density experimental data. A-C. Steady state activation/inactivation curves calculated from voltage-clamp simulations (dashed lines) compared to corresponding mean ± SEM experimental data (symbols) from diestrous (black) and proestrus (magenta) groups. **D-F**. Peak current density for various conductances. Experimental data for K^+ current subcomponents are the same as in Figures 2-3 and 2-4 and replotted here for ease of comparison. Data points for NaP (E) and CaT (C, F) are adapted from Wang et al., 2016.

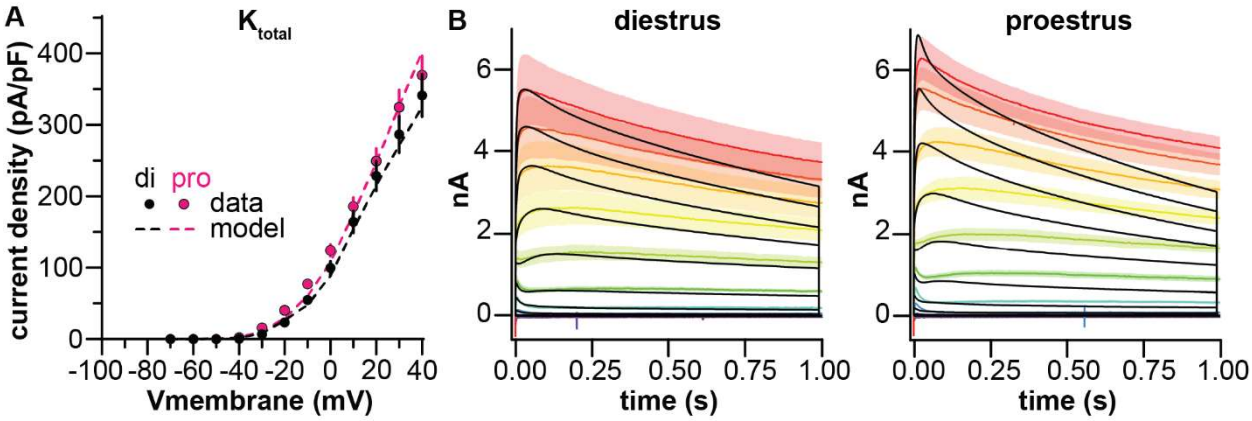

Figure 2-7 Reconstruction of the total K^+ current from the sum of the three subcomponents. **A.** Peak current density when I_{fast}, I_{slow}, and I_{resid} are simulated together in the same model (dashed lines) after $\bar{g}$ optimization to correct for suppression by TEA/4-AP. Mean ± SEM symbols (black: diestrus, magenta: proestrus) and voltage-clamp protocols are the same as shown in Figure 2-1A and 2-1D and are reproduced for ease of comparison. **B.** Mean ± SEM experimental current traces at different test pulses (rainbow colors) and model simulation (black).

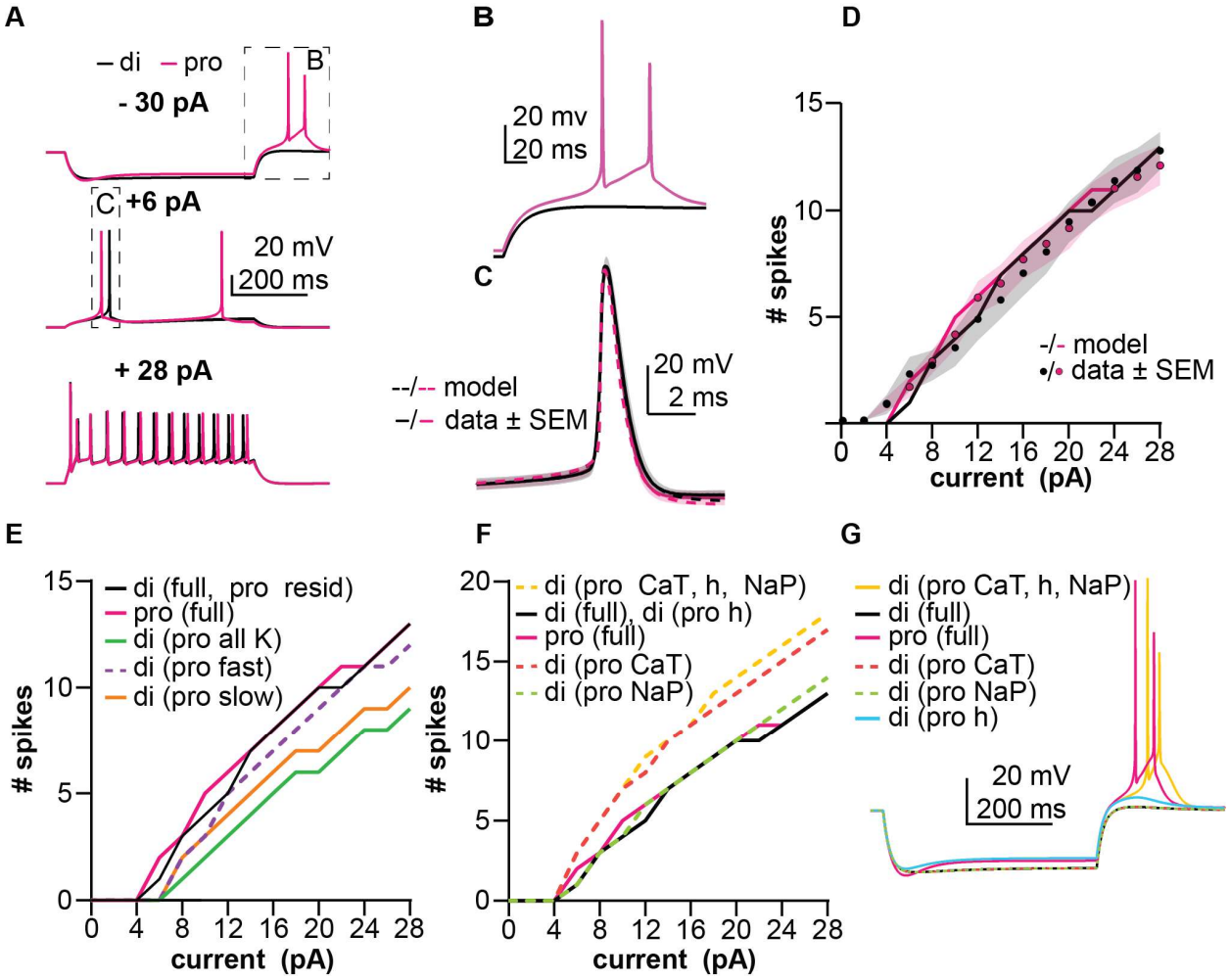

Figure 2-8 Simulations of firing from a baseline of -70 mV. **A.** Performance of diestrous (black) and proestrous (magenta) models in response to -30 pA (top), +6 pA (middle), and +28 pA (bottom) applied current. Boxed regions are shown with expanded axes in the indicated subfigure. **B.** Post-hyperpolarization rebound of diestrous and proestrus models from subfigure A. **C.** Rheobase action potentials for both models (dashed lines) from A (middle) and experimental counterparts (solid lines, mean ± SEM). **D.** Firing vs current (F-I) curves for diestrous and proestrous models (lines) and experimental counterparts (circles are means, shading is SEM). **E.** F-I performance of hybrid models in which one or multiple K^+ conductances in the diestrous model was substituted for a proestrous counterpart. Non-hybrid models from part D (di full and pro full) are reproduced here to facilitate comparison in this panel as well as F and G. **F.** F-I performance of hybrid models in which one or multiple subthreshold depolarizing currents in the diestrous model were replaced with proestrous counterparts. **G.** Rebound bursting performance of hybrid models in response to -30 pA current injection.

Tables

Table 2-1 Passive properties and statistical comparisons

By cycle stage	Diestrus	Proestrus		Mann Whitney U	Diff	p
Series resistance (MΩ)	15.8±0.3	15.5±0.4		2601	-0.1774	0.57
Input resistance (MΩ)	1045±46.3	917.1±59.4		2265	-86.68	0.07
Capacitance (pF)	17.3±0.5	18.1±0.7		2525	0.6704	0.4
Holding current (pA)	-21.6±2	-19.7±2.9		2601	0.0917	0.57
By drug	**none (total)**	**4- AP (slow)**	**TEA (fast)**	**Kruskal-Wallis**	**Diff**	**p**
Series resistance (MΩ)	15.7±0.5	16.4±0.4	15±0.5	4.87	-6.137 10.41 16.58;	0.09
Input resistance (MΩ)	816.8±50.0	1158±86.4	1179±84.4	16.31	-22.91 -25.98 -3.074;	<0.001
Capacitance (pF)	16.6±0.7	18.2±0.9	17.4±0.8	1.53	-8.139 -6.148 1.991;	0.47
Holding current (pA)	-18.7±4.1	-26.6±2.2	-18.9±3.3	3.154	-0.7543 -12.02 -11.27	0.21

Table 2-2 Two-way ANOVA analyses of K^+ current properties. Bold font indicates p<0.05**.**

	n cells, n animals		estrous stage	estrous stage x Vm or duration interaction
TOTAL	**di**	**pro**		
density	10, 4	17,5	Diff, -15.42 [CI -40.49, 9.660] F(1, 25) = 1.603; p=0.217	F (11, 275) = 0.6496 p=0.785
SLOW				
density	12, 5	13, 5	Diff, 24.07 [CI -5.523, 53.66] F (1, 23) = 6.503; p=0.106	**F (8, 184) = 10.03 p<0.001**
activation	12, 5	13, 5	Diff, -0.01901 [CI -0.06921, 0.03120] F (1, 25) = 5.283; p=0.442	F (11, 275) = 3.336 p=0.169
inactivation	9, 4	12, 5	Diff, -0.0009547 [CI -0.06269, 0.06078] F(1, 20) = 0.1782; p=0.975	F (12, 240) = 0.1988 p>0.999
rate of inactivation	10, 7	9, 4	Diff, -0.03472 [CI -0.08026, 0.01082] F (1, 17) = 2.587; p=0.126	F (14, 238) = 1.336 p=0.187
rate of recovery	9, 5	13, 5	**Diff, -0.05901 [CI -0.09461, -0.02342] F (1, 20) = 10.52; p=0.002**	**F (14, 280) = 4.006 p<0.001**
FAST				
density	11, 4	13, 4	Diff, -6.607 [CI -22.53, 9.317] F (1, 22) = 0.7404; p=0.399	F (11, 242) = 0.9366 p=0.506
activation	11, 4	13, 4	Diff, 0.01876 [CI -0.03188, 0.06940] F (1, 23) = 0.6133; p=0.450	F (8, 184) = 1.475 p=0.981
inactivation	11, 4	12, 4	**Diff, -0.05682 [CI -0.1119, -0.001691] F (1, 21) = 4.594; p=0.044**	**F (9, 189) = 4.041 p<0.001**
rate of inactivation	10, 4	12, 4	Diff, -0.0085 [CI -0.03704, 0.02004] F (1, 20) = 0.3859; p=0.541	F (11, 220) = 0.4253 p=0.944
rate of recovery	10, 4	12, 4	Diff, -0.01081 [CI -0.03695, 0.01532] F (1, 20) = 0.7448; p=0.398	F (11, 220) = 0.3670 p=0.967
RESIDUAL				
density	11, 4	13, 4	Diff, 0.07334 [CI -3.263, 3.409] F (1, 22) = 0.002079; p=0.964	F (11, 242) = 0.05676 p>0.999
activation	11, 4	13, 4	Diff, 0.01068 [CI -0.03932, 0.06068] F (1, 22) = 0.1962; p=0.662	F (11, 242) = 0.2095 p=0.997

Table 2-3 Two-sample analyses of K^+ current properties. Bold font indicates p<0.05. Differences shown for means for normally-distributed data and medians for non-normally-distributed data.

	n cells, n animals		estrous stage	estrous stage x Vm or duration interaction
TOTAL	**di**	**pro**		
density	10, 4	17,5	Diff, -15.42 [CI -40.49, 9.660] F(1, 25) = 1.603; p=0.217	F (11, 275) = 0.6496 p=0.785
SLOW				
density	12, 5	13, 5	Diff, 24.07 [CI -5.523, 53.66] F (1, 23) = 6.503; p=0.106	**F (8, 184) = 10.03 p<0.001**
activation	12, 5	13, 5	Diff, -0.01901 [CI -0.06921, 0.03120] F (1, 25) = 5.283; p=0.442	F (11, 275) = 3.336 p=0.169
inactivation	9, 4	12, 5	Diff, -0.0009547 [CI -0.06269, 0.06078] F(1, 20) = 0.1782; p=0.975	F (12, 240) = 0.1988 p>0.999
rate of inactivation	10, 7	9, 4	Diff, -0.03472 [CI -0.08026, 0.01082] F (1, 17) = 2.587; p=0.126	F (14, 238) = 1.336 p=0.187
rate of recovery	9, 5	13, 5	**Diff, -0.05901 [CI -0.09461, -0.02342] F (1, 20) = 10.52; p=0.002**	**F (14, 280) = 4.006 p<0.001**
FAST				
density	11, 4	13, 4	Diff, -6.607 [CI -22.53, 9.317] F (1, 22) = 0.7404; p=0.399	F (11, 242) = 0.9366 p=0.506
activation	11, 4	13, 4	Diff, 0.01876 [CI -0.03188, 0.06940] F (1, 23) = 0.6133; p=0.450	F (8, 184) = 1.475 p=0.981
inactivation	11, 4	12, 4	**Diff, -0.05682 [CI -0.1119, -0.001691] F (1, 21) = 4.594; p=0.044**	**F (9, 189) = 4.041 p<0.001**
rate of inactivation	10, 4	12, 4	Diff, -0.0085 [CI -0.03704, 0.02004] F (1, 20) = 0.3859; p=0.541	F (11, 220) = 0.4253 p=0.944
rate of recovery	10, 4	12, 4	Diff, -0.01081 [CI -0.03695, 0.01532] F (1, 20) = 0.7448; p=0.398	F (11, 220) = 0.3670 p=0.967
RESIDUAL				
density	11, 4	13, 4	Diff, 0.07334 [CI -3.263, 3.409] F (1, 22) = 0.002079; p=0.964	F (11, 242) = 0.05676 p>0.999

			Diff, 0.01068 [CI -0.03932, 0.06068]	F (11, 242) = 0.2095
activation	11, 4	13, 4	F (1, 22) = 0.1962; p=0.662	p=0.997

Table 2-4 Model parameters for diestrus

	slow		fast		residual		NaP		CaT		h	leak
***E* (mV)**	-92.00		-92.00		-92.00		50.00		155.00		-19.90	-70.00
$\bar{g}$ **(nS)**	37.4		36.9		29.7		0.14		1.60		0.11	1.06
	m	***h***	***m***	***h***	***m***	***h***	***m***	***h***	***m***	***h***	***m***	
V50	-1.70	-43.84	-19.22	-57.95	-5.54	-39.16	50.45	31.84	-55.61	-76.02	-97.55	
K	-7.73	8.41	-7.84	6.33 h1=14.55 h2=113.55	-8.85	11.29	-3.72	3.20	-5.45	10.90	4.19	
tau	Eq 8	Eq 8	Eq 9		Eq 8	Eq 8	0.40	Eq 10	Eq 9	Eq 9	Eq 9	
va	1.40	64.50	0.53		0.93	64.50		67.30	1.85	15.58	201.00	
b	1.54	1401.00	0.00		16.39	1401.65		-27.50	1.65	70.15	0.00	
c	15.81	59.70	-8.68		44.02	59.77		67.30	-60.60	-57.66	-2.20	
d	-0.27	-6.42	7.88		-0.33	-6.42		27.50	5.00	3.61	-5.95	
e	8.67	1.34			0.13	1.34		4650.15				
f	2.89	-8.26			-6.77	-8.26		62.48				
g	8.50	1.82			7.76	1.82						
r								1		2	1	n/a

Table 2-5 Model parameters for proestrus

	slow		**fast**		**residual**		**NaP**		**CaT**		**h**	**leak**
***E* (mV)**	-92.00		-92.00		-92.00		50.00		155.00		-19.90	-70.00
$\bar{g}$ **(nS)**	42.0		45.7		32.9		0.20		2.0		0.64	0.88
	m	***h***	***m***	***h***	***m***	***h***	***m***	***h***	***m***	***h***	***m***	
V50	-3.71	-40.51	-19.22	-57.13	-5.54	-39.16	50.45	31.84	-54.87	-74.00	-97.55	
K	-9.01	8.41	-7.84	6.33	-8.85	11.29	-3.72	3.20	-5.45	10.90	4.19	
				h1=14.55								
				h2=113.55								
tau	Eq 8	Eq 8	Eq9		Eq 8	Eq 8	0.40	Eq 10	Eq 9	Eq 9	Eq 9	
a	1.40	64.50	0.47		0.93	64.50		67.30	1.85	15.58	201.00	
b	0.66	873.09	0.00		16.39	1401.65		-27.50	1.65	70.15	0.00	
c	20.02	46.89	-8.68		44.02	59.77		67.30	-60.60	-57.50	-2.20	
d	-0.20	-6.42	7.88		-0.33	-6.42		27.50	5.00	3.61	-5.95	
e	8.67	1.34			0.13	1.34		3980.90				
f	-8.10	-8.26			-6.77	-8.26		62.48				
g	10.50	1.82			7.76	1.82						
r								1		2	1	n/a

Table 2-6 NaT parameters

Di/Pro	NaT			
***E* (mV)**	50.00			
$\bar{g}$ **(nS)**	68.12			
	α(V)	**β(V)**	**r1(V)**	**r3(V)**
s	65.24	48.59	9.52	12.68
k	-6.05	5.09	-4.66	3.08
r	38.40	391.84	1.36	0.014

Chapter 3: Optogenetic Activation of AVPV Kisspeptin Neurons Evokes Similar Changes in GnRH Neuron Spike Rate During Estradiol Negative vs. Positive Feedback

Introduction

The ovarian steroids of the female reproductive cycle shape structure and function in many brain regions. Steroids influence neuroplasticity, evidenced by changes in synaptic architecture and transmission in areas such as the hippocampus, amygdala, and hypothalamus (Cooke and Woolley, 2005). They can also affect a range of cognitive functions, such as memory, emotion, and attention, and may contribute to increased vulnerability to certain neuropsychiatric disorders in women (Galea et al., 2017). The physiologic mechanisms controlling ovarian steroid synthesis and cyclicity are therefore important regulators of brain function and reproductive health.

The hypothalamo-pituitary-gonadal (HPG) axis drives the fluctuating synthesis of ovarian steroids during the female reproductive cycle. The HPG axis itself displays ovarian steroid-regulated functional changes during the cycle, mediated by steroid feedback loops that alter neurosecretory output of the hypothalamus (Neill et al., 1977; Moenter et al., 1991). During the female cycle, the neuroendocrine release of gonadotropin-releasing hormone (GnRH) is regulated by ovarian estradiol and progesterone. These form negative feedback loops that suppress the amplitude and/or frequency of GnRH pulses released from the median eminence (Karsch et al., 1987b; Evans et al., 1994). GnRH pulses promote pulsatile gonadotropin release from the pituitary, driving folliculogenesis and steroidogenesis at the ovary. During the late-follicular phase (proestrous afternoon in nocturnal rodents), high-concentration estradiol from the mature follicle(s) exerts positive feedback inducing a change from pulsatile GnRH release to continuous release lasting several hours, referred to as a preovulatory surge (Sarkar et al., 1976b; Moenter et al., 1991; Pau et al., 1993). The GnRH surge

induces a surge of luteinizing hormone (LH) release which triggers ovulation. The neural bases for this estradiol-positive-feedback-initiated transition in GnRH output are not fully understood.

Estrogen receptor α (ERa), necessary for estradiol feedback on the HPG, is not detected in GnRH neurons (Hrabovszky et al., 2000). Feedback, therefore, must be relayed by estradiol-sensitive afferents. For positive feedback, this role is thought to be played by kisspeptin neurons in the rostral hypothalamus (Dungan et al., 2006). In rodents, these cells reside in the anteroventral periventricular area (AVPV). Immunohistochemical and bioinformatic studies have revealed markers of several amino acid-derived and peptidergic mediators expressed by AVPV kisspeptin neurons (Cravo et al., 2011; Stephens and Kauffman, 2021), however, the question of which signals are directed by these cells towards the GnRH neuron can only be answered by functional studies, of which there have been few (Qiu et al., 2016; Piet et al., 2018). Furthermore, the possibility that modulation of the structural connectivity of this pathway during the estrous cycle contributes to the transition from pulse (negative feedback) to surge (positive feedback) GnRH secretion has not been functionally explored.

Here, we have interrogated transmission between AVPV kisspeptin and GnRH neurons in brain slices from diestrous, proestrous, and ovariectomized mice to test the hypothesis that this transmission pathway is plastic across ovarian hormonal states. We also examined time of day in an OVX/OVX+E daily surge model that exhibits diurnal shifts in estradiol feedback action. Cell-specific photoactivation of preoptic area projections of the AVPV kisspeptin population was coupled with electrical recordings of individual GnRH neurons. We designed photostimulation and recording protocols for characterizing ionotropic and metabotropic signaling modalities.

Materials and Methods

Animals.

The University of Michigan Institutional Animal Care and Use Committee approved all procedures. Adult female (80-185d) GnRH-GFP (Suter et al., 2000) Kiss-Cre; Kiss1-hrGFP (Cravo et al., 2011), and Kiss-Cre;GnRH-GFP mice were used for these studies. Mice were provided with Harlan 2916 chow and water *ad libitum* and were held on a 14:10 h light:dark cycle. Estrous cycle stage was monitored by daily vaginal cytology from the day of stereotaxic surgery until brain slice preparation. Uterine mass was measured after brain slice preparation to confirm cycle stage. Uterine mass >100 mg indicated *in vivo* exposure to a high concentration of estradiol, typical of proestrus, whereas mass <60 mg indicated exposure to low estradiol, typical of diestrus and OVX (Shim et al., 2000b).

Experimental design

Stereotaxic injection of virus with a floxed opsin payload (AAV-Syn-FLEX-rc[ChrimsonR-tdTomato]) was used to target the AVPV in kisspeptin-cre, kisspeptin-GFP mice (Cravo et al., 2011; Klapoetke et al., 2014). Infection was validated to be in the targeted cells using immunofluorescence and control experiments done to empirically determine parameters for optogenetic stimulation of kisspeptin neurons. Female kiss-Cre:GnRH-GFP mice similarly stereotaxically injected were used to record the response of GnRH neurons to activation of AVPV kisspeptin neurons, with recordings made in the late afternoon from diestrus, proestrus or ovariectomized (OVX) mice (Suter et al., 2000). OVX and OVX+E mice were also examined in the AM vs PM to look for diurnal changes. Initially, extracellular recordings were used to monitor firing response to activation. At the conclusion of the extracellular recording, the pipette was slowly retracted from the neuron and replaced with a new pipette filled with solution appropriate to measure postsynaptic currents, which was used to perform a whole-cell recording of the same cell. In some cells, only whole-cell recording of fast synaptic connections were made.

Stereotaxic surgery.

Mice were anesthetized with 1.5–2% isoflurane to effect. Carprofen (Zoetis, Inc., 5 mg/kg, sc) was given before and 24 h after surgery to alleviate postsurgical pain. After exposing the skill and performing a craniotomy, AVPV injections were targeted 0.2 mm anterior to Bregma, 5.4 mm ventral to Bregma, and ±0.2 mm lateral to the center of the superior sagittal sinus. Bilateral injections of 100 nl virus (AAV-Syn-FLEX-rc[ChrimsonR-tdTomato], Addgene viral prep # 62723-AAV5) were made at the target coordinates at ~5 nl/min (Klapoetke et al., 2014). The pipette was left in place for 5 min after injection to allow virus to diffuse into the brain, then raised 100 µm and left in place for another 5 min. Estrous cycle monitoring continued after surgery for up to 8 weeks.

Immunofluorescence

Mice (n=2) were anesthetized with isoflurane and transcardially perfused with PBS (15–20 mL) then 10% neutral-buffered formalin for 10 min (~50 mL). Brains were placed into the same fixative overnight, followed by 30% sucrose for ≥24 h for cryoprotection. The brain was then rapidly frozen in optical cutting temperature compound and sections (30 µm, four series) were cut on a cryostat (Leica CM3050S) and stored at −20°C in antifreeze solution (25% ethylene glycol, 25% glycerol in PBS). Sections were washed with PBS, then placed in blocking solution (PBS containing 0.1% TritonX-100, 4% normal goat serum, Jackson Immunoresearch) for 1 h at room temperature (21-23C), then incubated with chicken anti-GFP (Abcam 13970) and rabbit anti-RFP (Invitrogen 710530) in blocking solution overnight at 4 C. Sections were then washed with PBS and incubated with Alexa Fluor 488-conjugated goat anti-chicken and Alexa Fluor 594-conjugated goat anti-rabbit antibodies (Jackson Immunoresearch) for 90 min at room temperature on a Thermomixer at 100 RPM. Sections were then washed with PBS and mounted on Superfrost+ slides (Thermofisher) for imaging. Images were collected on a

Cytation 5 (Agilent) multimode reader. The number of immunoreactive GFP-only, tdTomato-only, and GFP/tdTomato cells were counted in the injected region. The arcuate region was examined to look for off target infection of kisspeptin neurons.

Ovariectomy

To examine the role of circulating ovarian factors, mice were ovariectomized (OVX) under isoflurane anesthesia (Abbott). These mice were studied 2d after surgery. For sham surgeries, the same procedure was followed but the ovaries were left intact. Vaginal smears were performed daily following sham surgery, and mice were selected for experiments on the appropriate cycle day 3-7 days after surgery. Some mice were OVX and also received a Silastic implant containing either 0.625µg estradiol 17ß or sesame oil vehicle subcutaneously in the scapular region. Bupivacaine (0.25%, APP Pharmaceuticals) was provided local to incisions as an analgesic for these procedures.

Brain slice preparation

Chemicals were purchased from Sigma-Aldrich unless noted. All solutions were bubbled with 95% O_2/5% CO_2 for at least 15 min before exposure to tissue. Mice were euthanized at ZT12, the expected peak of the LH surge (Christian et al., 2005a). The brain was rapidly removed and placed in ice-cold sucrose saline solution containing in mM: 250 sucrose, 3.5 KCl, 25 $NaHCO_3$, 10 D-glucose, 1.25 Na_2HPO_4, 1.2 $MgSO_4$, and 3.8 $MgCl_2$, and adjusted to pH 7.6 and 345 mOsm. Coronal (300 µm) slices were cut with a VT1200S vibrating microtome (Leica Biosystems). Slices were incubated for 30 min at room temperature in a 1:1 mixture of sucrose saline and artificial CSF (ACSF) containing in mM 135 NaCl, 3.5 KCl, 26 $NaHCO_3$, 10 D-glucose, 1.25 Na_2HPO_4, 1.2 $MgSO_4$, and 2.5 $CaCl_2$, and adjusted to pH 7.4 and 305 mOsm room temperature (~21–23°C). Slices were then transferred to 100% ACSF for an additional 30–180 min at room temperature before recording.

For recording, slices were placed into a chamber and perfused (3 ml/min) with carboxygenated ACSF kept at 31°C with an inline heating unit (Warner Instruments). All recordings (described below) were performed with an EPC-10USB patch-clamp amplifier and PatchMaster software (HEKA Elektronik). Recording pipettes were pulled from borosilicate capillary glass using a Flaming/Brown P-97 puller (Sutter Instruments) to obtain pipettes with a resistance of 2.5-3.5 MΩ. At the end of a recording session, the pipette was left in place and brightfield (differential interference contrast) and fluorescent (GFP, tdTomato) images were taken using 4x and 40x objectives to map the location of the cell and estimate its apposition by kisspeptin processes. Brain slices were placed in 10% phosphate-buffered formalin overnight at 4C, then either stored in 0.1M phosphate-buffer for up to two weeks or mounted on slides for post-hoc visualization of GFP and tdTomato expression.

Extracellular recordings

Targeted extracellular recordings were made to obtain firing patterns of GnRH-GFP or Kiss-Cre; Kiss1-hrGFP neurons (Nunemaker et al., 2003a). This method was used because it maintains internal milieu and has a minimal impact on the firing rate of neurons (Alcami et al., 2012). Pipettes were filled with a HEPES-buffered solution containing (in mm) 150 NaCl, 10 HEPES, 10 glucose, 2.5 CaCl2, 1.3 MgCl2, and 3.5 KCl, at pH 7.4 and 310 mOsm. GFP-expressing neurons were identified by brief (<2s) illumination at 470 nm. Low-resistance (< 50 MΩ) seals were formed between the pipette and neuron after first exposing the pipette to the slice tissue in the absence of positive tip pressure. Recordings were made in voltage-clamp mode with a 0 mV pipette holding potential. Signals were acquired at 20 kHz and filtered at 8.6 kHz. Resistance of the loose seal was checked frequently during first 3 min of recordings to ensure a stable baseline. Every minute, the offset potential was adjusted to set the baseline current to 0 pA. Cells that exhibited no spikes during recording were excluded from analysis, as the loose seal could not be verified as intact (n=3, OVX PM: 2, OVX+E PM: 1).

Whole-cell recordings

Whole-cell voltage-clamp recordings were made of spontaneous and light-evoked postsynaptic currents (PSCs) in GnRH-GFP neurons. Pipettes were wrapped with parafilm to reduce capacitance transients and filled with a solution containing (in mM): 140 KCl, 10 HEPES, 5 EGTA, 0.1 $CaCl_2$, 4 MgATP, and 0.4 NaGTP. All potentials reported were corrected on-line for a calculated liquid-junction potential of -4.9 mV (Barry, 1994). After achieving the on-cell configuration with seal resistance >2.0 GΩ, fast capacitive transients were minimized and the whole-cell configuration was achieved by rupturing the cell membrane with brief suction. The membrane potential was held at -65 mV during all voltage-clamp protocols, except during test pulses used to measure passive membrane properties. Passive membrane properties and voltage-clamp quality were calculated from the averaged current response (after on-cell capacitive current subtraction) to sixteen -5-mV, 20-ms test pulses from a holding potential of -65 mV performed immediately before and after each protocol. The following recording quality control criteria were required for analysis: series resistance (Rs) <25 MΩ, input resistance (Rinput) >500 MΩ, stable capacitance (Cm) between 8 and 30 pF, holding current (Ihold) between -60 and 10 pA.

Photostimulation hardware and pilot studies

A custom light-emitting diode (LED) system was coupled to the epifluorescence port of an Olympus BX51 microscope and used for widefield illumination and optical stimulation of brain slices via a 40x LUMPlanFl/IR water-immersion objective. For GFP excitation, a 470 nm (“blue”) LED was coupled with a 470 nm (40 nm FWHM) filter. For excitation of tdTomato, a neutral white (4100K) LED was coupled with a 542 nm (20 nm FWHM) filter. For excitation of ChrimsonR, the white LED was coupled with a 620 nm (58 nm FWHM) “red” filter. The appropriate LED-filter combination was pulsed using analog voltage output of the EPC-10USB patch-clamp amplifier, coupled to an externally-

dimmable direct-current driver (Luxeonstar). Peak optical power was measured using Thorlabs PM101/S170C power meter to be 15.5mW/mm2 when using 620 nm filter by placing distilled water on the sensor surface and lowering the 40x objective into the water to within working distance relative to the sensor surface. This power was used for all stimulations unless otherwise stated.

To determine the parameters effective for optogenetic stimulation of kisspeptin neurons, targeted extracellular recordings were made of GFP/tdTomato-coexpressing cells in slices from ovary-intact kisspeptin-GFP, kisspeptin-cre mice 3-4 wks after virus injection. Trains of 30 red light pulses were applied with varying pulse width (0.5-2ms) and pulse frequency (1-80 Hz). The range of these parameters was chosen based on previous studies (Klapoetke et al., 2014; Qiu et al., 2016; Piet et al., 2018). Spike fidelity was defined as the number of light pulses divided by the number of evoked spikes. Trains of 30 blue light pulses were also tested because of the need to illuminate the slice with 470nm light to identify GFP-expressing cells of interest for recording, combined with the substantial blue-end shoulder on ChrimsonR excitation. Blue light pulses at power needed to visualize GFP evoked spiking of ChrimsonR-expressing AVPV kisspeptin neurons. To determine if prolonged exposure to constant blue light impacts responsiveness to subsequent red light pulses, spike fidelity to red light was tested before and 5 minutes after a 15 second continuous exposure to blue light. This duration exceeded typical exposures used during GFP visualization, which typically lasted <~2s for each exposure.

The photostimulation paradigm for whole-cell recordings of GnRH-GFP neurons consisted of 60 trials of 1ms red light pulses. Inter-trial interval was 1s. Pulse durations were extended up to 50ms if the neuron did not display evoked PSCs in response to 1ms pulses; these also failed to evoke PSCs displaying monosynaptic characteristics (see below). For recordings from cycling mice, an additional photostimulus protocol was used to measure PSCs in response to a higher frequency stimulus. Spontaneous PSCs

were recorded for 30s prior to a 30s train of red light pulses (1 ms) at 20 Hz. Spontaneous PSCs were then recorded for an additional 30s post stimulus.

Extracellular recordings were performed to determine stimulus train parameters effective for evoking long-term changes in firing rate suggestive of peptidergic/metabotropic transmission. GnRH neurons were recorded extracellularly in slices from OVX and OVX+E mice. Baseline spontaneous firing rate was recorded for 2 min before two 10 Hz (duration of each pulse), 20s red light stimulus trains. Spontaneous firing was recorded for 5 min after each train to assess response. A 20 Hz, 30s red light stimulus train was then applied and firing recorded for an additional 5 min. These experiments suggested 20 Hz, 30s evoked responses in both animal groups; these parameters were thus chosen for future experiments examining the effect of cycle stage. For some neurons (n=5), pharmacology was used to identify transmitters mediating evoked PSCs. This involved applying a 60 trials of 1 ms red light pulses (1 s inter-trial interval) in the following sequence of conditions: baseline (ACSF), after addition of CNQX (10 μM), after addition of GABAzine (5 μM), and washout (ACSF). In some neurons (n=3), a similar paradigm was used to test if evoked PSCs were monosynaptic (Petreanu et al., 2009; Qiu et al., 2016). This involved sequential application of CNQX followed by TTX (5 μM) followed by 4-AP (0.5 mM). PSCs rescued by 4-AP were then challenged with GABAzine followed by washout.

Data analysis

For extracellular recordings, action currents were detected off-line using custom scripts in Igor Pro 9 (Wavemetrics). For recordings in daily surge mice, baseline spike rate was calculated as the mean spike rate during the first 2 min of recording. Response firing rate was calculated as the average firing rate during the 5 min starting at the beginning of each stimulus train. This period was chosen because it captured the peak response. For recordings in cycling mice, baseline for the during-stimulus interval was calculated

as the mean spike rate during the 30 seconds prior to the stimulus train. Baseline for the post-stimulus period was calculated as the mean spike rate during the 2 minutes prior to the stimulus train. The response period was calculated as the mean spike rate during the 5 minutes following the end of the stimulus train. For whole-cell recordings, PSCs were categorized as evoked and monosynaptic if they were <10 ms latency and low jitter (<3 ms standard deviation). Latency was calculated as the time between the beginning of each light pulse and the peak of the PSC. These values are based on pharmacologically-confirmed monosynaptic connections (described above).

Statistical analyses

Data were analyzed using Igor Pro 9 and Prism 9 (GraphPad). Shapiro-Wilk was used to test distribution of the data. Parameters (mean ± SEM) were compared between animal groups with unpaired statistical tests appropriate for experimental design and data distributions as indicated in the results section. The number of cells per group is indicated by n.

Results

ChrimsonR expression in AAV-injected mice was limited to the AVPV

Brain slices used for electrophysiology exhibited tdTomato expression in cell bodies and local projections in the AVPV (Fig 3-1A). The arcuate nucleus was also examined for off-target transfection. Figure 3-1 B depicts a representative sagittal slice exhibiting tdTomato-expressing somata and local projections in the AVPV but not the arcuate nucleus. In Figure 3-1C, a 30 µm coronal section from a perfused mouse shows tdTomato expression in fibers near the median eminence and in the arcuate nucleus but not in cell bodies. Innervation of the POA by tdTomato positive fibers was also seen (Fig. 3-D). In an initial attempt, we were unable to obtain anti-GFP immunostaining in 30

μm sections, precluding a detailed analysis of GFP/tdTomato coexpression analysis in injected Kiss-Cre;Kiss-hrGFP mice at this time.

Photoactivation of AVPV kisspeptin neurons

We used optogenetics to achieve cell-specific activation of AVPV kisspeptin neurons in brain slices. ChrimsonR, a red-activated channelrhodopsin with fast kinetics (Klapoetke et al., 2014), was chosen because we needed to identify GnRH neurons by GFP expression in Kiss-Cre;GnRH-GFP mice (Suter et al., 2000; Cravo et al., 2011). Initial spike-fidelity control experiments were performed in virus-injected Kiss-Cre;Kiss-hrGFP mice (Cravo et al., 2011). Neurons coexpressing tdTomato/GFP in the AVPV (Fig 3-2A) were targeted for extracellular recordings of action currents ("spikes") while delivering red-light pulses (Fig. 3-2B). Spike fidelity was maintained >95% on average up to 20 Hz but was reduced at stimulus frequencies ≥40 Hz (Fig. 3-2C). There was an effect of frequency but not pulse width within the range tested, and no interaction between these parameters (Table 3-1). A pulse width of 1ms was chosen for the remainder of experiments. These results indicated photostimulation could drive at least 20 Hz spiking of AVPV kisspeptin neurons.

To test if the red-shifted activation spectrum of ChrimsonR could circumvent cross-activation of blue-activated channelrhodopsins while visualizing GFP, activation by blue light was also tested. Blue-light pulses (1 ms) induced spikes in Kiss-Cre:Kiss-GFP neurons (Fig. 3-2D). To test if prolonged photoactivation caused by cross-activation during GFP visualization may impact responsiveness to subsequent photostimulation pulses, spike fidelity was examined (30 s of red-light pulses at 10 Hz) before and after 15 s constant blue light exposure (Fig. 3-2E). Mean±SEM spike fidelity was above >95% (before, 98.5±3.0%, after, 99.45±1.2%) and not different before vs after blue-light

exposure (Fig. 3-2F, Table 3-1). This indicated exposure to shorter duration blue light (<~2s) was unlikely to impact the spike fidelity of subsequent red-light stimulus trains.

Response of GnRH neurons to activation of AVPV kisspeptin neurons in brain slices from the daily LH surge mouse model

Whole-cell voltage-clamp recordings of GnRH-GFP neurons in sagittal brain slices from virus-injected Kiss-Cre;GnRH-GFP OVX and OVX+E mice were performed in the afternoon (ZT12). Sagittal slices were chosen for initial studies to attempt to preserve soma of projecting AVPV neurons as well as projections. GnRH-GFP neurons near td-Tomato ChrimsonR fibers were targeted for recording (Fig. 3-3A). ChrimsonR-positive fibers within the field of view were photoactivated by 1ms red light pulses at 1 Hz. An example recording showing 60 trials overlaid is shown in Figure 3-3B. None of the 20 GnRH-GFP neurons in OVX mice and 6 of 23 neurons recorded from OVX+E mice displayed evoked PSCs (Fig 3-3C). The classification of PSCs as evoked vs non-evoked was based on latency and jitter calculations from pharmacologically-confirmed monosynaptic PSCs observed in experiments discussed below. The mean±SD latency of evoked PSCs from OVX+E mice was 6.8±2.4 ms.

In separate cells, we next tested the effects of activation of AVPV kisspeptin neurons on GnRH neuron firing rates in sagittal slices from OVX and OVX+E mice. Slices were prepared during the morning (ZT4) vs afternoon (ZT12). Three photostimulus trains were applied with 5-min intertrain interval: 10 Hz (20s duration), 10 Hz (20s), and 20 Hz (30s) (Fig. 3-3D). These frequencies and durations were informed by prior studies that successfully evoked delayed, prolonged activation of GnRH neurons with photo- or electrical activation of AVPV neurons (Liu et al., 2011; Qiu et al., 2016; Piet et al., 2018). The baseline and response periods over which mean firing rates were calculated are shown in Figure 3-3D. There was no effect of steroid, time of day or steroid x time of

day interaction on baseline firing rate (Fig. 3-3E, Table 3-2). There was an increase in firing rate vs baseline during the 20 Hz response period but not during either 10 Hz response period (Table 3-2). There was no effect of steroid or time of day or interactions among any of these variables (Fig. 3-3F, Table 3-2), but some cells from both OVX and OVX+E mice exhibited a delayed increase in firing despite an apparent paucity of fast synaptic connections in the former. Serum LH measured in trunk blood collected at the time of brain slice preparation indicated estradiol implants did not induce LH surges in the afternoon, rather these mice displayed LH levels similar to OVX+E mice examined in the morning (ZT4) and indicative of negative feedback (Fig. 3-3G, Table 3-2). Uterine masses were higher in OVX+E mice compared to OVX independent of time of day (Table 3-2), typical of estradiol exposure.

Response of GnRH neurons to activation of AVPV kisspeptin neurons in brain slices from diestrous and proestrous mice

Based on lack of induction of positive feedback in the daily LH surge model, we switched to comparing diestrous and proestrous mice in the afternoon (ZT12) to test for differences between negative and positive feedback, respectively. Serum LH levels and uterine mass were higher in proestrous vs diestrous mice indicating positive feedback and increased estradiol exposure, respectively (Fig. 3-4A, Table 3-3). For studies in cycling mice, several changes were made. We adapted the photostimulation protocol during extracellular recordings to a single 20 Hz, 30s stimulus train (Fig. 3-4B, left), as this was the most effective at inducing a response in the above experiments. Given the paucity of fast synaptic transmission with the attempted preservation of AVPV soma within the slice, we switched to coronal brain slices as this provides more slices containing GnRH neurons per mouse. The baseline recording period and post-stimulus response period were extended to 15 min to acquire a more representative sample of spontaneous activity and capture longer-duration responses, respectively. Finally, due

to the finding that GnRH neurons from OVX mice could respond with a delayed increase in firing despite lack of detecting evoked PSCs in these mice, we modified our recording strategy by using sequential extracellular then whole-cell recordings for each neuron, providing firing rate and ionotropic connectivity data for each recorded cell, when successfully performed.

Extracellular recordings of GnRH-GFP neurons near tdTomato fibers were made while applying the adapted stimulus paradigm (Fig. 3-4B, left). Successful whole-cell recordings were obtained from 3 of 18 cells from diestrous mice and 3 of 14 cells from proestrus mice (Fig. 3-4C). As was observed in the daily surge model, a minority of cells demonstrated evoked PSCs in response to red-light pulses (Fig 3-4B top, Fig. 3-4C). This was similar to coronal slices in OVX+E mice indicating slice orientation did not have a major impact on these earler data. These cells were classified as “evoked” cells for analysis. Cells that did not display evoked PSCs were classified as “no-evoked” (Fig. 3-4B, bottom right).

Initial data indicated no effect of estrous cycle stage on baseline firing rate (Fig. 3-4E, Table 3-3). Firing rates were elevated compared to historical data (Silveira et al., 2017). We therefore tested if this was attributable to viral transfection, damage during surgical approach and/or ChrimsonR expression in the brain slice by performing similar recordings in unoperated diestrous GnRH-GFP mice. Baseline firing rates measured in these mice were not different from experimental groups (Fig. 3-4E, Table 3-3). When evoked/no-evoked classification was incorporated as a variable (two-way ANOVA; this precludes EC-only cells from analysis) there was no effect of cycle stage, evoked/no-evoked classification, or interaction on baseline firing rate (Table 3-3).

The average responses in all cells from diestrous and proestrous mice are shown in Figure 3-4D (top). Responses showed two phases: an immediate increase in firing rate

during the stimulus train and a delayed and prolonged increase in firing rate. Neurons from diestrous vs proestrous mice did not respond differently during the stimulus or during the post-stimulus phase (Figure 3-4F, Table 3-3). When evoked/no-evoked was incorporated as a variable (three-way repeated-measures ANOVA, this precludes EC-only cells from analysis), there was an effect of evoked/no-evoked and response period x evoked/no-evoked classification interaction (Figure 3-4F, Table 3-3), reflective of an increase in spike rates during the stimulus in evoked but not no-evoked cells (Table 3-3). There was no effect of cycle stage or interactions of cycle stage with other factors (Table 3-3).

Characterization of evoked postsynaptic currents in brain slices from diestrous and proestrous mice

Pharmacology was used to determine if evoked PSCs were monosynaptic as well as determine the transmitters involved (Fig. 3-5A) (Petreanu et al., 2009; Qiu et al., 2016). In all n=5 cells that met recording quality standards throughout testing, PSCs were blocked by gabazine (5 μM), but not CNQX (10μM); partial recovery after a 10min GABAzine washout period was observed in all neurons tested. In some cells (n=3), TTX (5 μM) was added to the perfusate to block action potential firing; this blocked evoked PSCs. Subsequent application of 4-AP (0.5 mM) recovered the evoked PSCs, indicating the connection was monosynaptic. The latency and jitter of evoked PSCs under these conditions (Fig. 3-5B) were used to classify PSCs as evoked/non-evoked in prior experiments.

Discussion

According to a prevailing model of the initiation of ovulation in nocturnal rodents, high concentration estradiol primes AVPV kisspeptin neurons for activation by a diurnal signal arriving a few hours before lights-off on proestrus. This priming involves

modulation of membrane properties to promote burst-firing and regulation of gene expression (Smith et al., 2005b; Mohr et al., 2021; Stephens and Kauffman, 2021; Göcz et al., 2022; Wang et al., 2016a; Starrett et al., 2021). The latter conspicuously involves upregulation of kisspeptin (*Kiss1*), but also includes changes in genes for other signals. These priming effects, in theory, increase the ability of AVPV kisspeptin neurons to activate downstream GnRH neurons, causing a GnRH surge when activated by the diurnal signal. Here, we tested aspects of this postulate by using optogenetics to stimulate AVPV kisspeptin neurons while measuring downstream activation of GnRH neurons in acute brain slices prepared from mice subjected to the daily LH surge model and from diestrous and proestrous mice.

Our hypotheses was that lack of circulating estrogenic priming of the AVPV to GnRH connection in OVX mice reduces GnRH neuron response to photoactivation of AVPV kisspeptin neurons and reduces synaptic innervation. In partial refutation, we found preoptic area GnRH neurons in slices from OVX and OVX+E mice responded to 20 Hz photoactivation of ChrimsonR-positive AVPV kisspeptin neuron projections/terminals with similar increases in firing rate. In contrast, AVPV neurons displayed different synaptic connectivity to GnRH neurons from OVX vs OVX+E mice. Specifically, PSCs were evoked in a low percentage of GnRH neurons in OVX+E mice but were not observed in neurons from OVX mice recorded in the afternoon, suggesting a possible positive effect of estradiol on synaptic connectivity. This apparent lack of ionotropic synaptic connectivity in OVX mice is particularly interesting because delayed increases in spike rate following 20 Hz photostimulation were nonetheless detected. Ovariectomy may induce pruning or retraction of synapses between AVPV kisspeptin and GnRH neurons within 48h. Systems relying on bulk-flow of transmitter may still be functional despite this pruning, and may be regulated by transcriptional and/or vesicle population changes that occur over a longer time period. This difference may also simply reflect an

ability of neuromodulators to diffuse further in the absence of active reuptake mechanisms.

There are several caveats to interpretation of the above data. Most notably estradiol treatment induced negative feedback on serum LH but not positive feedback. Uterine mass was increased by estradiol-treatment, but this is not necessarily an indicator that estradiol levels were sufficient for intact positive feedback were achieved. Notably, inconsistent LH surge induction also occurred in a contemporaneous experiment in the lab, which tested strain (E. Wagenmaker, personal communication). In that ongoing study, LH surge induction was consistent in mice on a B6-CBA hybrid background compared to the B6 mice used in the present study, suggesting genetic background may influence reliability of the daily LH surge model. Of note, the surge model was developed in the hybrid strain (Christian et al., 2005a). The estradiol threshold needed to induce positive feedback may differ among strains. This finding emphasizes the need for verifying the occurrence of estradiol feedback status with serum LH measurements when possible.

Historical data in the daily surge model show spontaneous firing rates of GnRH neurons are suppressed during negative feedback compared to those in OVX mice (Christian et al., 2005a). This is in line with decreased GnRH neuron firing rate causing decreased neuroendocrine GnRH release, ultimately reducing serum LH. In the present study, spontaneous firing rates were not different, yet LH was suppressed in OVX+E mice compared to OVX. This may be attributed to the fact that estradiol feedback effects occur at both the brain and the pituitary. It is possible the estradiol dose was sufficient for direct negative feedback effects at the level of the pituitary but not at the hypothalamus. Of note, the duration of baseline activity used in the present study was just 5 min vs an hour when the daily surge was characterized. GnRH neurons display spontaneous long-term changes in firing rate and 5-min samples of baseline activity

may not be reflective of the overall average spontaneous activity of each neuron (Nunemaker et al., 2003b; Constantin et al., 2022). Further, activity in the beginning of a recording is more likely to be influenced by attaining the recording configuration.

The apparent discrepancy between fast synaptic and longer-term modulation of neurons being differentially sensitive to removing circulating ovarian steroids led us to attempt sequential recordings of firing rate and synaptic transmission from the same neuron. These early studies revealed that cells with evoked PSCs did not always respond with a change in firing rate, and that cells with changes in firing rate did not always exhibit evoked PSCs. Based on these and the above observations, we adapted our design in several ways. First, the duration of baseline and response periods was increased. Second, the photostimulus was simplified to a single 30s application of 20Hz light pulses as this was most effective in inducing delayed increases in GnRH neuron firing rate. Third, to determine if delayed increases in firing could indeed occur in the absence of ionotropic monosynaptic connections, we performed sequential recordings of firing rate (extracellular) and PSCs (whole-cell) from the same GnRH neuron. This allowed measurement of spike rates without diluting the cytosol, which may be necessary for delayed responses, and also provided information about ionotropic synaptic transmission. Fourth, we switched to coronal slices. Finally, we performed studies in the afternoon from diestrous (negative feedback) vs proestrous (positive feedback) mice.

LH levels were elevated to values typical of positive feedback in proestrous vs diestrous mice. Despite this difference in feedback state, no diestrous vs proestrous differences were observed in baseline firing rate or in firing rate increases; cells from both diestrous and proestrous mice consistently increased firing rate following photostimulation. Interestingly, subsequent whole-cell recordings revealed low percentages of cells receiving ionotropic transmission in both diestrous and proestrous mice, similar to cells from OVX+E mice. In all cases of monosynaptic transmission, PSCs were GABAergic,

consistent with prior immunofluorescence data suggesting AVPV kisspeptin neurons express vesicular GABA transporters (Zhang et al., 2013; Stephens and Kauffman, 2021). In the preceding extracellular recordings of these cells, immediate increases in firing were observed during the photostimulus. We interpret this finding as evidence of excitatory GABAergic transmission at GnRH neurons (Herbison and Moenter, 2011; Watanabe et al., 2014a). Although there was no statistical interaction of cycle stage with evoked/non-evoked classification for either immediate or delayed responses, these comparisons likely did not have statistical power to detect differences due to the lower number of evoked-PSC cells in both groups.

Contrary our hypothesis, studies in cycling mice indicated AVPV kisspeptin neurons possess similar capacities for increasing GnRH neuron spike rate in cycle stages reflecting negative and positive feedback. This interpretation must be tempered by consideration of caveats involved in our approach. A primary caveat concerns the characteristics of the stimulus used to activate AVPV kisspeptin neurons. The pattern of activity of these cells leading up to the surge has not been measured *in vivo*. Thus, it is not clear if the duration and/or frequency of the photostimulation chosen could reveal differences in GnRH neuron responses that may impact surge induction. Our choice of stimulus parameters was based on prior optogenetics studies of this circuit (Qiu et al., 2016; Piet et al., 2018). In brain slice recordings of AVPV kisspeptin neurons, however, mean firing rates of these cells over a 5-minute period during proestrus were reported in the range of ~2-8 Hz compared to 1-4 Hz during diestrus (Wang et al., 2016a). In our experiments, a 20 Hz stimulus was applied equally to slices from both groups of mice, and generated similar increases in GnRH neuron firing rate. It may be that the main factor driving surge induction is the increase in AVPV kisspeptin neuron firing activity during proestrus. This would place increased emphasis on estradiol's regulation of the firing activity of these cells and their responsiveness to afferents, which are also estradiol sensitive.

Notably, photostimulus-induced increases in GnRH neuron spike rate during diestrus and proestrus lasted ~15 minutes, whereas LH surges can last longer than this (Czieselsky et al., 2016). It is likely AVPV kisspeptin neurons maintain high firing rates for longer than 30s *in vivo* during the surge, as the central changes induced by positive feedback likely last longer than the 30s stimulus used. Prolonged activation of AVPV kisspeptin neurons *in vivo* may produce more prolonged activation of GnRH neurons than we observed here. Neurons in proestrous/OVX+E mice may be able to release kisspeptin for longer periods than neurons from diestrous mice because of larger kisspeptin stores and/or faster replenishment of kisspeptin at release sites. This difference would likely not be detectable by our design. It is also possible AVPV kisspeptin neurons release kisspeptin at lower spike rates during proestrus vs diestrus. If, for example, release probability reaches a maximum at 12 Hz in proestrous mice but 18 Hz in diestrous mice, release probabilities would be equal during the 20 Hz stimulus used in our experiments. When during positive feedback a stimulus is applied may also make a difference given this phase lasts a couple of hours.

The percentage of GnRH neurons with evoked PSCs in cycling mice was similar to OVX+E mice and increased compared to OVX, suggesting ovariectomy may induce more dramatic changes to the synaptic connectivity of these cell types compared to steroid changes of estrous cycle. The low degree of connectivity was unexpected given previous anatomical (light-microscopy) studies and our own observation of a high number of tdTomato/ChrimsonR positive fibers near GnRH neurons (Wintermantel et al., 2006; Kumar et al., 2015; Stincic et al., 2021). GnRH neurons not exhibiting evoked ionotropic input nonetheless displayed delayed increases in spike rate, indicating direct ionotropic input from AVPV kisspeptin neurons was not necessary for these cells to increase GnRH neuron spike rate. This raises the question of how AVPV neuron activation is relayed to the GnRHs neuron in such cases. It is possible this occurs

indirectly, involving interneurons in a delayed manner. These interneurons could be GnRH neurons, i.e., direct activation of only a small percentage of GnRH neurons may be sufficient to initiate activation of the network. Kisspeptin can indirectly activate GnRH neurons by modulating GABA/glutamate transmission, consistent with this hypothesis (Pielecka-Fortuna et al., 2008). It is also possible additional metabotropic signals may be released by AVPV kisspeptin neurons in the absence of co-transmission with glutamate or GABA, including extrasynaptically. In this regard, a high proportion of AVPV kisspeptin neurons co-express tyrosine hydroxylase (Cravo et al., 2011; Stephens and Kauffman, 2021). Our data suggest signaling in absence of GABA/gluamate co-transmission may in fact be the primary mode of transmission between AVPV kisspeptin and GnRH neurons regardless of cycle stage. The existence of such “silent” transmission modes should be considered more broadly in circuit mapping experiments. Many experiments examine only ionotropic transmission, however, lack of an evoked ionotropic response does not indicate a lack of signaling between cell types.

Figures and Legends

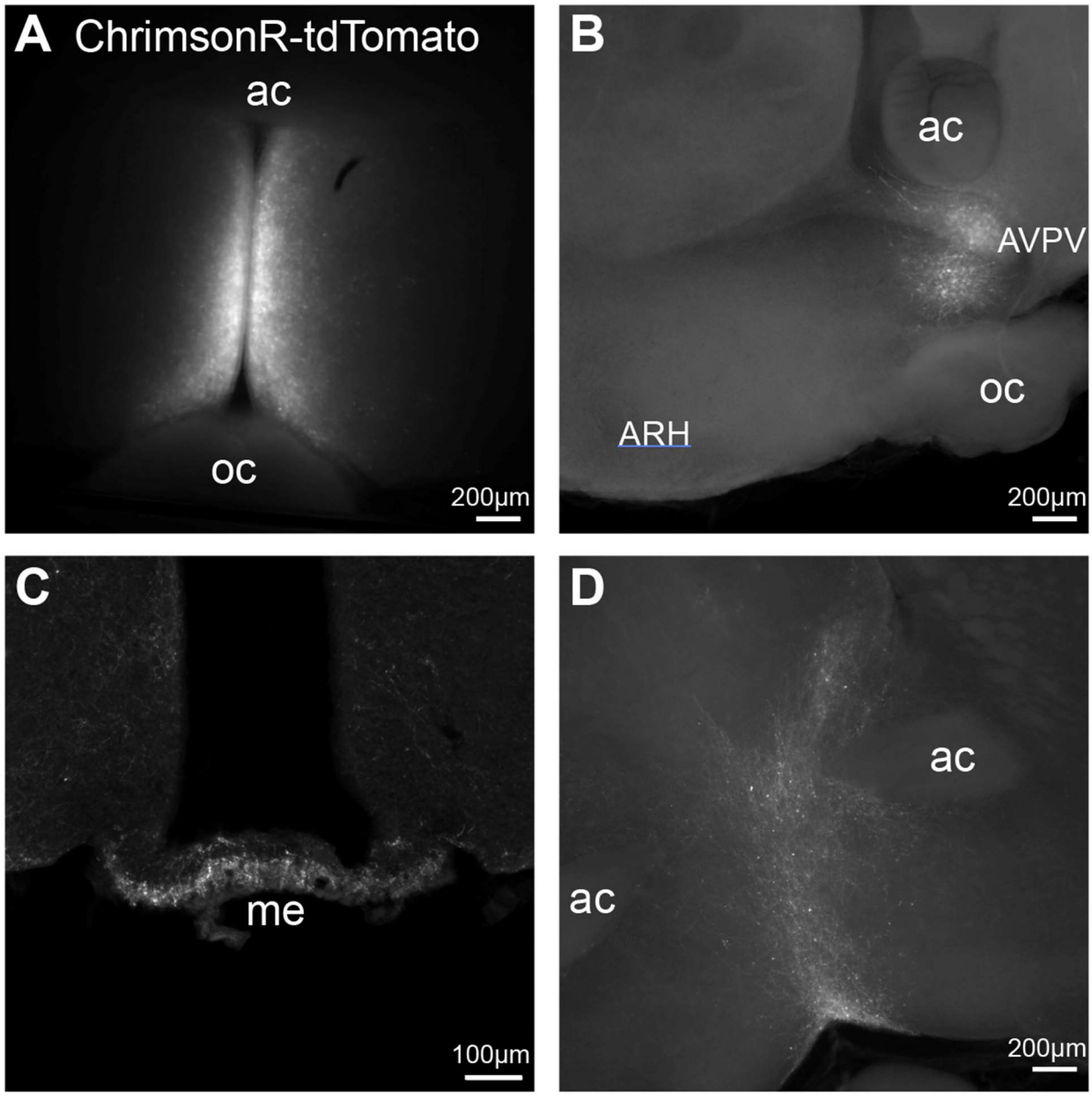

Figure 3-1 tdTomato expression in Kiss-Cre mice injected with AAV-FLEX-ChrimsonR-tdTomato. **A,** ChrimsonR-tdTomato expression in the AVPV of a coronal slice prepared for electrophysiology, ac, anterior commissure; oc, optic chiasm. **B,** Sagittal slice displaying ChrimsonR-tdTomato expression in the AVPV but not arcuate (ARH). **C,** Cryostat coronal

section of the median eminence (me) and arcuate region. **D,** Coronal slice exhibiting ChrimsonR-tdTomato expressing fibers in the preoptic area.

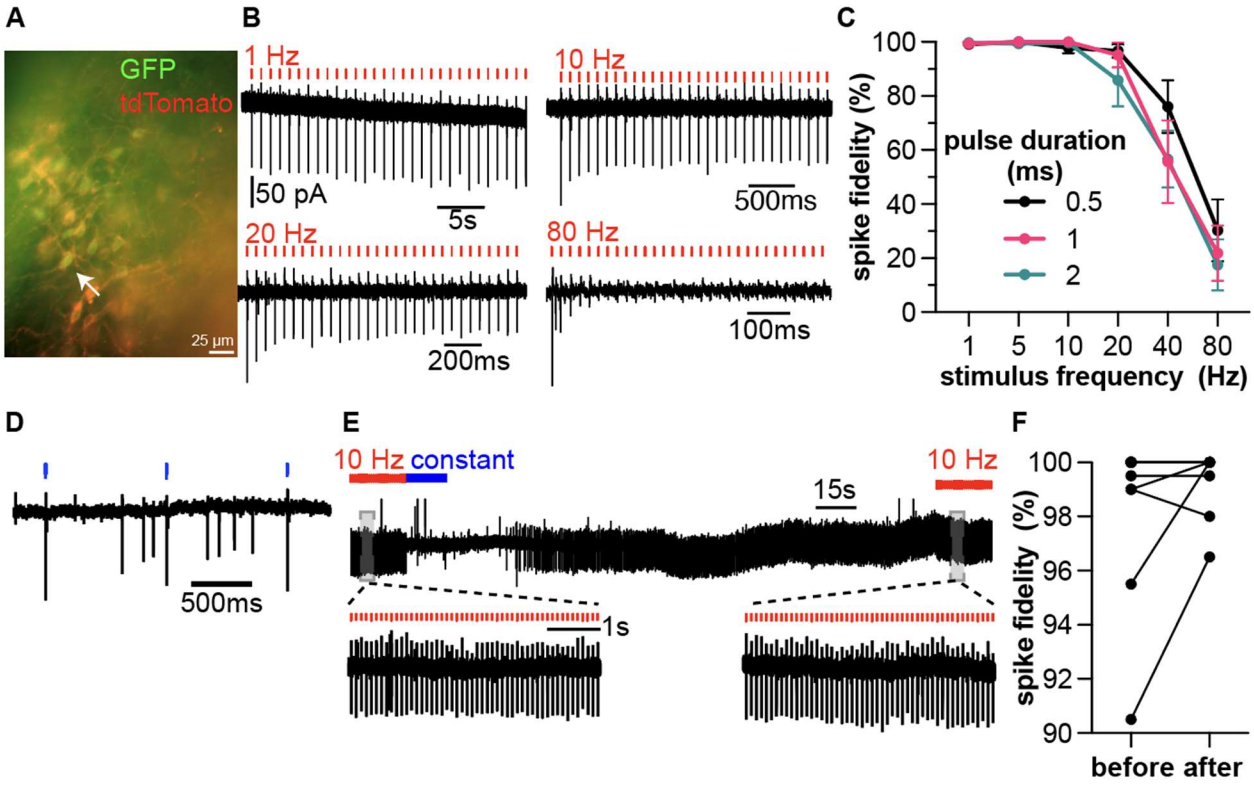

Figure 3-2 Photostimulation drives spiking by ChrimsonR-expressing AVPV kisspeptin neurons. **A,** Post-hoc image from a 300µm-thick brain slice from AAV-injected Kiss-Cre;Kiss-hrGFP mouse. Arrow indicates an example GFP/tdTomato co-expressing neuron that would be targeted for extracellular recording **B,** Representative extracellular recordings showing the responses of an AVPV Kiss1-GFP:Kiss-Cre neuron to 30 1ms red-light pulses delivered at 1, 10, 20, and 80 Hz; note differences in time scale; 50 pA current scale applies to all traces in figure. **C,** Mean±SEM spike fidelity as a function of photostimulus frequency for 0.5, 1, and 2 ms red-light pulses. **D,** Representative extracellular recording showing a ChrimsonR-expressing AVPV kisspeptin neuron firing in response to 1 ms blue light pulses at 1 Hz. Spontaneous spikes occurred between light pulses. **E,** Representative extracellular recording showing spike fidelity tests (30 s of 1 ms red-light pulses at 10 Hz) before and after 15 s exposure to constant blue light. Expanded regions show light-evoked spikes during each fidelity test. **F,** Spike fidelity before and after constant blue-light exposure in 11 neurons; note y-axis begins at 90%.

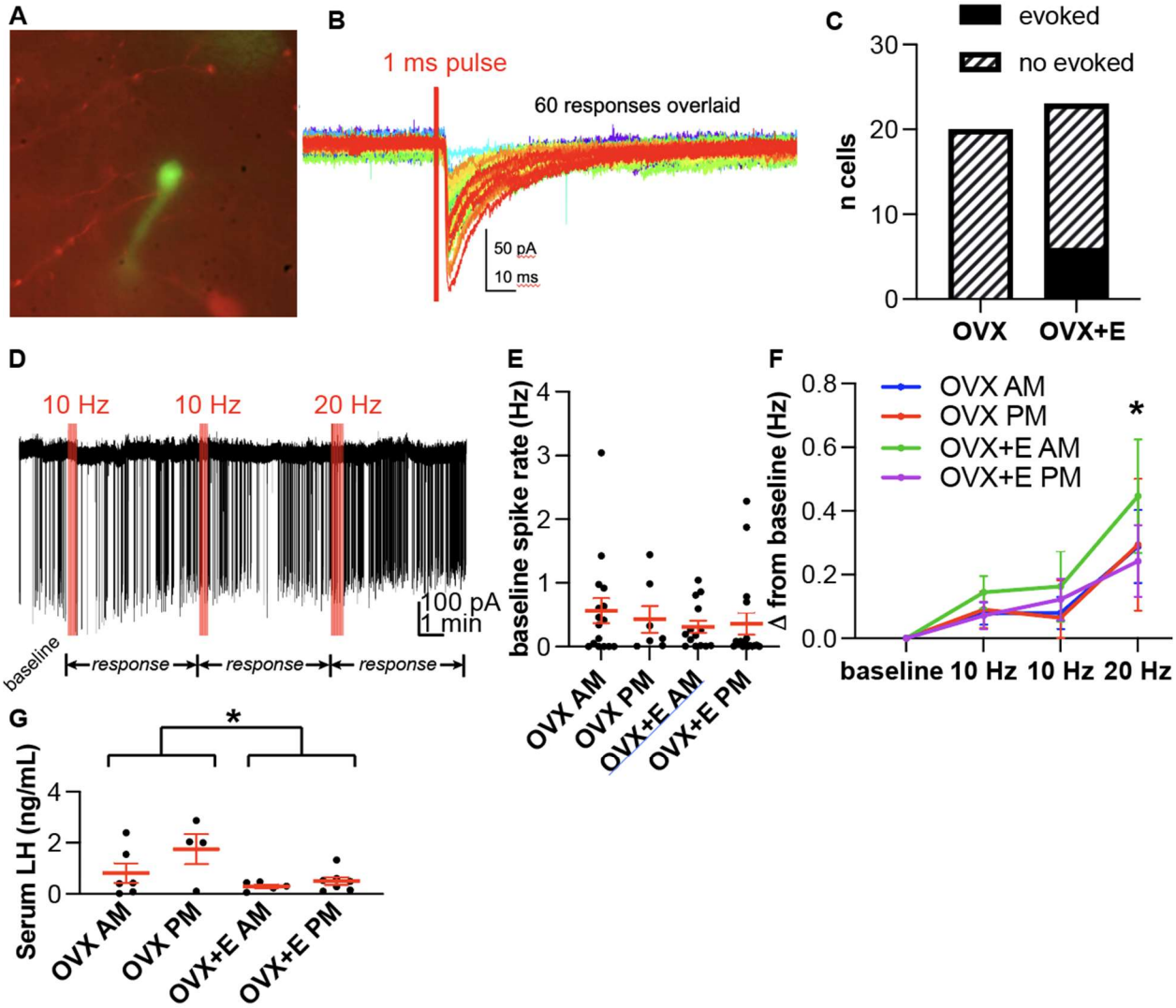

Figure 3-3 Photoactivation of AVPV Kiss1-Cre neurons in the daily LH surge model. ***A,*** Image from 300 µm brain slice showing an example targeted GnRH-GFP neuron near tdTomato-positive fibers. ***B,*** Example whole-cell voltage-clamp recording showing evoked post-synaptic currents (PSCs) in response to red-light pulses. ***C,*** Proportion of recorded cells in slices from OVX and OVX+E mice exhibiting evoked PSCs. **D,** Representative extracellular recording of a GnRH-GFP neuron from a an OVX+E (AM) mouse showing the stimulus paradigm and periods where firing rates were calculated for E and F. ***E,*** Individual values and mean±SEM baseline firing rates. ***F,*** Mean±SEM change (∆) in firing rate from the baseline period during periods shown in D. ***G,*** Individual values and mean±SEM serum LH values.

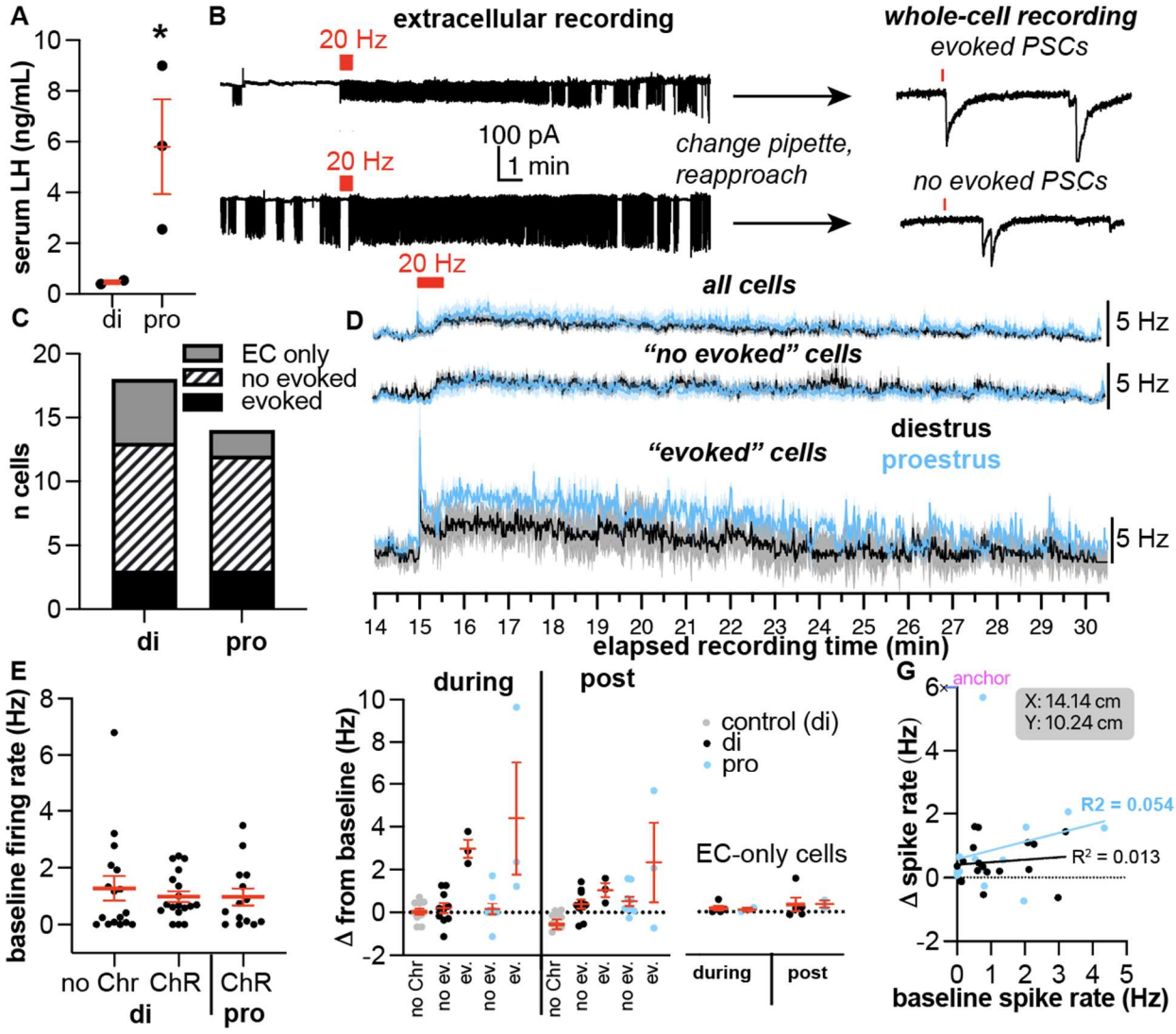

Figure 3-4 Photoactivation of AVPV Kiss1 to GnRH neuron pathway in brain slices from diestrous and proestrous mice. **A,** Mean±SEM and individual serum LH values in diestrous and proestrous mice, **B,** Left: representative extracellular and whole-cell voltage-clamp (right) recordings from a neuron exhibiting evoked PSCs (top) and one not exhibiting evoked PSCs (bottom). The baseline recording is truncated. Right: follow-up whole-cell recordings from cells on left. **C,** cells per animal group for extracellular (EC)-only (failed whole-cell attempt), and sequential extracellular/whole-cell recordings classified as "evoked" or "no-evoked". **D,** top, Mean±SEM firing rate time course (1 s bins) during extracellular recordings in all cells from diestrus (black) and proestrus (blue) mice; middle, no-evoked cells only; bottom evoked-cells only. **E,** Mean±SEM and individual baseline GnRH neuron firing rates in slices from ChrimsonR-injected (ChR) diestrous and proestrous and non-injected (no Chr) control diestrous mice. **F,** Change (Δ) in spike rate (during the stimulus (left) and during the 5-min post-stimulus period

(right) in evoked and no-evoked cells in control, diestrous, and proestrous mice. **G,** Baseline spike rate vs change from baseline plot. Each point represents a cell and the colors denote cycle stage. Lines are linear fit to each group.

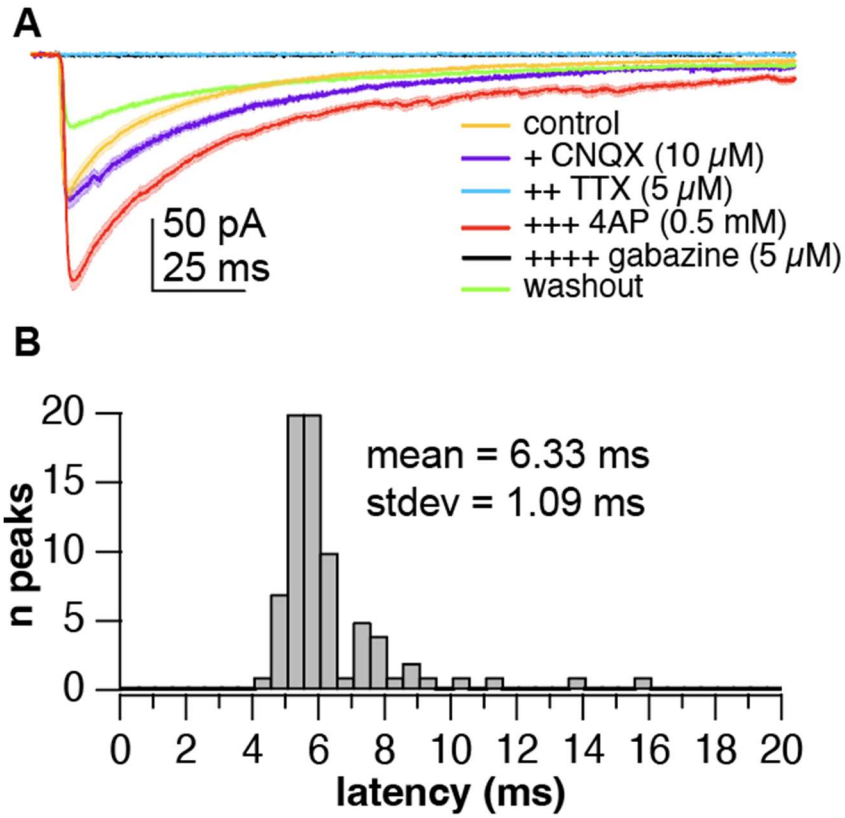

Figure 3-5 Photostimulation of AVPV Kiss1-ChrimsonR fibers evokes monosynaptic GABAergic PSCs in GnRH neurons. **A,** Mean±SEM timecourses of evoked PSCs in an example neuron from a proestrous mouse. PSCs were challenged with sequential additions of drugs to determine if they were monosynaptic and the mediating transmitter(s). Increasing number of + denotes the order of additions. **B,** Histogram of latency to PSC peak in the presence of 4AP+TTX for the neuron shown in A.

Tables

Table 3-1 Sample sizes and statistical test results for spike fidelity and blue-exposure experiments in Figure 3-2.

	(n cells, n animals)
0.5 ms	(12,3)
1 ms	(12,3)
2 ms	(11,3)
spike fidelity	
two-way repeated measures ANOVA	
frequency	F (2.284, 73.08) = 69.34, p<0.0001***
width	F (2, 32) = 0.8867, p=0.4219
frequency x width	F (10, 160) = 0.6664, p=0.7543
blue exposure test - spike fidelity	**(n cells, n animals)**
before	(11,3)
after	(11,3)
paired two-tailed t-test	
before vs after	Diff=0.9545, CI=-0.5208 to 2.430, t=1.442, df=10, p=0.18

*p<0.05; **p<0.01; ***p<0.001.

Table 3-2 Sample sizes and statistical test results for experiments involving the daily LH surge model from Figure 3-3.

baseline	**(n cells, n animals)**
OVX AM	(16, 4)
OVX PM	(7,4)
OVX+E AM	(14, 5)
OVX+E PM	(17, 4)
two-way repeated measures ANOVA	
steroid	F (1, 50) = 0.7425, p=0.3930
time of day	F (1, 50) = 0.05472, p=0.8160
steroid x time of day	F (1, 50) = 0.2377, p=0.6280
change from baseline	
three-way repeated measures ANOVA	
steroid	F (1, 50) = 0.3263, p=0.5704
time of day	F (1, 50) = 0.3726, p=0.5443
stimulus	F (3, 150) = 12.65, p<0.0001***
steroid x stimulus	F (3, 150) = 0.1723, p=0.9150
steroid x time of day	F (1, 50) = 0.3803, p=0.5403
time of day x stimulus	F (3, 150) = 0.3139, p=0.8153
stimulus x steroid x time of day	F (3, 150) = 0.3849, p=0.7641
Tukey's multiple comparisons	
baseline vs. 10 Hz	Diff=-0.0961, CI=-0.2345 to 0.04227, df=150, p=0.2753
baseline vs. 10 Hz	Diff=-0.1073, CI=-0.2457 to 0.03103, df=150, p=0.1869
baseline vs. 20 Hz	Diff = -0.3178, CI = -0.4562 to -0.1795, df=150, p<0.0001***
10 Hz vs. 10 Hz	Diff=-0.01124, CI=-0.1496 to 0.1271, df=150, p=0.9967
10 Hz vs. 20 Hz	Diff= 0.2217, CI= 0.3601 to -0.08336, df=150, p=0.0003***
10 Hz vs. 20 Hz	Diff=-0.2105, CI=-0.3489 to -0.07212, df=150, p=0.0007***
serum LH	**n animals**
OVX AM	6
OVX PM	4
OVX+E AM	5
OVX+E PM	6
two-way ANOVA	
steroid	F (1, 18) = 7.581, p=0.0131*
time of day	F (1, 18) = 3.173, p=0.0917
steroid x time of day	F (1, 18) = 1.333, p=0.2634

uterine mass	**n animals**
OVX AM	6
OVX PM	4
OVX+E AM	5
OVX+E PM	6
two-way ANOVA	
steroid	F (1, 17) = 178.2, p<0.0001***
time of day	F (1, 17) = 0.7612, p=0.3951
steroid x time of day	F (1, 17) = 0.9291, p=0.3486

*p<0.05; **p<0.01; ***p<0.001.

Table 3-3 Sample sizes and statistical test results for experiments involving the estrous cycle from Figure 3-4

serum LH	**n animals**
diestrus	2
proestrus	3
two-tailed t-test	
diestrus vs proestrus	Diff=5.334±2.403, CI=-2.313 to 12.98, t=2.220, df=3, p=0.1131
uterine mass	**n animals**
diestrus	2
proestrus	3
two-tailed t-test	
diestrus vs proestrus	Diff=77.52 ± 19.76, CI=14.63 to 140.4, t=3.923, df=3, p=0.0295*
baseline spike rate	**(n cells, n animals)**
control	(15,5)
diestrus	(18,4)
proestrus	(14,4)
one-way ANOVA	
control vs diestrus vs proestrus	F (2, 46) = 0.2812, p=0.3090
change from baseline	
two-way repeated measures ANOVA	
cycle stage	F (1, 30) = 0.5529, p=0.4629,
response period (during stim/delayed)	F (1, 30) = 9.605, p=0.0042**
cycle stage x response period	F (1, 30) = 0.2289, p=0.6358
baseline spike rate nonEv/Ev	**(n cells, n animals)**
diestrus - nonEv	(10, 4)

diestrus - Ev	(3,2)
proestrus -nonEv	(9,3)
proestrus - Ev	(3,4)
two-way ANOVA	
cycle stage (di vs pro)	F (1, 21) = 0.1626, p=0.6909
Ev/nonEv	F (1, 21) = 0.3800, p=0.5442
cycle stage x Ev/nonEv	F (1, 21) = 1.326, p=0.2624
change from baseline nonEv/Ev - immediate	
two-way repeated measures ANOVA	
cycle stage	F (1, 21) = 0.8792, p=0.3591
Ev/nonEv	F (1, 21) = 22.44, p=0.0001***
cycle stage x Ev/nonEv	F (1, 21) = 0.9876, p=0.3316
change from baseline nonEv/Ev - delayed	
two-way repeated emasures ANOVA	
cycle stage	F (1, 21) = 1.695, p=0.2070
Ev/nonEv	F (1, 21) = 5.098, p=0.0347*
cycle stage x Ev/nonEv	F (1, 21) = 1.129, p=0.3000

Chapter 4: Conclusion

During the preovulatory phase of the reproductive cycle of spontaneously-ovulating mammals, high concentration circulating estradiol causes a surge of GnRH released by the hypothalamus (Sarkar et al., 1976a; Moenter et al., 1990, 1992a; Pau et al., 1993). This process, known as estradiol positive feedback, initiates a cascade of neural and endocrine events that culminate in ovulation. It is therefore vital for fertility. The central neurons that synthesize and secrete GnRH do not detectably express the receptor necessary for estradiol feedback effects (Hrabovszky et al., 2000), indicating afferent estradiol-sensitive neurons are essential. At the start of this dissertation, accumulating evidence suggested a necessary site of estradiol positive-feedback action is kisspeptin neurons in the anteroventral-periventricular area (AVPV) of the hypothalamus. Despite an understanding that these cells are critical, there was incomplete knowledge of how they become activated by estradiol and how this activation is communicated to GnRH neurons. Three main questions therefore formed the basis of this dissertation: 1) how do kisspeptin neurons in the AVPV become electrically activated during estradiol positive feedback? 2) how do these cells communicate with GnRH neurons? 3) does this communication take on a new form during positive feedback?

Chapter 2: how do kisspeptin neurons in the AVPV become electrically activated during estradiol positive feedback?

A biophysical approach was used to address this question. The central hypothesis was that changes in voltage-gated conductances promote increased spiking and burst-firing activity during proestrus. Previous studies had reported multiple voltage-gated conductances differ in diestrous vs proestrous mice or in the daily surge model (Piet et al., 2013a; Zhang et al., 2015; Wang et al., 2016a). However, information about voltage-gated potassium currents, major determinants of activity in neurons, was lacking and this precluded modeling firing dynamics rigorously. To address this, voltage-gated potassium currents were biophysically characterized in acute brain slices from diestrous and proestous mice. These data, along with data from the literature, were used to create *in silico* neuron models with conductances fit to data from diestrous vs proestrous mice. The models were used to perform simulations of firing behavior, which suggested that rebound burst firing, a firing pattern that may be associated with neuropeptide release, is enabled by proestrus-related increases in the amplitudes of three currents in unison: T-type calcium, hyperpolarization-activated, and persistent-sodium currents. Concomitant changes in voltage-gated potassium currents during proestrus caused similar excitability in response to simulated depolarizing current injection compared to diestrus, without restraining rebound-burst capability.

This work generates new questions about the electrophysiology of AVPV kisspeptin neurons and provides both tools and directions for future research. While a definitive

answer as to how these cells become more electrically active during positive feedback remains elusive, it is now clear that seemingly inhibitory forms of input must be considered alongside the capacity of these cells for rebound burst firing, which our work suggests is enabled by increases in T-type calcium, persistent sodium, and hyperpolarization-activated currents acting in unison during proestrus. An intriguing possible source of fast hyperpolarizing input to drive this burst activity is the AVPV itself. A majority of AVPV kisspeptin neurons are GABAergic (Cravo et al., 2011). In a pilot experiment, I found optogenetic activation of the AVPV kisspeptin neuron population evoked PSCs in an opsin-negative AVPV kisspeptin neuron (Figure 4-1A). The PSCs appeared monosynaptic and GABAergic based on latency and decay times, though this was not pharmacologically tested.

Local, possibly reciprocal, connections among rebound burst-firing AVPV kisspeptin neurons may be a mechanism that facilitates ramping-up of activity during estradiol positive feedback. This process may be initiated by an incoming diurnal signal, such as GABAergic input from the SCN. Notably, if GABA does act as a major source of hyperpolarizing input during positive feedback, one might expect spontaneous GABA PSC frequency at AVPV kisspeptin neurons to be higher in OVX+E mice in the afternoon vs. morning, but a previous study found the opposite trend (DeFazio et al., 2014a). It is possible hyperpolarization is supplied by metabotropic signals coming from within the AVPV, since kisspeptin neurons in the AVPV co-express typically

hyperpolarizing neuropeptides such as galanin metenkephalin, and the catecholamine dopamine (Porteous et al., 2011; Stephens and Kauffman, 2021; Göcz et al., 2022). According to a recent study that measured actively-translated transcripts in AVPV kisspeptin neurons of OVX vs OVX+E mice, tyrosine hydroxylase is more highly expressed in OVX+E mice (Stephens and Kauffman, 2021). The study also found that AVPV kisspeptin neurons express primarily D2-type receptors, with other receptors not detected, suggesting dopamine has a primarily inhibitory effect on these cells. Although the effects of inhibitory GPCRs like D2 are likely not acute enough to induce rebounding, it is possible slow-acting, hyperpolarizing GPCR activation puts AVPV kisspeptin neurons into a more burst-prone state, from which bursts may be activated by acute depolarizing input such as glutamate. Consistent with this, AVPV kisspeptin neurons receive increased glutamatergic input during positive feedback (Wang et al., 2018).

Possible dynamics of combined excitatory/inhibitory input streams and the interconnectedness of AVPV kisspeptin neurons could be explored with network models, with the spiking properties of individual AVPV neurons supplied by the models created in the present work. A useful evolution of the AVPV kisspeptin neuron spiking model we created may come from future experiments measuring the fast voltage-gated sodium current in these cells, which we did not model in the current edition (though we did base its parameters on action potential shape). Dynamic clamp, a hybrid

model/wet-lab approach, could also be used to increase our understanding of how AVPV kisspeptin neurons integrate synaptic inputs. The present work replicated previous findings in that AVPV neurons (and models) from diestrous and proestrous mice showed similar excitability in response to depolarizing square current injections lasting 500 ms – a stimulus that seems unlikely to exist in normal physiology (Wang et al., 2016a). It is possible differences in excitability are displayed in response to more physiologic stimuli, which could be tested by using dynamic clamp to apply simulated post-synaptic conductances to AVPV kisspeptin neurons from diestrous and proestrous mice while observing the resulting change in membrane potential. This may reveal that rebound burst firing is primarily a signature of increased excitability during proestrus rather than the root cause of increased spike rate and burst firing during this time.

The possibility that AVPV kisspeptin neurons form a local positive-feedback system that promotes an exponential increase in activity leading up to the GnRH surge is intriguing. Communication among these cells is understudied especially in comparison to cells in the arcuate nucleus, where reciprocal connections among kisspeptin neurons have been hypothesized as a component of pulse-generator activity (Goodman et al., 2022). However, there remains a strong possibility that activation of AVPV kisspeptin neurons during positive feedback is driven primarily by input from neurons that project to the area from outside the AVPV. In this case, increased firing rates of AVPV kisspeptin neurons in slices from proestrus mice may represent only a fraction of what occurs

when circuitry is intact *in vivo.* It is likely the *in vivo* activity of AVPV kisspeptin neurons will be measured in the near future as this has been accomplished recently in the ARH (Moore et al., 2022; Han et al., 2023). A time series of activity of AVPV kisspeptin neurons across the proestrus phase within a single mouse would provide useful information about GnRH surge induction mechanisms. Combined with rapid advances in volumetric *in vivo* imaging of fluorescent indicators for neuromodulators and neurotransmitters, work in intact animals will likely bring new understanding of how the AVPV is involved in surge generation.

Chapter 3: How do AVPV kisspeptin neurons communicate with GnRH neurons? Does this communication take on a new form during estradiol positive feedback?

To address the first question, optogenetics was used to specifically activate AVPV kisspeptin neurons/projections in acute brain slices while recording downstream changes in firing rate and evoked PSCs at GnRH neurons. The second question was addressed by performing these experiments in slices from OVX,OVX+E, diestrous, and proestrous mice. The central hypothesis was that estrogenic priming of ionotropic and kisspeptin signaling facilitates GnRH surge initiation. The prediction stemming from this was that activation of AVPV kisspeptin neurons in brain slices from proestrous and OVX+E (PM) mice would produce lesser downstream activation of GnRH neurons, compared to diestrus and OVX mice.

The experiments yielded interesting and unexpected results. Given the proposed critical role of AVPV kisspeptin neurons as potent activators of GnRH neurons and initiators of the GnRH surge, it was surprising that the prevalence of ionotropic transmission between these cell types was low. This finding is, however, in line with early electron microscopy studies of GnRH neurons, which consistently reported a low degree of synaptic innervation of GnRH neurons in multiple species, although quantification of synapses at GnRH neurons in mice has not been performed (Silverman et al., 1994). Notably, in our experiments, PSCs were not evoked in ovariectomized mice possibly due to loss of ovarian estradiol causing pruning and/or retraction of synapses at GnRH neurons. It is possible ovariectomy engages a similar mechanism that may be at play in long-term (>6wk) OVX rhesus monkeys, which display decreases in synaptic innervation of GnRH neurons and increases in the number of glial appositions (Witkin 1991). Notably the post-ovariectomy duration we used (2 days) was not long-term. This could explain why, in OVX mice, though fast synaptic innervation appears to have been lost, delayed increases in GnRH neuron firing rate could still be induced to a similar degree as in OVX+E mice in negative feedback. Delayed firing in OVX mice may be attributable to neuromodulators, such as kisspeptin, not requiring synapses to activate GnRH neurons, and kisspeptin may diffuse extensively given lack of reuptake transporters. The amount of readily-releasable and near-releasable kisspeptin stores in neurons in OVX and OVX+E mice may not have been different in our experiments,

suggested by OVX+E mice not exhibiting LH surges. It is also possible delayed responses were equal in OVX and OVX+E mice for reasons related to glia. For example, it is possible estradiol makes GnRH neurons more accessible to kisspeptin by reducing glial ensheathment. This process may take longer than the 2 days used in our experiments, hence GnRH neurons in OVX mice were still accessible. At the median eminence, estradiol reduces tanycyte ensheathment of GnRH nerve terminals, which restrict access to the perivascular space (Prevot et al., 2010). This process can initiate suddenly and takes place over hours, rather than days, however, it is not clear if tanycyte ensheathment of nerve terminals and astrocytic ensheathment of GnRH cell bodies and proximal fibers in the preoptic area engage similar mechanisms. Mice 2-3 days post ovariectomy are still responsive to kisspeptin but longer post-OVX durations have not been tested (Pielecka-Fortuna et al., 2008; Adams et al., 2018b). Importantly, changes in glial architecture are likely more impactful for endogenously-released kisspeptin compared to drug applications to brain slices; the latter involves widespread action throughout the slice whereas the former occurs is more focal. The possibility of ovariectomy causing a loss of the delayed firing response of GnRH neurons will be explored further with experiments involving longer-term (5-7 days) ovariectomy using comparison to sham-operated diestrous and proestrous controls.

The number of GnRH neurons with evoked PSCs was not different between diestrous and proestrous mice suggesting synaptic connectivity may not change during the

estrous cycle. In both cycle stages, photo-evoked PSCs were consistently GABAergic; glutamatergic PSCs were not evoked. This is consistent with recordings of spontaneous PSCs in GnRH neurons suggesting a paucity of spontaneous glutamatergic transmission and with immunofluorescence and bioinformatic studies of AVPV kisspeptin neurons reporting VGAT expression in these cells(Zhang et al., 2013; Constantin et al., 2022). GnRH neurons that received GABAergic PSCs exhibited immediate increases in firing during the stimulus train providing the first direct evidence of excitatory GABAergic transmission from AVPV kisspeptin neurons. Due to the low number of synaptically-connected cells, we did not have the statistical power to detect differences between diestrous and proestrous mice in terms of the amplitude of the immediate or delayed GnRH neuron firing responses to AVPV stimulation. This also precluded comparison of GABAergic PSC characteristics between these groups. To increase yield per mouse, responsive (evoked-PSC) GnRH neurons could be more rapidly identified in the slice by returning to a “whole-cell only” approach, rather than sequential extracellular-whole cell strategy. Alternatively, if both extracellular recordings of spike rate and whole-cell recordings of individual neurons are desired, extracellular recordings could begin with an initial “trial” phase in which the GnRH neuron is tested for an immediate spike-rate increase in response to photostimulation, which the present data suggest is typically indicative of a synaptic connection. Cells not exhibiting immediate responses would not be recorded further.

GnRH neurons that exhibited delayed increases in firing in response to high-frequency photostimulation of the AVPV were often not recipients of evoked ionotropic transmission. This indicates co-transmission of metabotropic and ionotropic signals by AVPV kisspeptin neurons does not always occur. Whether or not the delayed and prolonged increases in firing can be attributed to kisspeptin would be difficult to determine because there is not a consistently-effective antagonist for the kisspeptin receptor; in our pilot studies, antagonists failed to block increased firing of GnRH neurons from applied kisspeptin. However, the latency and amplitude of the response to our photostimulus was consistent with responses to exogenous kisspeptin reported by prior studies (Pielecka-Fortuna et al., 2008; Rønnekleiv and Kelly, 2013; Adams et al., 2018b). The duration of responses to exogenous kisspeptin are, however, more prolonged than the optogenetically-evoked responses we observed. An explanation for this returns to the idea that optogenetically-evoked kisspeptin release is likely more spatially confined compared to treatment of the entire slice as occurs in pharmacological experiments. An intriguing possibility is that evoking endogenous kisspeptin release with optogenetics engages co-release of additional substances from AVPV neurons that modulate the GnRH neuron response.

An unexpected result from this study was that activation of the AVPV produced similar increases in firing rate (both immediate and delayed) in GnRH neurons from diestrous and proestrous mice. This was surprising because of evidence indicating AVPV neurons

express more kisspeptin during estradiol positive feedback and estradiol potentiates the response to kisspeptin during this time (Smith et al., 2005a; Pielecka-Fortuna et al., 2008). We used an equivalent photostimulation paradigm during diestrous and proestrous, and it produced similar responses downstream, indicating the capability of AVPV kisspeptin neurons to activate GnRH neurons does not change across these estrous cycle stages. This challenges the predominant model of how estradiol modulates this circuit across negative vs positive feedback, which postulates estradiol primes the circuit for activation by a diurnal signal arriving on the afternoon of proestrus.

A more important target of estradiol in this circuit may be the spontaneous activity of AVPV kisspeptin neurons and the responsiveness of these cells to a diurnal signal. The basal spike rate of AVPV kisspeptin neurons during proestrus measured in brain slices increases to about twice that of diestrus (Wang et al., 2016a). In our work, however, we used an equivalent photostimulus between diestrous and proestrous mice. As we did not test a range of stimulus parameters in cycling mice, it is not clear if lower frequencies and/or durations of AVPV activation produce comparatively weaker responses in GnRH neurons, or whether the AVPV-activation/GnRH neuron-response relationship is consistent across cycle stages. Dose-response curves involving a range of stimulus frequencies and durations could be constructed from experiments in diestrous and proestrous mice to determine if this is the case.

As discussed, the average response to the 30 second , 20 Hz stimulus lasted ~15 minutes, yet the LH surge in mice can last more than an hour and GnRH surges measured in rats last multiple hours (Sarkar et al., 1976a). cFos expression in AVPV kisspeptin neurons is elevated starring in the late-morning proestrus and remains elevated through the surge in the later afternoon (Robertson et al., 2009), suggesting these cells remain active for a prolonged period leading up to and during the GnRH surge. This brings into question whether the stimulus parameters we used are reflective of the natural physiology. Higher kisspeptin expression in AVPV kisspeptin neurons during proestrus, compared to diestrus, may provide longer-lasting stores that enable them to activate GnRH neurons over a long period. The comparatively short duration of our photostimulus paradigm may have precluded observing this difference. A longer stimulus train could address this question in future experiments. In an experiment involving in-vivo activation of AVPV kisspeptin neurons, increases in LH to surge-like levels were measured starting at 5-10 minutes into a 15 minute, 10 Hz stimulus train (Piet et al., 2018). These parameters may serve as a starting point in designing long-term stimulation experiments for experiments in brain slices.

Using optogenetics to functionally map the central reproductive neurocircuitry, and the growing prevalence of in vivo techniques

AVPV and arcuate kisspeptin neurons are often thought dichotomous in relation to their contributions to the two forms of estradiol feedback, but these two hypothalamic kisspeptin populations interact both anatomically and functionally. AVPV and arcuate kisspeptin neurons appose one another in rodents (Kumar et al., 2015; Stincic et al., 2021), but evidence suggests this interaction is limited in sheep (Merkley et al., 2015). A possible role for arcuate kisspeptin neurons in surge generation is suggested by the substantial blunting of estradiol-induced LH surges in rats that had a > 90% reduction in the number of kisspeptin-positive neurons in the arcuate (Nagae et al., 2021). Optogenetic stimulation of arcuate neurons evokes monosynaptic glutamatergic PSCs in AVPV kisspeptin neurons in mice (Qiu et al., 2016), consistent with most arcuate neurons expressing VGluT2 (Cravo et al., 2011). It is also possible that KNDy neurons modulate AVPV kisspeptin neuron activity via neurokinin B and dynorphin, since AVPV kisspeptin neurons express neurokinin receptors 1 and 3 (Navarro et al., 2015), and κ-opioid receptors (κOR, activated by dynorphin) (Zhang et al., 2013). Local arcuate injection of NKB conjugated to saporin to ablate KNDY neurons notably increases the amplitude of the LH surge, perhaps via reduced dynorphin signaling (Mittelman-Smith et al., 2016). While this may appear to contradict the above study in which reducing the number of intact arcuate kisspeptin neurons reduced surge amplitude, the methods produce rather different outcomes at the cellular level, with the entire neuron and all its connections and transmitters being removed by saporin ablation vs targeted peptide removal in the former case.

The interplay between the AVPV and ARH kisspeptin populations is likely not solely unidirectional from the arcuate to the AVPV. Neuronal projections from the AVPV population are also found apposed to arcuate kisspeptin neurons (Kumar et al., 2015). In a pilot experiment, I found optogenetic activation of projections from the AVPV in ARH evoked PSCs in an ARH kisspeptin neuron (Figure 4-1 left). These PSCs appeared monosynaptic and GABAergic based on latency and decay time. Besides via direct projections, it is also possible the hypothalamic kisspeptin neuron populations interact indirectly via interneurons, including interneurons outside of the AVPV and arcuate since projections from both populations are found in hypothalamic areas such as the dorsomedial and paraventricular hypothalamus, bed nucleus of the stria terminals, and the organum vasculosum of the laminae terminalis (Stincic et al., 2021). The physiological relevance of arcuate/AVPV kisspeptin neuron interactions has not been determined and is an intriguing area for future research. Another interesting and unexplored area is GnRH-neuron transmission to kisspeptin neurons. GnRH-positive appositions are found near AVPV and arcuate kisspeptin neurons yet the possibility of GnRH neurons playing a more active role in the kisspeptin system has not been explored functionally.

Summary

The work described in this dissertation increases our understanding of the physiology of neurons theorized as critical for the neuroendocrine control of ovulation: kisspeptin-expressing neurons in the rostral hypothalamus. It identified three subthreshold voltage-gated currents that are important for regulating spike patterns of these cells in mice, and in the process created a computational tool that can be used for future studies of the central reproductive network. It also revealed new information about how these cells transmit information to GnRH neurons, and how this transmission changes across the reproductive cycle or when ovarian hormones are absent.

Figures and Legends

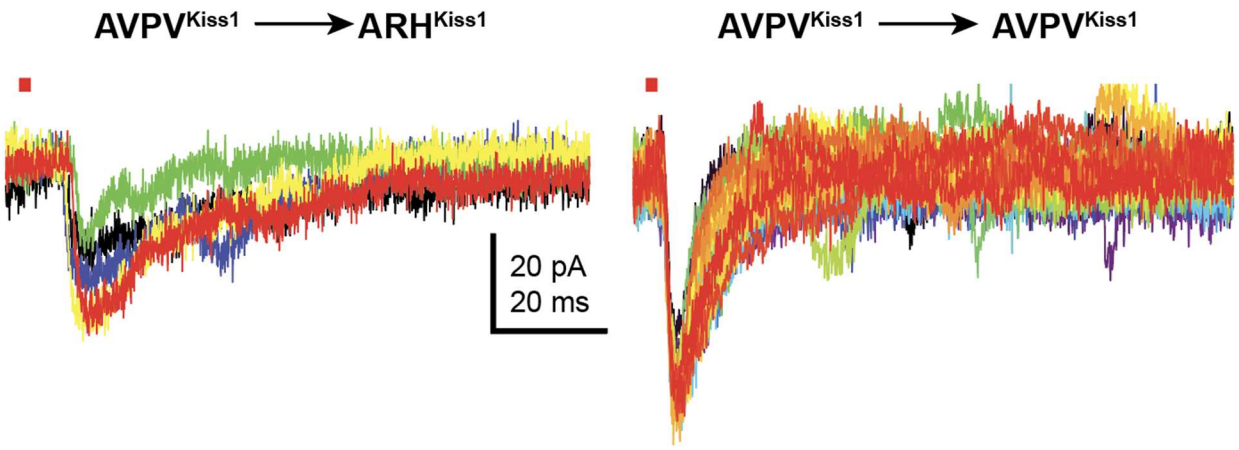

Figure 4-1 Photostimulation of AVPV kisspeptin neurons evokes post-synaptic currents (PSCs) in GFP-identified kisspeptin neurons in the AVPV and arcuate. **Left:** Voltage-clamp recording of a GFP-positive, tdTomato-negative neuron in the arcuate nucleus of an AAV-hSyn-FLEX-ChrimsonR-tdTomato injected Kiss-Cre;Kiss-hrGFP female mouse. Colors denote overlaid responses to repeated 1 ms red-light stimuli trials (1s inter-trial interval, top). **Right:** From the same mouse studied in the left, PSCs were evoked in a GFP-positive, tdTomato-negative neuron in the AVPV. AVPV, anteroventral periventricular nucleus. ARH, arcuate nucleus. Kiss1, kisspeptin.

Bibliography

Adachi S, Yamada S, Takatsu Y, Matsui H, Kinoshita M, Takase K, Sugiura H, Ohtaki T, Matsumoto H, Uenoyama Y, Tsukamura H, Inoue K, Maeda K-I (2007) Involvement of anteroventral periventricular metastin/kisspeptin neurons in estrogen positive feedback action on luteinizing hormone release in female rats. J Reprod Dev 53:367–378.

Adams C, Chen X, Moenter SM (2018a) Changes in GABAergic Transmission to and Intrinsic Excitability of Gonadotropin-Releasing Hormone (GnRH) Neurons during the Estrous Cycle in Mice. eNeuro 5.

Adams C, Stroberg W, DeFazio RA, Schnell S, Moenter SM (2018b) Gonadotropin-Releasing Hormone (GnRH) Neuron Excitability Is Regulated by Estradiol Feedback and Kisspeptin. J Neurosci 38:1249–1263.

Adams VL, Goodman RL, Salm AK, Coolen LM, Karsch FJ, Lehman MN (2006) Morphological Plasticity in the Neural Circuitry Responsible for Seasonal Breeding in the Ewe. Endocrinology 147:4843–4851.

Adler BA, Crowley WR (1986) Evidence for gamma-aminobutyric acid modulation of ovarian hormonal effects on luteinizing hormone secretion and hypothalamic catecholamine activity in the female rat. Endocrinology 118:91–97.

Alcami P, Franconville R, Llano I, Marty A (2012) Measuring the firing rate of high-resistance neurons with cell-attached recording. J Neurosci 32:3118–3130.

Armstrong CM, Bezanilla F (1977) Inactivation of the sodium channel. II. Gating current experiments. J Gen Physiol 70:567–590.

As K, Ml G, J R, Ac B, A C, Dk C, Ge H, Ra S, M T-S (2007) Sexual differentiation of Kiss1 gene expression in the brain of the rat. Endocrinology 148 Available at: https://pubmed.ncbi.nlm.nih.gov/17204549/ [Accessed October 3, 2022].

Banciu A, Banciu DD, Mustaciosu CC, Radu M, Cretoiu D, Xiao J, Cretoiu SM, Suciu N, Radu BM (2018) Beta-Estradiol Regulates Voltage-Gated Calcium Channels and Estrogen Receptors in Telocytes from Human Myometrium. Int J Mol Sci 19:1413.

Barry PH (1994) JPCalc, a software package for calculating liquid junction potential corrections in patch-clamp, intracellular, epithelial and bilayer measurements and for correcting junction potential measurements. J Neurosci Methods 51:107–116.

Belchetz PE, Plant TM, Nakai Y, Keogh EJ, Knobil E (1978) Hypophysial responses to continuous and intermittent delivery of hypopthalamic gonadotropin-releasing hormone. Science 202:631–633.

Bennett GW, Edwardson JA, Holland D, Jeffcoate SL, White N (1975) Release of immunoreactive luteinising hormone-releasing hormone and thyrotrophin-releasing hormone from hypothalamus. Nature 257:323–325.

Berson SA, Yalow RS, Bauman A, Rothschild MA, Newerly K (1956) INSULIN-I131 METABOLISM IN HUMAN SUBJECTS: DEMONSTRATION OF INSULIN BINDING GLOBULIN IN THE CIRCULATION OF INSULIN TREATED SUBJECTS 1. J Clin Invest 35:170–190.

Bevan MD, Wilson CJ (1999) Mechanisms Underlying Spontaneous Oscillation and Rhythmic Firing in Rat Subthalamic Neurons. J Neurosci 19:7617–7628.

Bicknell RJ, Flint APF, Leng G, Sheldrick EL (1982) Phasic pattern of electrical stimulation enhances oxytocin secretion from the isolated neurohypophysis. Neuroscience Letters 30:47–50.

Bosch MA, Tonsfeldt KJ, Rønnekleiv OK (2013) mRNA expression of ion channels in GnRH neurons: Subtype-specific regulation by 17β-estradiol. Molecular and Cellular Endocrinology 367:85–97.

Bronson FH, Vom Saal FS (1979) Control of the preovulatory release of luteinizing hormone by steroids in the mouse. Endocrinology 104:1247–1255.

Brown-Grant K, Exley D, Naftolin F (1970) Peripheral plasma oestradiol and luteinizing hormone concentrations during the oestrous cycle of the rat. J Endocrinol 48:295–296.

Burgus R, Butcher M, Amoss M, Ling N, Monahan M, Rivier J, Fellows R, Blackwell R, Vale W, Guillemin R (1972) Primary structure of the ovine hypothalamic luteinizing hormone-releasing factor (LRF) (LH-hypothalamus-LRF-gas chromatography-mass spectrometry-decapeptide-Edman degradation). Proc Natl Acad Sci U S A 69:278–282.

Campbell RE, Coolen LM, Hoffman GE, Hrabovszky E (2022) Highlights of neuroanatomical discoveries of the mammalian gonadotropin-releasing hormone system. Journal of Neuroendocrinology 34:e13115.

Campbell RE, Ducret E, Porteous R, Liu X, Herde MK, Wellerhaus K, Sonntag S, Willecke K, Herbison AE (2011) Gap junctions between neuronal inputs but not

gonadotropin-releasing hormone neurons control estrous cycles in the mouse. Endocrinology 152:2290–2301.

Campbell RE, Gaidamaka G, Han S-K, Herbison AE (2009) Dendro-dendritic bundling and shared synapses between gonadotropin-releasing hormone neurons. Proc Natl Acad Sci U S A 106:10835–10840.

Campbell RE, Han S-K, Herbison AE (2005) Biocytin filling of adult gonadotropin-releasing hormone neurons in situ reveals extensive, spiny, dendritic processes. Endocrinology 146:1163–1169.

Campos P, Herbison AE (2014) Optogenetic activation of GnRH neurons reveals minimal requirements for pulsatile luteinizing hormone secretion. Proceedings of the National Academy of Sciences 111:18387–18392.

Caraty A, Locatelli A, Martin GB (1989) Biphasic response in the secretion of gonadotrophin-releasing hormone in ovariectomized ewes injected with oestradiol. J Endocrinol 123:375–382.

Caraty A, Lomet D, Sébert ME, Guillaume D, Beltramo M, Evans NP (2013) Gonadotrophin-releasing hormone release into the hypophyseal portal blood of the ewe mirrors both pulsatile and continuous intravenous infusion of kisspeptin: an insight into kisspeptin's mechanism of action. J Neuroendocrinol 25:537–546.

Caraty A, Orgeur P, Thiery JC (1982) [Demonstration of the pulsatile secretion of LH-RH into hypophysial portal blood of ewes using an original technic for multiple samples]. C R Seances Acad Sci III 295:103–106.

Carmel PW, Araki S, Ferin M (1976) Pituitary stalk portal blood collection in rhesus monkeys: evidence for pulsatile release of gonadotropin-releasing hormone (GnRH). Endocrinology 99:243–248.

Chachlaki K et al. (2022) NOS1 mutations cause hypogonadotropic hypogonadism with sensory and cognitive deficits that can be reversed in infantile mice. Sci Transl Med 14:eabh2369.

Chan H, Prescott M, Ong Z, Herde MK, Herbison AE, Campbell RE (2011) Dendritic spine plasticity in gonadatropin-releasing hormone (GnRH) neurons activated at the time of the preovulatory surge. Endocrinology 152:4906–4914.

Chen X, Moenter S (2021) Relationship between action potentials and hormone release in gonadotropin-releasing hormone (GnRH) neurons is modified by gonadal feedback.

Cheong RY, Czieselsky K, Porteous R, Herbison AE (2015) Expression of ESR1 in Glutamatergic and GABAergic Neurons Is Essential for Normal Puberty Onset, Estrogen Feedback, and Fertility in Female Mice. J Neurosci 35:14533–14543.

Cheong RY, Porteous R, Chambon P, Abrahám I, Herbison AE (2014) Effects of neuron-specific estrogen receptor (ER) α and ERβ deletion on the acute estrogen negative feedback mechanism in adult female mice. Endocrinology 155:1418–1427.

Cholanian M, Krajewski-Hall SJ, Levine RB, McMullen NT, Rance NE (2014) Electrophysiology of arcuate neurokinin B neurons in female Tac2-EGFP transgenic mice. Endocrinology 155:2555–2565.

Choquet D, Korn H (1992) Mechanism of 4-aminopyridine action on voltage-gated potassium channels in lymphocytes. J Gen Physiol 99:217–240.

Christian CA, Mobley JL, Moenter SM (2005a) Diurnal and estradiol-dependent changes in gonadotropin-releasing hormone neuron firing activity. Proc Natl Acad Sci U S A 102:15682–15687.

Christian CA, Mobley JL, Moenter SM (2005b) Diurnal and estradiol-dependent changes in gonadotropin-releasing hormone neuron firing activity. PNAS 102:15682–15687.

Christian CA, Moenter SM (2007) Estradiol induces diurnal shifts in GABA transmission to gonadotropin-releasing hormone neurons to provide a neural signal for ovulation. J Neurosci 27:1913–1921.

Christian CA, Pielecka-Fortuna J, Moenter SM (2009) Estradiol suppresses glutamatergic transmission to gonadotropin-releasing hormone neurons in a model of negative feedback in mice. Biol Reprod 80:1128–1135.

Chu Z, Tomaiuolo M, Bertram R, Moenter SM (2012) Two types of burst firing in gonadotrophin-releasing hormone neurones. J Neuroendocrinol 24:1065–1077.

Clarke IJ, Cummins JT (1982) The temporal relationship between gonadotropin releasing hormone (GnRH) and luteinizing hormone (LH) secretion in ovariectomized ewes. Endocrinology 111:1737–1739.

Clarkson J, d'Anglemont de Tassigny X, Moreno AS, Colledge WH, Herbison AE (2008) Kisspeptin-GPR54 signaling is essential for preovulatory gonadotropin-releasing hormone neuron activation and the luteinizing hormone surge. J Neurosci 28:8691–8697.

Clarkson J, Herbison AE (2006) Postnatal development of kisspeptin neurons in mouse hypothalamus; sexual dimorphism and projections to gonadotropin-releasing hormone neurons. Endocrinology 147:5817–5825.

Clay JR (2000) Determining K+ channel activation curves from K+ channel currents. Eur Biophys J 29:555–557.

Clay JR (2009) Determining k channel activation curves from k channel currents often requires the goldman-hodgkin-katz equation. Front Cell Neurosci 3:20.

Coetzee WA, Amarillo Y, Chiu J, Chow A, Lau D, McCormack T, Moreno H, Nadal MS, Ozaita A, Pountney D, Saganich M, Vega-Saenz de Miera E, Rudy B (1999) Molecular diversity of K+ channels. Ann N Y Acad Sci 868:233–285.

Conn PM, Huckle WR, Andrews WV, McArdle CA (1987) The molecular mechanism of action of gonadotropin releasing hormone (GnRH) in the pituitary. Recent Prog Horm Res 43:29–68.

Constantin S, Moenter SM, Piet R (2022) The electrophysiologic properties of gonadotropin-releasing hormone neurons. J Neuroendocrinol 34:e13073.

Cooke BM, Woolley CS (2005) Gonadal hormone modulation of dendrites in the mammalian CNS. Journal of neurobiology 64:34–46.

Couse JF, Yates MM, Walker VR, Korach KS (2003) Characterization of the hypothalamic-pituitary-gonadal axis in estrogen receptor (ER) Null mice reveals hypergonadism and endocrine sex reversal in females lacking ERalpha but not ERbeta. Mol Endocrinol 17:1039–1053.

Cravo RM, Margatho LO, Osborne-Lawrence S, Donato J, Atkin S, Bookout AL, Rovinsky S, Frazão R, Lee CE, Gautron L, Zigman JM, Elias CF (2011) Characterization of Kiss1 neurons using transgenic mouse models. Neuroscience 173:37–56.

Cropper EC, Jing J, Vilim FS, Weiss KR (2018) Peptide Cotransmitters as Dynamic, Intrinsic Modulators of Network Activity. Front Neural Circuits 12:78.

Czieselsky K, Prescott M, Porteous R, Campos P, Clarkson J, Steyn FJ, Campbell RE, Herbison AE (2016) Pulse and Surge Profiles of Luteinizing Hormone Secretion in the Mouse. Endocrinology 157:4794–4802.

Dalkin AC, Haisenleder DJ, Ortolano GA, Ellis TR, Marshall JC (1989) The Frequency of Gonadotropin-Releasing-Hormone Stimulation Differentially Regulates

Gonadotropin Subunit Messenger Ribonucleic Acid Expression*. Endocrinology 125:917–923.

D'Amour FE (1940) Further Studies on Hormone Excretion During the Menstrual Cycle. American Journal of Obstetrics & Gynecology 40:958–965.

de Croft S, Piet R, Mayer C, Mai O, Boehm U, Herbison AE (2012a) Spontaneous kisspeptin neuron firing in the adult mouse reveals marked sex and brain region differences but no support for a direct role in negative feedback. Endocrinology 153:5384–5393.

de Croft S, Piet R, Mayer C, Mai O, Boehm U, Herbison AE (2012b) Spontaneous Kisspeptin Neuron Firing in the Adult Mouse Reveals Marked Sex and Brain Region Differences but No Support for a Direct Role in Negative Feedback. Endocrinology 153:5384–5393.

de Roux N, Genin E, Carel J-C, Matsuda F, Chaussain J-L, Milgrom E (2003) Hypogonadotropic hypogonadism due to loss of function of the KiSS1-derived peptide receptor GPR54. Proc Natl Acad Sci U S A 100:10972–10976.

DeFazio RA, Elias CF, Moenter SM (2014a) GABAergic transmission to kisspeptin neurons is differentially regulated by time of day and estradiol in female mice. J Neurosci 34:16296–16308.

DeFazio RA, Elias CF, Moenter SM (2014b) GABAergic transmission to kisspeptin neurons is differentially regulated by time of day and estradiol in female mice. J Neurosci 34:16296–16308.

DeFazio RA, Heger S, Ojeda SR, Moenter SM (2002a) Activation of A-type gamma-aminobutyric acid receptors excites gonadotropin-releasing hormone neurons. Mol Endocrinol 16:2872–2891.

DeFazio RA, Heger S, Ojeda SR, Moenter SM (2002b) Activation of A-type gamma-aminobutyric acid receptors excites gonadotropin-releasing hormone neurons. Mol Endocrinol 16:2872–2891.

DeFazio RA, Moenter SM (2002) Estradiol feedback alters potassium currents and firing properties of gonadotropin-releasing hormone neurons. Mol Endocrinol 16:2255–2265.

DeFazio RA, Navarro MA, Adams CE, Milescu LS, Moenter SM (2019) Estradiol Enhances the Depolarizing Response to GABA and AMPA Synaptic

Conductances in Arcuate Kisspeptin Neurons by Diminishing Voltage-Gated Potassium Currents. J Neurosci 39:9532–9545.

Deisseroth K (2015) Optogenetics: 10 years of microbial opsins in neuroscience. Nat Neurosci 18:1213–1225.

Dhillo WS, Chaudhri OB, Thompson EL, Murphy KG, Patterson M, Ramachandran R, Nijher GK, Amber V, Kokkinos A, Donaldson M, Ghatei MA, Bloom SR (2007) Kisspeptin-54 stimulates gonadotropin release most potently during the preovulatory phase of the menstrual cycle in women. J Clin Endocrinol Metab 92:3958–3966.

Dierschke DJ, Bhattacharya AN, Atkinson LE, Knobil E (1970) Circhoral oscillations of plasma LH levels in the ovariectomized rhesus monkey. Endocrinology 87:850–853.

Döcke F, Dörner G (1965) The mechanism of the induction of ovulation by oestrogens. J Endocrinol 33:491–499.

Du J, Wang Q, Hu F, Wang J, Ding H, Gao R, Xiao H, Wang L (2014) Effects of estradiol on voltage-gated potassium channels in mouse dorsal root ganglion neurons. J Membr Biol 247:541–548.

Dungan HM, Clifton DK, Steiner RA (2006) Minireview: kisspeptin neurons as central processors in the regulation of gonadotropin-releasing hormone secretion. Endocrinology 147:1154–1158.

Dutton A, Dyball RE (1979a) Phasic firing enhances vasopressin release from the rat neurohypophysis. J Physiol 290:433–440.

Dutton A, Dyball REJ (1979b) Phasic firing enhances vasopressin release from the rat neurohypophysis. J Physiol 290:433–440.

Dyer RG, Dyball RE (1974) Evidence for a direct effect of LRF and TRF on single unit activity in the rostral hypothalamus. Nature 252:486–488.

Evans NP, Dahl GE, Glover BH, Karsch FJ (1994) Central regulation of pulsatile gonadotropin-releasing hormone (GnRH) secretion by estradiol during the period leading up to the preovulatory GnRH surge in the ewe. Endocrinology 134:1806–1811.

Evans NP, Dahl GE, Mauger D, Karsch FJ (1995) Estradiol induces both qualitative and quantitative changes in the pattern of gonadotropin-releasing hormone secretion during the presurge period in the ewe. Endocrinology 136:1603–1609.

Frazão R, Cravo RM, Donato J, Ratra DV, Clegg DJ, Elmquist JK, Zigman JM, Williams KW, Elias CF (2013) Shift in Kiss1 Cell Activity Requires Estrogen Receptor α. J Neurosci 33:2807–2820.

Galea LAM, Frick KM, Hampson E, Sohrabji F, Choleris E (2017) Why estrogens matter for behavior and brain health. Neuroscience & Biobehavioral Reviews 76:363–379.

Glanowska KM, Moenter SM (2015) Differential regulation of GnRH secretion in the preoptic area (POA) and the median eminence (ME) in male mice. Endocrinology 156:231–241.

Glanowska KM, Venton BJ, Moenter SM (2012) Fast Scan Cyclic Voltammetry as a Novel Method for Detection of Real-Time Gonadotropin-Releasing Hormone Release in Mouse Brain Slices. J Neurosci 32:14664–14669.

Göcz B, Takács S, Skrapits K, Rumpler É, Solymosi N, Póliska S, Colledge WH, Hrabovszky E, Sárvári M (2022) Estrogen differentially regulates transcriptional landscapes of preoptic and arcuate kisspeptin neuron populations. Front Endocrinol (Lausanne) 13:960769.

Gold MS, Shuster MJ, Levine JD (1996) Characterization of six voltage-gated K+ currents in adult rat sensory neurons. J Neurophysiol 75:2629–2646.

Goldsmith PC, Thind KK, Perera AD, Plant TM (1994) Glutamate-immunoreactive neurons and their gonadotropin-releasing hormone-neuronal interactions in the monkey hypothalamus. Endocrinology 134:858–868.

Goodman RL (1978) The Site of the Positive Feedback Action of Estradiol in the Rat. Endocrinology 102:151–159.

Goodman RL, Herbison AE, Lehman MN, Navarro VM (2022) Neuroendocrine control of gonadotropin-releasing hormone: Pulsatile and surge modes of secretion. J Neuroendocrinol 34:e13094.

Goodman RL, Hileman SM, Nestor CC, Porter KL, Connors JM, Hardy SL, Millar RP, Cernea M, Coolen LM, Lehman MN (2013) Kisspeptin, neurokinin B, and dynorphin act in the arcuate nucleus to control activity of the GnRH pulse generator in ewes. Endocrinology 154:4259–4269.

Goodman RL, Karsch FJ (1980) Pulsatile secretion of luteinizing hormone: differential suppression by ovarian steroids. Endocrinology 107:1286–1290.

Gorur-Shandilya S, Hoyland A, Marder E (2018) Xolotl: An Intuitive and Approachable Neuron and Network Simulator for Research and Teaching. Front Neuroinform 12:87.

Gottsch ML, Clifton DK, Steiner RA (2006) Kisspepeptin-GPR54 signaling in the neuroendocrine reproductive axis. Mol Cell Endocrinol 254–255:91–96.

Gottsch ML, Clifton DK, Steiner RA (2009) From KISS1 to kisspeptins: An historical perspective and suggested nomenclature. Peptides 30:4–9.

Gottsch ML, Cunningham MJ, Smith JT, Popa SM, Acohido BV, Crowley WF, Seminara S, Clifton DK, Steiner RA (2004) A role for kisspeptins in the regulation of gonadotropin secretion in the mouse. Endocrinology 145:4073–4077.

Granados ST, Castillo K, Bravo-Moraga F, Sepúlveda RV, Carrasquel-Ursulaez W, Rojas M, Carmona E, Lorenzo-Ceballos Y, González-Nilo F, González C, Latorre R, Torres YP (2019) The molecular nature of the 17β-Estradiol binding site in the voltage- and Ca 2+ -activated K + (BK) channel β1 subunit. Sci Rep 9:9965.

Greenwald-Yarnell ML, Marsh C, Allison MB, Patterson CM, Kasper C, MacKenzie A, Cravo R, Elias CF, Moenter SM, Myers MG (2016) ERα in Tac2 Neurons Regulates Puberty Onset in Female Mice. Endocrinology 157:1555–1565.

Greep RO, Van Dyke HB, Chow BF (1942) Gonadotropins of the swine pituitary I. Various biological effects of purified Thylakentrin (FSH) and pure metakentrin (ICSH). Endocrinology 30:635–649.

Gusmao DO, Vieira HR, Mansano NS, Tavares MR, de Sousa LMM, Wasinski F, Frazao R, Donato Jr J (2022) Pattern of gonadotropin secretion along the estrous cycle of C57BL/6 female mice. Physiological Reports 10:e15460.

Gyurko R, Leupen S, Huang PL (2002) Deletion of exon 6 of the neuronal nitric oxide synthase gene in mice results in hypogonadism and infertility. Endocrinology 143:2767–2774.

Haisenleder DJ, Dalkin AC, Ortolano GA, Marshall JC, Shupnik MA (1991) A pulsatile gonadotropin-releasing hormone stimulus is required to increase transcription of the gonadotropin subunit genes: evidence for differential regulation of transcription by pulse frequency in vivo. Endocrinology 128:509–517.

Han S-K, Gottsch ML, Lee KJ, Popa SM, Smith JT, Jakawich SK, Clifton DK, Steiner RA, Herbison AE (2005) Activation of gonadotropin-releasing hormone neurons by kisspeptin as a neuroendocrine switch for the onset of puberty. J Neurosci 25:11349–11356.

Han S-K, Todman MG, Herbison AE (2004) Endogenous GABA release inhibits the firing of adult gonadotropin-releasing hormone neurons. Endocrinology 145:495–499.

Han SY, Kane G, Cheong I, Herbison AE (2019) Characterization of GnRH Pulse Generator Activity in Male Mice Using GCaMP Fiber Photometry. Endocrinology 160:557–567.

Han SY, McLennan T, Czieselsky K, Herbison AE (2015) Selective optogenetic activation of arcuate kisspeptin neurons generates pulsatile luteinizing hormone secretion. Proc Natl Acad Sci U S A 112:13109–13114.

Han SY, Morris PG, Kim J-C, Guru S, Pardo-Navarro M, Yeo S-H, McQuillan HJ, Herbison AE (2023) Mechanism of kisspeptin neuron synchronization for pulsatile hormone secretion in male mice. Cell Rep 42:111914.

Hanchate NK, Parkash J, Bellefontaine N, Mazur D, Colledge WH, d'Anglemont de Tassigny X, Prevot V (2012) Kisspeptin-GPR54 signaling in mouse NO-synthesizing neurons participates in the hypothalamic control of ovulation. J Neurosci 32:932–945.

Herbison AE, Moenter SM (2011) Depolarising and hyperpolarising actions of GABA(A) receptor activation on gonadotrophin-releasing hormone neurones: towards an emerging consensus. J Neuroendocrinol 23:557–569.

Herde MK, Iremonger KJ, Constantin S, Herbison AE (2013) GnRH neurons elaborate a long-range projection with shared axonal and dendritic functions. J Neurosci 33:12689–12697.

Herdegen T, Leah JD (1998) Inducible and constitutive transcription factors in the mammalian nervous system: control of gene expression by Jun, Fos and Krox, and CREB/ATF proteins. Brain Research Reviews 28:370–490.

Hille B (2001) Ion Channels of Excitable Membranes, 3 edition. Sunderland, Mass: Sinauer Associates is an imprint of Oxford University Press.

Hisano S, Kawano H, Maki Y, Daikoku S (1981) Electron microscopic study of immunoreactive LHRH perikarya with special reference to neuronal regulation. Cell Tissue Res 220:511–518.

Hoffman GE, Berghorn KA (1997) Gonadotropin-releasing hormone neurons: their structure and function. Semin Reprod Endocrinol 15:5–17.

Hoffman GE, Finch CE (1986) LHRH neurons in the female C57BL/6J mouse brain during reproductive aging: no loss up to middle age. Neurobiol Aging 7:45–48.

Hoffman GE, Le WW, Franceschini I, Caraty A, Advis JP (2011) Expression of fos and in vivo median eminence release of LHRH identifies an active role for preoptic area kisspeptin neurons in synchronized surges of LH and LHRH in the ewe. Endocrinology 152:214–222.

Hrabovszky E, Shughrue PJ, Merchenthaler I, Hajszán T, Carpenter CD, Liposits Z, Petersen SL (2000) Detection of estrogen receptor-beta messenger ribonucleic acid and 125I-estrogen binding sites in luteinizing hormone-releasing hormone neurons of the rat brain. Endocrinology 141:3506–3509.

Huang L, Ledochowitsch P, Knoblich U, Lecoq J, Murphy GJ, Reid RC, de Vries SE, Koch C, Zeng H, Buice MA, Waters J, Li L (2021) Relationship between simultaneously recorded spiking activity and fluorescence signal in GCaMP6 transgenic mice. Elife 10:e51675.

Hunzicker-Dunn M, Mayo K (2006) Gonadotropin signaling in the ovary. In: Knobil and Neill's Physiology of Reproduction, pp 547–592. Elsevier Inc. Available at: http://www.scopus.com/inward/record.url?scp=69549126164&partnerID=8YFLogxK [Accessed March 7, 2023].

Irvine CH, Alexander SL (1994) The dynamics of gonadotrophin-releasing hormone, LH and FSH secretion during the spontaneous ovulatory surge of the mare as revealed by intensive sampling of pituitary venous blood. J Endocrinol 140:283–295.

Jamieson BB, Bouwer GT, Campbell RE, Piet R (2021) Estrous Cycle Plasticity in the Central Clock Output to Kisspeptin Neurons: Implications for the Preovulatory Surge. Endocrinology 162:bqab071.

Jamieson BB, Piet R (2022) Kisspeptin neuron electrophysiology: Intrinsic properties, hormonal modulation, and regulation of homeostatic circuits. Frontiers in Neuroendocrinology 66:101006.

Jarry H, Leonhardt S, Wuttke W (1991) Gamma-aminobutyric acid neurons in the preoptic/anterior hypothalamic area synchronize the phasic activity of the gonadotropin-releasing hormone pulse generator in ovariectomized rats. Neuroendocrinology 53:261–267.

Jennes L, Stumpf WE, Sheedy ME (1985) Ultrastructural characterization of gonadotropin-releasing hormone (GnRH)-producing neurons. J Comp Neurol 232:534–547.

Kalra PS, McCann SM (1975) The stimulatory effect on gonadotropin release of implants of estradiol or progesterone in certain sites in the central nervous system. Neuroendocrinology 19:289–302.

Karsch FJ, Cummins JT, Thomas GB, Clarke IJ (1987a) Steroid feedback inhibition of pulsatile secretion of gonadotropin-releasing hormone in the ewe. Biol Reprod 36:1207–1218.

Karsch FJ, Cummins JT, Thomas GB, Clarke IJ (1987b) Steroid feedback inhibition of pulsatile secretion of gonadotropin-releasing hormone in the ewe. Biol Reprod 36:1207–1218.

Kawakami M, Uemura T, Hayashi R (1982) Electrophysiological correlates of pulsatile gonadotropin release in rats. Neuroendocrinology 35:63–67.

Kaynard AH, Pau KY, Hess DL, Spies HG (1990) Gonadotropin-releasing hormone and norepinephrine release from the rabbit mediobasal and anterior hypothalamus during the mating-induced luteinizing hormone surge. Endocrinology 127:1176–1185.

Kehl SJ (2017) A Model of the Block of Voltage-Gated Potassium Kv4.2 Ionic Currents by 4-Aminopyridine. J Pharmacol Exp Ther 363:184–195.

Kelly MJ, Qiu J (2010) Estrogen Signaling in Hypothalamic Circuits Controling Reproduction. Brain Res 1364:44–52.

Kerdelhué B, Brown S, Lenoir V, Queenan JT, Jones GS, Scholler R, Jones HW (2002) Timing of initiation of the preovulatory luteinizing hormone surge and its relationship with the circadian cortisol rhythm in the human. Neuroendocrinology 75:158–163.

Kim SJ, Foster DL, Wood RI (1999) Prenatal testosterone masculinizes synaptic input to gonadotropin-releasing hormone neurons in sheep. Biol Reprod 61:599–605.

Kimm T, Khaliq ZM, Bean BP (2015) Differential Regulation of Action Potential Shape and Burst-Frequency Firing by BK and Kv2 Channels in Substantia Nigra Dopaminergic Neurons. J Neurosci 35:16404–16417.

Kimura F, Jinnai K (1994) Bicuculline infusions advance the timing of luteinizing hormone surge in proestrous rats: comparisons with naloxone effects. Horm Behav 28:424–430.

Klapoetke NC et al. (2014) Independent optical excitation of distinct neural populations. Nat Methods 11:338–346.

Knobil E (1988) The neuroendocrine control of ovulation. Hum Reprod 3:469–472.

Knobil E, Plant TM, Wildt L, Belchetz PE, Marshall G (1980) Control of the rhesus monkey menstrual cycle: permissive role of hypothalamic gonadotropin-releasing hormone. Science 207:1371–1373.

Kovács KJ (2008) Measurement of Immediate-Early Gene Activation- c-fos and Beyond. Journal of Neuroendocrinology 20:665–672.

Kozlowski GP, Chu L, Hostetter G, Kerdelhué B (1980) Cellular characteristics of immunolabeled luteinizing hormone releasing hormone (LHRH) neurons. Peptides 1:37–46.

Kress GJ, Dowling MJ, Eisenman LN, Mennerick S (2010) Axonal sodium channel distribution shapes the depolarized action potential threshold of dentate granule neurons. Hippocampus 20:558–571.

Kumar D, Candlish M, Periasamy V, Avcu N, Mayer C, Boehm U (2015) Specialized subpopulations of kisspeptin neurons communicate with GnRH neurons in female mice. Endocrinology 156:32–38.

Lee K, Porteous R, Campbell RE, Lüscher B, Herbison AE (2010) Knockdown of GABA(A) receptor signaling in GnRH neurons has minimal effects upon fertility. Endocrinology 151:4428–4436.

Lee SK, Ryu PD, Lee SY (2013) Estrogen replacement modulates voltage-gated potassium channels in rat presympathetic paraventricular nucleus neurons. BMC Neurosci 14:134.

Lehman MN, Goodman RL, Karsch FJ, Jackson GL, Berriman SJ, Jansen HT (1997) The GnRH System of Seasonal Breeders: Anatomy and Plasticity. Brain Research Bulletin 44:445–457.

Lehman MN, Hileman SM, Goodman RL (2013) Neuroanatomy of the Kisspeptin Signaling System in Mammals: Comparative and Developmental Aspects. Adv Exp Med Biol 784:27–62.

Lehman MN, Karsch FJ, Robinson JE, Silverman A-J (1988) Ultrastructure and synaptic organization of luteinizing hormone-releasing hormone (LHRH) neurons in the anestrous ewe. Journal of Comparative Neurology 273:447–458.

Lehman MN, Silverman AJ (1988) Ultrastructure of luteinizing hormone-releasing hormone (LHRH) neurons and their projections in the golden hamster. Brain Res Bull 20:211–221.

Leranth C, MacLusky NJ, Sakamoto H, Shanabrough M, Naftolin F (1985a) Glutamic acid decarboxylase-containing axons synapse on LHRH neurons in the rat medial preoptic area. Neuroendocrinology 40:536–539.

Leranth C, Segura LM, Palkovits M, MacLusky NJ, Shanabrough M, Naftolin F (1985b) The LH-RH-containing neuronal network in the preoptic area of the rat: demonstration of LH-RH-containing nerve terminals in synaptic contact with LH-RH neurons. Brain Res 345:332–336.

Levine JE, Norman RL, Gliessman PM, Oyama TT, Bangsberg DR, Spies HG (1985) In Vivo Gonadotropin-Releasing Hormone Release and Serum Luteinizing Hormone Measurements in Ovariectomized, Estrogen-Treated Rhesus Macaques. Endocrinology 117:711–721.

Levine JE, Ramirez VD (1982) Luteinizing Hormone-Releasing Hormone Release during the Rat Estrous Cycle and after Ovariectomy, as Estimated with Push-Pull Cannulae. Endocrinology 111:1439–1448.

Levitan IB (2006) Signaling protein complexes associated with neuronal ion channels. Nat Neurosci 9:305–310.

Lin MZ, Schnitzer MJ (2016) Genetically encoded indicators of neuronal activity. Nat Neurosci 19:1142–1153.

Liu X, Porteous R, Herbison AE (2017) Dynamics of GnRH Neuron Ionotropic GABA and Glutamate Synaptic Receptors Are Unchanged during Estrogen Positive and Negative Feedback in Female Mice. eNeuro 4:ENEURO.0259-17.2017.

Liu X, Porteous R, Tassigny X d'Anglemont de, Colledge WH, Millar R, Petersen SL, Herbison AE (2011) Frequency-Dependent Recruitment of Fast Amino Acid and

Slow Neuropeptide Neurotransmitter Release Controls Gonadotropin-Releasing Hormone Neuron Excitability. J Neurosci 31:2421–2430.

Lüthi A, McCormick DA (1998) H-current: properties of a neuronal and network pacemaker. Neuron 21:9–12.

Marni F, Wang Y, Morishima M, Shimaoka T, Uchino T, Zheng M, Kaku T, Ono K (2009) 17β-Estradiol Modulates Expression of Low-Voltage-Activated CaV3.2 T-Type Calcium Channel via Extracellularly Regulated Kinase Pathway in Cardiomyocytes. Endocrinology 150:879–888.

Martin GB, Thiéry JC (1987) Hypothalamic multiunit activity and LH secretion in conscious sheep. Exp Brain Res 67:469–478.

Martin K, Santoro N, Hall J, Filicori M, Wierman M, Crowley WF (1990) Clinical review 15: Management of ovulatory disorders with pulsatile gonadotropin-releasing hormone. J Clin Endocrinol Metab 71:1081A-1081G.

Matsuda F, Nakatsukasa K, Suetomi Y, Naniwa Y, Ito D, Inoue N, Wakabayashi Y, Okamura H, Maeda K-I, Uenoyama Y, Tsukamura H, Ohkura S (2015) The Luteinising Hormone Surge-Generating System is Functional in Male Goats as in Females: Involvement of Kisspeptin Neurones in the Medial Preoptic Area. Journal of Neuroendocrinology 27:57–65.

Mayer C, Acosta-Martinez M, Dubois SL, Wolfe A, Radovick S, Boehm U, Levine JE (2010) Timing and completion of puberty in female mice depend on estrogen receptor α-signaling in kisspeptin neurons. Proceedings of the National Academy of Sciences 107:22693–22698.

Mayer C, Boehm U (2011) Female reproductive maturation in the absence of kisspeptin/GPR54 signaling. Nat Neurosci 14:704–710.

Mendonça PRF, Kyle V, Yeo S-H, Colledge WH, Robinson HPC (2018) Kv4.2 channel activity controls intrinsic firing dynamics of arcuate kisspeptin neurons. J Physiol (Lond) 596:885–899.

Merkley CM, Coolen LM, Goodman RL, Lehman MN (2015) Evidence for Changes in Numbers of Synaptic Inputs onto KNDy and GnRH Neurones during the Preovulatory LH Surge in the Ewe. Journal of Neuroendocrinology 27:624–635.

Merkley CM, Porter KL, Coolen LM, Hileman SM, Billings HJ, Drews S, Goodman RL, Lehman MN (2012) KNDy (kisspeptin/neurokinin B/dynorphin) neurons are

activated during both pulsatile and surge secretion of LH in the ewe. Endocrinology 153:5406–5414.

Messager S, Chatzidaki EE, Ma D, Hendrick AG, Zahn D, Dixon J, Thresher RR, Malinge I, Lomet D, Carlton MBL, Colledge WH, Caraty A, Aparicio SAJR (2005) Kisspeptin directly stimulates gonadotropin-releasing hormone release via G protein-coupled receptor 54. Proc Natl Acad Sci U S A 102:1761–1766.

Mittelman-Smith MA, Krajewski-Hall SJ, McMullen NT, Rance NE (2016) Ablation of KNDy Neurons Results in Hypogonadotropic Hypogonadism and Amplifies the Steroid-Induced LH Surge in Female Rats. Endocrinology 157:2015–2027.

Moenter SM (2015) Leap of Faith: Does Serum Luteinizing Hormone Always Accurately Reflect Central Reproductive Neuroendocrine Activity? Neuroendocrinology 102:256–266.

Moenter SM, Brand RC, Karsch FJ (1992a) Dynamics of gonadotropin-releasing hormone (GnRH) secretion during the GnRH surge: insights into the mechanism of GnRH surge induction. Endocrinology 130:2978–2984.

Moenter SM, Brand RC, Karsch FJ (1992b) Dynamics of gonadotropin-releasing hormone (GnRH) secretion during the GnRH surge: insights into the mechanism of GnRH surge induction. Endocrinology 130:2978–2984.

Moenter SM, Brand RM, Midgley AR, Karsch FJ (1992c) Dynamics of gonadotropin-releasing hormone release during a pulse. Endocrinology 130:503–510.

Moenter SM, Caraty A, Karsch FJ (1990) The estradiol-induced surge of gonadotropin-releasing hormone in the ewe. Endocrinology 127:1375–1384.

Moenter SM, Caraty A, Locatelli A, Karsch FJ (1991) Pattern of Gonadotropin-Releasing Hormone (GnRH) Secretion Leading up to Ovulation in the Ewe: Existence of a Preovulatory GnRH Surge. Endocrinology 129:1175–1182.

Moenter SM, Evans NP (2022) Gonadotropin-releasing hormone (GnRH) measurements in pituitary portal blood: A history. J Neuroendocrinol 34:e13065.

Mohr MA, Wong AM, Sukumar G, Dalgard CL, Hong W, Wu TJ, Wu YE, Micevych PE (2021) RNA-sequencing of AVPV and ARH reveals vastly different temporal and transcriptomic responses to estradiol in the female rat hypothalamus. PLoS One 16:e0256148.

Moore AM, Coolen LM, Lehman MN (2022) In vivo imaging of the GnRH pulse generator reveals a temporal order of neuronal activation and synchronization during each pulse. Proceedings of the National Academy of Sciences 119:e2117767119.

Moore AM, Prescott M, Czieselsky K, Desroziers E, Yip SH, Campbell RE, Herbison AE (2018) Synaptic Innervation of the GnRH Neuron Distal Dendron in Female Mice. Endocrinology 159:3200–3208.

Moore CR, Price D (1932) Gonad hormone functions, and the reciprocal influence between gonads and hypophysis with its bearing on the problem of sex hormone antagonism. American Journal of Anatomy 50:13–71.

Moran S, Moenter SM, Khadra A (2016) A unified model for two modes of bursting in GnRH neurons. J Comput Neurosci 40:297–315.

Mori Y, Nishihara M, Tanaka T, Shimizu T, Yamaguchi M, Takeuchi Y, Hoshino K (1991) Chronic recording of electrophysiological manifestation of the hypothalamic gonadotropin-releasing hormone pulse generator activity in the goat. Neuroendocrinology 53:392–395.

Moss RL, Dudley CA (1978) Changes in responsiveness of medial preoptic neurons to the microelectrophoresis of releasing hormones as a function of ovarian hormones. Brain Res 149:511–515.

Nagae M, Uenoyama Y, Okamoto S, Tsuchida H, Ikegami K, Goto T, Majarune S, Nakamura S, Sanbo M, Hirabayashi M, Kobayashi K, Inoue N, Tsukamura H (2021) Direct evidence that KNDy neurons maintain gonadotropin pulses and folliculogenesis as the GnRH pulse generator. Proc Natl Acad Sci U S A 118:e2009156118.

Narayanaswamy S, Jayasena CN, Ng N, Ratnasabapathy R, Prague JK, Papadopoulou D, Abbara A, Comninos AN, Bassett P, Bloom SR, Veldhuis JD, Dhillo WS (2016) Subcutaneous infusion of kisspeptin-54 stimulates gonadotrophin release in women and the response correlates with basal oestradiol levels. Clin Endocrinol (Oxf) 84:939–945.

Navarro VM, Bosch MA, León S, Simavli S, True C, Pinilla L, Carroll RS, Seminara SB, Tena-Sempere M, Rønnekleiv OK, Kaiser UB (2015) The integrated hypothalamic tachykinin-kisspeptin system as a central coordinator for reproduction. Endocrinology 156:627–637.

Navarro VM, Gottsch ML, Chavkin C, Okamura H, Clifton DK, Steiner RA (2009) Regulation of gonadotropin-releasing hormone secretion by kisspeptin/dynorphin/neurokinin B neurons in the arcuate nucleus of the mouse. J Neurosci 29:11859–11866.

Neill JD, Patton JM, Dailey RA, Tsou RC, Tindall GT (1977) Luteinizing hormone releasing hormone (LHRH) in pituitary stalk blood of rhesus monkeys: relationship to level of LH release. Endocrinology 101:430–434.

Nottebohm F (1981) A brain for all seasons: cyclical anatomical changes in song control nuclei of the canary brain. Science 214:1368–1370.

Novaira HJ, Sonko ML, Hoffman G, Koo Y, Ko C, Wolfe A, Radovick S (2014) Disrupted Kisspeptin Signaling in GnRH Neurons Leads to Hypogonadotrophic Hypogonadism. Mol Endocrinol 28:225–238.

Nunemaker CS, DeFazio RA, Moenter SM (2002) Estradiol-sensitive afferents modulate long-term episodic firing patterns of GnRH neurons. Endocrinology 143:2284–2292.

Nunemaker CS, DeFazio RA, Moenter SM (2003a) A targeted extracellular approach for recording long-term firing patterns of excitable cells: a practical guide. Biol Proced Online 5:53–62.

Nunemaker CS, Straume M, DeFazio RA, Moenter SM (2003b) Gonadotropin-releasing hormone neurons generate interacting rhythms in multiple time domains. Endocrinology 144:823–831.

Oakley AE, Clifton DK, Steiner RA (2009a) Kisspeptin signaling in the brain. Endocr Rev 30:713–743.

Oakley AE, Clifton DK, Steiner RA (2009b) Kisspeptin signaling in the brain. Endocr Rev 30:713–743.

Padilla SL, Perez JG, Ben-Hamo M, Johnson CW, Sanchez REA, Bussi IL, Palmiter RD, de la Iglesia HO (2019) Kisspeptin Neurons in the Arcuate Nucleus of the Hypothalamus Orchestrate Circadian Rhythms and Metabolism. Curr Biol 29:592-604.e4.

Pau KY, Berria M, Hess DL, Spies HG (1993) Preovulatory gonadotropin-releasing hormone surge in ovarian-intact rhesus macaques. Endocrinology 133:1650–1656.

Pelletier G, Labrie F, Puviani R, Arimura A, Schally AV (1974) Immunohistochemical localization of luteinizing hormone-releasing hormone in the rat median eminence. Endocrinology 95:314–317.

Perez-Reyes E (2003) Molecular physiology of low-voltage-activated t-type calcium channels. Physiol Rev 83:117–161.

Petersen SL, Barraclough CA (1989) Suppression of spontaneous LH surges in estrogen-treated ovariectomized rats by microimplants of antiestrogens into the preoptic brain. Brain Res 484:279–289.

Petersen SL, Cheuk C, Hartman RD, Barraclough CA (1989) Medial preoptic microimplants of the antiestrogen, keoxifene, affect luteinizing hormone-releasing hormone mRNA levels, median eminence luteinizing hormone-releasing hormone concentrations and luteinizing hormone release in ovariectomized, estrogen-treated rats. J Neuroendocrinol 1:279–283.

Petreanu L, Mao T, Sternson SM, Svoboda K (2009) The subcellular organization of neocortical excitatory connections. Nature 457:1142–1145.

Phumsatitpong C, De Guzman RM, Zuloaga DG, Moenter SM (2020) A CRH Receptor Type 1 Agonist Increases GABA Transmission to GnRH Neurons in a Circulating-Estradiol-Dependent Manner. Endocrinology 161:bqaa140.

Pielecka-Fortuna J, Chu Z, Moenter SM (2008) Kisspeptin acts directly and indirectly to increase gonadotropin-releasing hormone neuron activity and its effects are modulated by estradiol. Endocrinology 149:1979–1986.

Pielecka-Fortuna J, DeFazio RA, Moenter SM (2011) Voltage-Gated Potassium Currents Are Targets of Diurnal Changes in Estradiol Feedback Regulation and Kisspeptin Action on Gonadotropin-Releasing Hormone Neurons in Mice. Biol Reprod 85:987–995.

Piet R, Boehm U, Herbison AE (2013a) Estrous cycle plasticity in the hyperpolarization-activated current ih is mediated by circulating 17β-estradiol in preoptic area kisspeptin neurons. J Neurosci 33:10828–10839.

Piet R, Boehm U, Herbison AE (2013b) Estrous cycle plasticity in the hyperpolarization-activated current ih is mediated by circulating 17β-estradiol in preoptic area kisspeptin neurons. J Neurosci 33:10828–10839.

Piet R, Kalil B, McLennan T, Porteous R, Czieselsky K, Herbison AE (2018) Dominant Neuropeptide Cotransmission in Kisspeptin-GABA Regulation of GnRH Neuron Firing Driving Ovulation. J Neurosci 38:6310–6322.

Ping L, Mahesh VB, Bhat GK, Brann DW (1997) Regulation of gonadotropin-releasing hormone and luteinizing hormone secretion by AMPA receptors. Evidence for a physiological role of AMPA receptors in the steroid-induced luteinizing hormone surge. Neuroendocrinology 66:246–253.

Plant TM, Krey LC, Moossy J, McCormack JT, Hess DL, Knobil E (1978) The arcuate nucleus and the control of gonadotropin and prolactin secretion in the female rhesus monkey (Macaca mulatta). Endocrinology 102:52–62.

Porteous R, Herbison AE (2019) Genetic Deletion of Esr1 in the Mouse Preoptic Area Disrupts the LH Surge and Estrous Cyclicity. Endocrinology 160:1821–1829.

Porteous R, Petersen SL, Yeo SH, Bhattarai JP, Ciofi P, de Tassigny XD, Colledge WH, Caraty A, Herbison AE (2011) Kisspeptin neurons co-express met-enkephalin and galanin in the rostral periventricular region of the female mouse hypothalamus. J Comp Neurol 519:3456–3469.

Prevot V, Hanchate NK, Bellefontaine N, Sharif A, Parkash J, Estrella C, Allet C, de Seranno S, Campagne C, de Tassigny X d'Anglemont, Baroncini M (2010) Function-related structural plasticity of the GnRH system: a role for neuronal-glial-endothelial interactions. Front Neuroendocrinol 31:241–258.

Qiu J, Bosch MA, Jamali K, Xue C, Kelly MJ, Rønnekleiv OK (2006) Estrogen upregulates T-type calcium channels in the hypothalamus and pituitary. J Neurosci 26:11072–11082.

Qiu J, Nestor CC, Zhang C, Padilla SL, Palmiter RD, Kelly MJ, Rønnekleiv OK (2016) High-frequency stimulation-induced peptide release synchronizes arcuate kisspeptin neurons and excites GnRH neurons. Elife 5:e16246.

Roberts WM, Almers W (1992) Patch voltage clamping with low-resistance seals: loose patch clamp. Methods Enzymol 207:155–176.

Robertson JL, Clifton DK, de la Iglesia HO, Steiner RA, Kauffman AS (2009) Circadian regulation of Kiss1 neurons: implications for timing the preovulatory gonadotropin-releasing hormone/luteinizing hormone surge. Endocrinology 150:3664–3671.

Roepke TA, Malyala A, Bosch MA, Kelly MJ, Rønnekleiv OK (2007) Estrogen regulation of genes important for K+ channel signaling in the arcuate nucleus. Endocrinology 148:4937–4951.

Romero MT, Silverman AJ, Wise PM, Witkin JW (1994) Ultrastructural changes in gonadotropin-releasing hormone neurons as a function of age and ovariectomy in rats. Neuroscience 58:217–225.

Rønnekleiv OK, Kelly MJ (2013) Kisspeptin excitation of GnRH neurons. Adv Exp Med Biol 784:113–131.

Ronnekleiv OK, Naylor BR, Bond CT, Adelman JP (1989) Combined immunohistochemistry for gonadotropin-releasing hormone (GnRH) and pro-GnRH, and in situ hybridization for GnRH messenger ribonucleic acid in rat brain. Mol Endocrinol 3:363–371.

Rønnekleiv OK, Zhang C, Bosch MA, Kelly MJ (2015) Kisspeptin and GnRH Neuronal Excitability: Molecular Mechanisms Driven by 17β-Estradiol. Neuroendocrinology 102:184–193.

Roth BL (2016) DREADDs for Neuroscientists. Neuron 89:683–694.

Ruka KA, Burger LL, Moenter SM (2013) Regulation of arcuate neurons coexpressing kisspeptin, neurokinin B, and dynorphin by modulators of neurokinin 3 and κ-opioid receptors in adult male mice. Endocrinology 154:2761–2771.

Sakmann B, Neher E (1995) Single Channel Recording, 2nd ed. New York, NY: Springer.

Sanz E, Yang L, Su T, Morris DR, McKnight GS, Amieux PS (2009) Cell-type-specific isolation of ribosome-associated mRNA from complex tissues. Proceedings of the National Academy of Sciences 106:13939–13944.

Sarkar DK, Chiappa SA, Fink G, Sherwood NM (1976a) Gonadotropin-releasing hormone surge in pro-oestrous rats. Nature 264:461–463.

Sarkar DK, Chiappa SA, Fink G, Sherwood NM (1976b) Gonadotropin-releasing hormone surge in pro-oestrous rats. Nature 264:461–463.

Schally AV, Arimura A, Kastin AJ, Matsuo H, Baba Y, Redding TW, Nair RM, Debeljuk L, White WF (1971) Gonadotropin-releasing hormone: one polypeptide regulates secretion of luteinizing and follicle-stimulating hormones. Science 173:1036–1038.

Seminara SB et al. (2003) The GPR54 gene as a regulator of puberty. N Engl J Med 349:1614–1627.

Sergeeva A, Jansen HT (2009) Neuroanatomical plasticity in the gonadotropin-releasing hormone system of the ewe: Seasonal variation in glutamatergic and γ-aminobutyric acidergic afferents. Journal of Comparative Neurology 515:615–628.

Shim WS, Conaway M, Masamura S, Yue W, Wang JP, Kmar R, Santen RJ (2000a) Estradiol hypersensitivity and mitogen-activated protein kinase expression in long-term estrogen deprived human breast cancer cells in vivo. Endocrinology 141:396–405.

Shim WS, Conaway M, Masamura S, Yue W, Wang JP, Kmar R, Santen RJ (2000b) Estradiol hypersensitivity and mitogen-activated protein kinase expression in long-term estrogen deprived human breast cancer cells in vivo. Endocrinology 141:396–405.

Silveira MA, Burger LL, DeFazio RA, Wagenmaker ER, Moenter SM (2017) GnRH Neuron Activity and Pituitary Response in Estradiol-Induced vs Proestrous Luteinizing Hormone Surges in Female Mice. Endocrinology 158:356–366.

Silverman AJ (1984) Luteinizing hormone releasing hormone containing synapses in the diagonal band and preoptic area of the guinea pig. J Comp Neurol 227:452–458.

Silverman AJ, Livne I, Witkin JW (1994) The gondotropin-releasing hormone (GnRH) neuronal systems: immunocytochemistry and in situ hybridization. In: The physiology of reproduction, II., pp 1683–1706. New York.

Silverman AJ, Witkin JW (1985) Synaptic interactions of luteinizing hormone-releasing hormone (LHRH) neurons in the guinea pig preoptic area. J Histochem Cytochem 33:69–72.

Simerly RB (1998a) Organization and regulation of sexually dimorphic neuroendocrine pathways. Behav Brain Res 92:195–203.

Simerly RB (1998b) Organization and regulation of sexually dimorphic neuroendocrine pathways. Behav Brain Res 92:195–203.

Skinner DC, Evans NP, Delaleu B, Goodman RL, Bouchard P, Caraty A (1998) The negative feedback actions of progesterone on gonadotropin-releasing hormone secretion are transduced by the classical progesterone receptor. Proc Natl Acad Sci U S A 95:10978–10983.

Smith JT, Cunningham MJ, Rissman EF, Clifton DK, Steiner RA (2005a) Regulation of Kiss1 gene expression in the brain of the female mouse. Endocrinology 146:3686–3692.

Smith JT, Dungan HM, Stoll EA, Gottsch ML, Braun RE, Eacker SM, Clifton DK, Steiner RA (2005b) Differential regulation of KiSS-1 mRNA expression by sex steroids in the brain of the male mouse. Endocrinology 146:2976–2984.

Smith JT, Li Q, Pereira A, Clarke IJ (2009) Kisspeptin Neurons in the Ovine Arcuate Nucleus and Preoptic Area Are Involved in the Preovulatory Luteinizing Hormone Surge. Endocrinology 150:5530–5538.

Smith JT, Popa SM, Clifton DK, Hoffman GE, Steiner RA (2006) Kiss1 neurons in the forebrain as central processors for generating the preovulatory luteinizing hormone surge. J Neurosci 26:6687–6694.

Smith LB, Walker WH (2014) Hormone Signaling in the Testis. Knobil and Neill's Physiology of Reproduction: Two-Volume Set:637–690.

Soper BD, Weick RF (1980) Hypothalamic and extrahypothalamic mediation of pulsatile discharges of luteinizing hormone in the ovariectomized rat. Endocrinology 106:348–355.

Spergel DJ, Krüth U, Hanley DF, Sprengel R, Seeburg PH (1999) GABA- and glutamate-activated channels in green fluorescent protein-tagged gonadotropin-releasing hormone neurons in transgenic mice. J Neurosci 19:2037–2050.

Standish LJ, Adams LA, Vician L, Clifton DK, Steiner RA (1987) Neuroanatomical localization of cells containing gonadotropin-releasing hormone messenger ribonucleic acid in the primate brain by in situ hybridization histochemistry. Mol Endocrinol 1:371–376.

Starrett JR, DeFazio RA, Moenter SM (2021) Reciprocal Changes in Voltage-Gated Potassium and Subthreshold Inward Currents Help Maintain Firing Dynamics of AVPV Kisspeptin Neurons during the Estrous Cycle. eNeuro 8 Available at: https://www.eneuro.org/content/8/5/ENEURO.0324-21.2021 [Accessed May 5, 2022].

Stephens SBZ, Kauffman AS (2021) Estrogen Regulation of the Molecular Phenotype and Active Translatome of AVPV Kisspeptin Neurons. Endocrinology 162:bqab080.

Stincic TL, Qiu J, Connors AM, Kelly MJ, Rønnekleiv OK (2021) Arcuate and Preoptic Kisspeptin Neurons Exhibit Differential Projections to Hypothalamic Nuclei and Exert Opposite Postsynaptic Effects on Hypothalamic Paraventricular and Dorsomedial Nuclei in the Female Mouse. eNeuro 8:ENEURO.0093-21.2021.

Sun J, Chu Z, Moenter SM (2010) Diurnal In Vivo and Rapid In Vitro Effects of Estradiol on Voltage-Gated Calcium Channels in Gonadotropin-Releasing Hormone Neurons. J Neurosci 30:3912–3923.

Suter KJ, Song WJ, Sampson TL, Wuarin JP, Saunders JT, Dudek FE, Moenter SM (2000) Genetic targeting of green fluorescent protein to gonadotropin-releasing hormone neurons: characterization of whole-cell electrophysiological properties and morphology. Endocrinology 141:412–419.

Terasawa E (1994) Steroid modulation of pulsatile LHRH release in the rhesus monkey. Horm Behav 28:406–416.

Thind KK, Goldsmith PC (1988) Infundibular Gonadotropin-Releasing Hormone Neurons Are Inhibited by Direct Opioid and Autoregulatory Synapses in Juvenile Monkeys. NEN 47:203–216.

Tovar S, Vázquez MJ, Navarro VM, Fernández-Fernández R, Castellano JM, Vigo E, Roa J, Casanueva FF, Aguilar E, Pinilla L, Dieguez C, Tena-Sempere M (2006) Effects of single or repeated intravenous administration of kisspeptin upon dynamic LH secretion in conscious male rats. Endocrinology 147:2696–2704.

Urbanski HF, Ojeda SR (1987) Activation of luteinizing hormone-releasing hormone release advances the onset of female puberty. Neuroendocrinology 46:273–276.

van der Beek EM (1996) Circadian control of reproduction in the female rat. Prog Brain Res 111:295–320.

Vanacker C, Moya MR, DeFazio RA, Johnson ML, Moenter SM (2017) Long-Term Recordings of Arcuate Nucleus Kisspeptin Neurons Reveal Patterned Activity That Is Modulated by Gonadal Steroids in Male Mice. Endocrinology 158:3553–3564.

Vastagh C, Solymosi N, Farkas I, Liposits Z (2019) Proestrus Differentially Regulates Expression of Ion Channel and Calcium Homeostasis Genes in GnRH Neurons of Mice. Front Mol Neurosci 12:137.

Vida B, Deli L, Hrabovszky E, Kalamatianos T, Caraty A, Coen CW, Liposits Z, Kalló I (2010) Evidence for suprachiasmatic vasopressin neurones innervating

kisspeptin neurones in the rostral periventricular area of the mouse brain: regulation by oestrogen. J Neuroendocrinol 22:1032–1039.

Vida B, Hrabovszky E, Kalamatianos T, Coen CW, Liposits Z, Kalló I (2008) Oestrogen receptor alpha and beta immunoreactive cells in the suprachiasmatic nucleus of mice: distribution, sex differences and regulation by gonadal hormones. J Neuroendocrinol 20:1270–1277.

Wakabayashi Y, Nakada T, Murata K, Ohkura S, Mogi K, Navarro VM, Clifton DK, Mori Y, Tsukamura H, Maeda K-I, Steiner RA, Okamura H (2010) Neurokinin B and dynorphin A in kisspeptin neurons of the arcuate nucleus participate in generation of periodic oscillation of neural activity driving pulsatile gonadotropin-releasing hormone secretion in the goat. J Neurosci 30:3124–3132.

Wang L, Burger LL, Greenwald-Yarnell ML, Myers MG, Moenter SM (2018) Glutamatergic Transmission to Hypothalamic Kisspeptin Neurons Is Differentially Regulated by Estradiol through Estrogen Receptor α in Adult Female Mice. J Neurosci 38:1061–1072.

Wang L, DeFazio RA, Moenter SM (2016a) Excitability and Burst Generation of AVPV Kisspeptin Neurons Are Regulated by the Estrous Cycle Via Multiple Conductances Modulated by Estradiol Action. eNeuro 3:ENEURO.0094-16.2016.

Wang L, DeFazio RA, Moenter SM (2016b) Excitability and Burst Generation of AVPV Kisspeptin Neurons Are Regulated by the Estrous Cycle Via Multiple Conductances Modulated by Estradiol Action. eNeuro 3.

Wang L, Vanacker C, Burger LL, Barnes T, Shah YM, Myers MG, Moenter SM (2019a) Genetic dissection of the different roles of hypothalamic kisspeptin neurons in regulating female reproduction Elmquist JK, Dulac C, Prevot V, eds. eLife 8:e43999.

Wang L, Vanacker C, Burger LL, Barnes T, Shah YM, Myers MG, Moenter SM (2019b) Genetic dissection of the different roles of hypothalamic kisspeptin neurons in regulating female reproduction. Elife 8.

Watanabe M, Fukuda A, Nabekura J (2014a) The role of GABA in the regulation of GnRH neurons. Front Neurosci 8:387.

Watanabe Y, Uenoyama Y, Suzuki J, Takase K, Suetomi Y, Ohkura S, Inoue N, Maeda K-I, Tsukamura H (2014b) Oestrogen-induced activation of preoptic kisspeptin

neurones may be involved in the luteinising hormone surge in male and female Japanese monkeys. J Neuroendocrinol 26:909–917.

Watson RE, Langub MC, Engle MG, Maley BE (1995) Estrogen-receptive neurons in the anteroventral periventricular nucleus are synaptic targets of the suprachiasmatic nucleus and peri-suprachiasmatic region. Brain Res 689:254–264.

Wiegand SJ, Terasawa E (1982) Discrete lesions reveal functional heterogeneity of suprachiasmatic structures in regulation of gonadotropin secretion in the female rat. Neuroendocrinology 34:395–404.

Wiegand SJ, Terasawa E, Bridson WE (1978) Persistent estrus and blockade of progesterone-induced LH release follows lesions which do not damage the suprachiasmatic nucleus. Endocrinology 102:1645–1648.

Wiegand SJ, Terasawa E, Bridson WE, Goy RW (1980) Effects of Discrete Lesions of Preoptic and Suprachiasmatic Structures in the Female Rat. NEN 31:147–157.

Wildt L, Häusler A, Marshall G, Hutchison JS, Plant TM, Belchetz PE, Knobil E (1981) Frequency and amplitude of gonadotropin-releasing hormone stimulation and gonadotropin secretion in the rhesus monkey. Endocrinology 109:376–385.

Wilson RC, Kesner JS, Kaufman JM, Uemura T, Akema T, Knobil E (1984) Central electrophysiologic correlates of pulsatile luteinizing hormone secretion in the rhesus monkey. Neuroendocrinology 39:256–260.

Wintermantel TM, Campbell RE, Porteous R, Bock D, Gröne H-J, Todman MG, Korach KS, Greiner E, Pérez CA, Schütz G, Herbison AE (2006) Definition of estrogen receptor pathway critical for estrogen positive feedback to gonadotropin-releasing hormone neurons and fertility. Neuron 52:271–280.

Witkin JW (1987) Aging changes in synaptology of luteinizing hormone-releasing hormone neurons in male rat preoptic area. Neuroscience 22:1003–1013.

Witkin JW (1989) Synaptology of luteinizing hormone-releasing hormone neurons in the preoptic area of the male rat: effects of gonadectomy. Neuroscience 29:385–390.

Witkin JW (1992a) Reproductive history affects the synaptology of the ageing gonadotropin-releasing hormone system in the male rat. J Neuroendocrinol 4:427–432.

Witkin JW (1992b) Increased synaptic input to gonadotropin-releasing hormone neurons in aged, virgin, male Sprague-Dawley rats. Neurobiol Aging 13:681–686.

Witkin JW, Ferin M, Popilskis SJ, Silverman AJ (1991) Effects of gonadal steroids on the ultrastructure of GnRH neurons in the rhesus monkey: synaptic input and glial apposition. Endocrinology 129:1083–1092.

Witkin JW, O'Sullivan H, Ferin M (1995) Glial ensheathment of GnRH neurons in pubertal female rhesus macaques. J Neuroendocrinol 7:665–671.

Witkin JW, Romero M-T (1995) Comparison of ultrastructural characteristics of gonadotropin-releasing hormone neurons in prepubertal and adult male rats. Neuroscience 64:1145–1151.

Witkin JW, Silverman AJ (1985) Synaptology of luteinizing hormone-releasing hormone neurons in rat preoptic area. Peptides 6:263–271.

Woolley CS, Weiland NG, McEwen BS, Schwartzkroin PA (1997) Estradiol Increases the Sensitivity of Hippocampal CA1 Pyramidal Cells to NMDA Receptor-Mediated Synaptic Input: Correlation with Dendritic Spine Density. J Neurosci 17:1848–1859.

Wray S, Hoffman G (1986) Postnatal morphological changes in rat LHRH neurons correlated with sexual maturation. Neuroendocrinology 43:93–97.

Wu FC, Irby DC, Clarke IJ, Cummins JT, de Kretser DM (1987) Effects of gonadotropin-releasing hormone pulse-frequency modulation on luteinizing hormone, follicle-stimulating hormone and testosterone secretion in hypothalamo/pituitary-disconnected rams. Biol Reprod 37:501–510.

Xia L, Van Vugt D, Alston EJ, Luckhaus J, Ferin M (1992) A surge of gonadotropin-releasing hormone accompanies the estradiol-induced gonadotropin surge in the rhesus monkey. Endocrinology 131:2812–2820.

Xiong JJ, Karsch FJ, Lehman MN (1997) Evidence for seasonal plasticity in the gonadotropin-releasing hormone (GnRH) system of the ewe: changes in synaptic inputs onto GnRH neurons. Endocrinology 138:1240–1250.

Yang JA, Mamounis KJ, Yasrebi A, Roepke TA (2016) Regulation of gene expression by 17β-estradiol in the arcuate nucleus of the mouse through ERE-dependent and ERE-independent mechanisms. Steroids 107:128–138.

Yip SH, Boehm U, Herbison AE, Campbell RE (2015) Conditional Viral Tract Tracing Delineates the Projections of the Distinct Kisspeptin Neuron Populations to Gonadotropin-Releasing Hormone (GnRH) Neurons in the Mouse. Endocrinology 156:2582–2594.

Yip SH, Campos P, Liu X, Porteous R, Herbison AE (2021) Innervation of GnRH Neuron Distal Projections and Activation by Kisspeptin in a New GnRH-Cre Rat Model. Endocrinology 162:bqaa186.

Zhang C, Bosch MA, Qiu J, Rønnekleiv OK, Kelly MJ (2015) 17β-Estradiol increases persistent Na(+) current and excitability of AVPV/PeN Kiss1 neurons in female mice. Mol Endocrinol 29:518–527.

Zhang C, Bosch MA, Rick EA, Kelly MJ, Rønnekleiv OK (2009) 17Beta-estradiol regulation of T-type calcium channels in gonadotropin-releasing hormone neurons. J Neurosci 29:10552–10562.

Zhang C, Kelly MJ, Rønnekleiv OK (2010) 17 β-estradiol rapidly increases ATP-sensitive potassium channel activity in gonadotropin-releasing hormone neurons [corrected] via a protein kinase signaling pathway. Endocrinology 151:4477–4484.

Zhang C, Roepke TA, Kelly MJ, Rønnekleiv OK (2008) Kisspeptin Depolarizes Gonadotropin-Releasing Hormone Neurons through Activation of TRPC-Like Cationic Channels. J Neurosci 28:4423–4434.

Zhang C, Tonsfeldt KJ, Qiu J, Bosch MA, Kobayashi K, Steiner RA, Kelly MJ, Rønnekleiv OK (2013) Molecular mechanisms that drive estradiol-dependent burst firing of Kiss1 neurons in the rostral periventricular preoptic area. Am J Physiol Endocrinol Metab 305:E1384-1397.

Zoeller RT, Seeburg PH, Young WS (1988) In situ hybridization histochemistry for messenger ribonucleic acid (mRNA) encoding gonadotropin-releasing hormone (GnRH): effect of estrogen on cellular levels of GnRH mRNA in female rat brain. Endocrinology 122:2570–2577.